

**POLITECNICO DI TORINO**

Master Degree in Physics of Complex Systems



Master Degree Thesis

**Bosonic Binary Mixture in a 4-well Ring**

Supervisor

Prof. Vittorio Penna

Candidate

Alessandra Contestabile

October 2020



## Abstract

The aim of this thesis is to show that, depending on the ratio between the inter- and the intra-species repulsive interactions, a mixture of two Bose-Einstein condensates trapped in a  $L$ -well potential with periodic boundary conditions (and  $L = 4$ ) exhibits various macroscopic ground-state configurations which differ in the degree of mixing and in the space distribution. The latter were found and investigated, thanks to the use of the Coherent-State picture, with reference to previous work on the dimer (two potential wells) and on the trimer (three wells). Moreover, by studying the energy behavior described by the Hamiltonian of the Bose-Hubbard model, it has been possible to derive the complete mixing-demixing phase diagram, both in the case with the hopping parameter set to zero ( $T=0$ ) and in the case with the latter different from zero (more realistic and interesting from an experimental point of view). The mixing properties of the two quantum fluids, which are shown to be strongly affected by the fragmented character of the confining potential, are also shown to depend only on two effective parameters incorporating the asymmetry between the heteronuclear species. The study of the case  $L = 4$ , developed in continuity with the  $L < 4$  ring lattices' one, allowed us to discover significant differences with respect to cases with  $L = 2, 3$  and, moreover, it highlighted new and interesting properties concerning the demixing mechanism and the quantum phases in ring lattices.

# Acknowledgements

I take this opportunity to thank Prof. Vittorio Penna for his valuable guidance, encouragement and help. I am also grateful to him for providing all the material useful for the correct understanding of the subject of this thesis, as well as for the clear and comprehensive explanations. A particular recognition for the patience with which he helped me to carry out the project despite the only working mode available was smart-working, during the difficult months that have just passed.

I would also like to thank Dr. Andrea Richaud for all the support, the clarifications and for sharing with me the knowledge gained during his PhD experience. Moreover, a very special thank to him for the help in the computational part.

A heartfelt thanks is due to my father, Mauro, for always encouraging me to give my best, to challenge my limits and to always look forward. He always told me to keep the "starboard" and, even though he thinks I didn't listen to him, he doesn't know how many times I've followed his advice. I take this opportunity to tell him that we are too similar to think I don't want to follow his example.

An enormous thanks to my mother, Caterina. If she hadn't been there to listen to my repetitions aloud of the programs of almost all subjects I would probably still be here with many exams to take. So, thank you Mom for always taking my side (well, almost always), for pushing me and for taking care: I couldn't have done it without you.

Another heartfelt thanks goes to my brother, Domenico; otherwise, if I don't mention him, he gets angry. Ok, just kidding! Thank you, little brother, for always supporting and never abandoning me: you will always be my greatest partner in

crime.

A big thank you goes to my grandparents, Luciana, Fernando and Francesca, who are my biggest fans, together with my aunts Graziella and Gianna, my uncles, cousins and all relatives.

I also want to address a small thought to those who are no longer here: grandfather Domenico, grandfather Vincenzo and grandmother Anna. I know that if you had still been with us you would have formed the "north curve" of my supporters.

Last but not least, a "thank you" as big as the Polytechnic to all my friends and colleagues. To both near and far ones. To those I met in these years of travel and changes and to those I have known since time immemorial. Thank you, friends, for supporting and putting up with me: you are in my heart.

Alessandra Contestabile



# Table of Contents

<b>List of Figures</b>	VII
<b>Acronyms</b>	XII
<b>1 Introduction</b>	1
1.1 Physics of Ultracold Atoms and Binary Mixtures . . . . .	1
1.1.1 Bose-Einstein condensation . . . . .	1
1.1.2 Mixtures of Bose-Einstein condensates . . . . .	3
1.1.3 Ultracold atoms in optical lattices . . . . .	4
1.1.4 Binary mixtures in optical lattices . . . . .	6
1.2 The Bose-Hubbard Model . . . . .	8
1.2.1 Derivation of the BH model through the space-mode approx- imation . . . . .	10
1.2.2 The BH-Model Phase Diagram . . . . .	14
1.2.3 The Coherent-State Picture of the Bose-Hubbard Model . .	15
<b>2 Phase Separation in <math>L = 2, 3</math> Ring Lattices</b>	19
2.1 The dimer . . . . .	20
2.1.1 The Continuous-Variable Picture . . . . .	20
2.1.2 The Mixing-Supermixing Phase Diagram in the large popu- lations limit . . . . .	24
2.1.3 The Mixing-Demixing Phase Diagram in the large popula- tions limit . . . . .	26
2.2 The trimer . . . . .	32
2.2.1 Phase Diagram in the large population limit . . . . .	34
2.2.2 Phases and Degree of Mixing . . . . .	36
<b>3 The Ground State in the large-population limit</b>	39
3.1 The Coherent-State Variational Picture . . . . .	40
3.1.1 Solutions for $T_a = T_b = 0$ . . . . .	41

<b>4</b>	<b>Phase Diagram</b>	<b>52</b>
4.1	Evaluation of the energy associated to the found solutions . . . . .	52
4.1.1	Case 1: completely mixed phase . . . . .	53
4.1.2	Case 2: half-demixed phase . . . . .	53
4.1.3	Case 3: phase with mixing in a single well . . . . .	54
4.1.4	Case 4: partially demixed double-dimer . . . . .	54
4.1.5	Case 5: quasi-uniform phase . . . . .	55
4.1.6	Case 6: dimer-like demixed phase . . . . .	55
4.1.7	Case 7: trimer-like demixed phase . . . . .	55
4.2	Comparison between the values of the energy in the different configurations . . . . .	56
4.2.1	Comparison between case 1 and case 6 . . . . .	56
4.2.2	Comparison between case 1 and case 7 . . . . .	56
4.2.3	Comparison between case 6 and case 7 . . . . .	57
4.2.4	Comparison with case 2 in the symmetrical case . . . . .	57
4.2.5	Comparisons in the asymmetrical cases for the partially demixed phases . . . . .	59
4.3	Phase Diagram . . . . .	64
4.3.1	Behaviour of minimum-energy configuration $(\vec{n}, \vec{m})$ . . . . .	66
4.3.2	Phases and degree of mixing . . . . .	69
4.3.3	Phases and Free Energy . . . . .	70
4.3.4	Phases and Location Entropy . . . . .	73
<b>5</b>	<b>Finite-Size Effects on the Mixing-Demixing Transitions</b>	<b>75</b>
5.1	GS configuration with non-vanishing hopping terms . . . . .	75
5.2	The border of the fully-mixed phase . . . . .	80
5.3	Mixing and Location Entropy . . . . .	81
<b>A</b>	<b>The finding-minima Numerical Algorithm</b>	<b>85</b>
<b>B</b>	<b>The link between the CVP and the Coherent-State method</b>	<b>91</b>
	<b>Bibliography</b>	<b>94</b>

# List of Figures

1.1	An illustration of a "super-photon" created when physicists turned photons of light into a state of matter called a Bose-Einstein condensate. (Image: © Jan Klaers, University of Bonn) . . . . .	2
1.2	Illustration of Cold Atoms in an Optical Lattice. . . . .	4
1.3	A schematic representation of the fragmentation in many space components of the condensate in the lattice. Different heights of the wells correspond to different values of the tunneling amplitude $J$ . . . . .	9
1.4	BH-Model Phase Diagram. The grey domains (lobes) represent the portions of the plane where the system is in the MI-phase. For each lobe, the filling is specified. Outside the domains, the system is in the SF-regime. . . . .	15
2.1	Probability densities of the ground state for $U/T = 0.01$ , $N = M = 30$ , and (from top to bottom) $W/T = 0.001, 0.085, 0.093, 0.170$ . Right column: probability density obtained within the CV method. Left column: probability amplitudes for the exact ground state calculated numerically. . . . .	22
2.2	First 15 energy levels as a function of interspecies interaction $W$ for intraspecies interaction $U = 0.01$ (energy units in $J$ ) and total boson number $N = 60$ with $N = M$ . The plots compare numerical results (continuous lines) with the analytical eigenvalues (dotted lines) computed within the CV method. . . . .	23
2.3	Phase diagram of a bosonic binary mixture characterized by attractive inter-species interaction and confined in a generic L-site potential. Phase M is the uniform and mixed one, phase PL features a soliton just in the minority species, while phase SM exhibits the presence of a supermixed soliton. Red dashed (solid) line corresponds to a phase transition where the first (second) derivative of the effective potential of the CVP, associated to this case, with respect to $\alpha$ is discontinuous. . . . .	25

2.4	The Mixing-Demixing Phase Diagram of a binary mixture in a dimer. Each of the three phases corresponds to a different functional relationship between the minimum-energy configuration and the effective model parameters $\alpha$ and $\beta$ . Each phase has been labelled with the same number used to label the Hamiltonian in the relevant configuration. . . . .	31
2.5	Phase diagram of a binary mixture in a ring trimer. Each of the four phases is related to a different functional relationship between the minimum-energy configuration and effective model parameters $\alpha$ and $\beta$ . This behaviour has a direct impact on the mixing properties of the system and on its GS energy. Red dashed (solid) line represents a mixing-demixing transition across which the components $x_j$ and $y_j$ of the minimum-energy configuration feature a jump discontinuity (are continuous). The plot has been obtained by means of a fully-analytic minimization of potential (2.41) under the constraints (2.37) and (2.38). . . . .	35
2.6	Entropy of mixing, $S_{mix}$ , in the four phases. Phase 1 (in blue) features perfect mixing and $S_{mix}$ takes the biggest possible value, i.e. $\log 2 \approx 0.69$ . Conversely, phase 3 (in purple) features perfect demixing and $S_{mix}$ is therefore zero. . . . .	36
2.7	Mixing Entropy associated to the configurations $(\vec{x}, \vec{y})$ which minimize effective potential (2.41) sweeping model parameters $\alpha$ and $\beta$ . The following values/intervals have been chosen: $U_a = U_b = 1$ , $N = 15$ , $M \in [0, 15] \rightarrow \beta \in [0, 1]$ , $W \in [0, 3] \rightarrow \alpha \in [0, 3]$ , $T_a = T_b = T$ , where $T = 0.1, 0.2, 0.5$ in the left, central and right panel respectively. Colors have been employed as a guide to the eye: blue is used when $S_{mix} = \log 2$ , purple when $S_{mix} < 0.05$ , green for all intermediate values except the domain corresponding to phase 2 and therefore colored in orange. . . . .	38
3.1	Possible phase-separation mechanisms for a binary mixture in a 4-well potential with PBC. Blue (red) color corresponds to species A (B). On the left, the fully mixed configurations is depicted. On the right, some examples of demixed configurations (from top to bottom: complete demixing with emulsion-like structure, complete demixing with well separated structure, and partial demixing). Left panel corresponds to $W/U < 1$ , right panels to $W/U = 1$ . $T/U = 0$ has been chosen for all plots. . . . .	40
3.2	Case 1: Mixed (Uniform) phase. . . . .	42
3.3	Case 2: Partially demixed phase that recalls the trimer's phase 2. We can call this one the "half-demixed phase". . . . .	42

3.4	Case 3: Partially demixed phase that recalls the trimer's phase 4. We can call this one "phase with mixing in a single well". . . . .	42
3.5	Case 4: Partially demixed phase that recalls the dimer's phase 2; let's call it the "partially demixed double dimer". . . . .	42
3.6	Case 5: Partially demixed phase consisting in the union of a filled well and a trimer in uniform configuration: a totally new guess. We can call this one the "quasi-uniform phase". . . . .	43
3.7	Case 6: Completely demixed phase that recalls the dimer one. Let's call it "dimer-like". . . . .	43
3.8	Case 7: Completely demixed phase that recalls the trimer one. Let's call it "trimer-like". . . . .	43
3.9	Case 2 solutions: Range of validity. . . . .	48
4.1	Comparison between case 4 partially demixed phase and the dimer-like totally demixed phase. . . . .	61
4.2	Comparison between case 4 partially demixed phase and the trimer-like totally demixed phase. . . . .	62
4.3	This is nothing but the graph of figure (3.2) seen from above. The two straight lines are put there in order to highlight the small surviving yellow corner, where the energy of case 4 is smaller than the one of the demixed phase. . . . .	62
4.4	The interval of validity of the case 2 solutions (represented by the triangle) lays entirely in the region where $H_{dd}$ is the minimal (the outer curve). . . . .	63
4.5	Phase diagram of a binary mixture in a ring tetramer. Each of the five phases corresponds to a different functional relationship between the minimum-energy configuration and effective model parameters $\alpha$ and $\beta$ . This circumstance has a direct impact on the mixing properties of the system and on its GS energy. The labels of each phase are the numbers corresponding to the name of the cases which were "winners" of the comparisons referred to in the previous paragraphs. . . . .	64
4.6	For convenience, we report here the schematic representations of the configurations that have become part of the Phase Diagram in Fig. (4.5) . . . . .	66
4.7	Behaviour of species A in the 1 <sup>st</sup> well. . . . .	67
4.8	Behaviour of species A in the 2 <sup>nd</sup> well. . . . .	67
4.9	Behaviour of species A in the 3 <sup>rd</sup> well. . . . .	67
4.10	Behaviour of species A in the 4 <sup>th</sup> well. . . . .	67
4.11	Behaviour of species B in the 1 <sup>st</sup> well. . . . .	68
4.12	Behaviour of species B in the 2 <sup>nd</sup> well. . . . .	68

4.13	Behaviour of species B in the 3 <sup>rd</sup> well. . . . .	68
4.14	Behaviour of species B in the 4 <sup>th</sup> well. . . . .	68
4.15	Entropy of mixing, $S_{mix}$ , in the five phases. Phase 1 (in orange) features perfect mixing and $S_{mix}$ takes the biggest possible value, i.e. $\log 2 \approx 0.69$ . Conversely, phase 6 and 7 (in green and yellow) features perfect demixing and $S_{mix}$ is therefore zero. . . . .	69
4.16	Hamiltonian relevant to the minimum-energy configuration as a function of the model parameters $\alpha$ and $\beta$ . . . . .	71
4.17	First derivative with respect to $\alpha$ of the Hamiltonian relevant to the minimum-energy configuration, as a function of the model parameters $\alpha$ and $\beta$ . . . . .	72
4.18	Second derivative with respect to $\alpha$ of the Hamiltonian relevant to the minimum-energy configuration, as a function of the model parameters $\alpha$ and $\beta$ . . . . .	72
4.19	Second derivative of energy seen from below. This different point of view is presented with the intention of emphasizing the new jumps present at the transitions 4-6 and 3-7. . . . .	72
4.20	Location Entropy, $S_{loc}$ , in the five phases. Thanks to the use of this indicator, one can finally observe the critical behavior at transition 6-7, between the two demixed phases, as well as at the transitions 1-4, 4-7 and 1-3 already observed in the Entropy of Mixing. . . . .	74
5.1	Scatter plot of the minimum-energy configuration $(\vec{x}, \vec{y})$ for $T = 0.1, 0.2, 0.5$ (going from top to bottom). The orange color has been chosen to mark the region in which the mixed phase persists. All the other phases are colored in blue. The occurrence of a phase transition at $\beta = 1/\sqrt{3}$ is clearly recognizable and still discontinuous for the lowest value of the hopping amplitude $T$ (first panel), but it start to become smoother as $T$ increases (second and third panels). . . . .	78
5.2	Scatter plot of the Mixing Entropy associated to the ground state for $T = 0.1$ (the one on the upper left corner), $T = 0.2$ (the one on the upper right corner), $T = 0.5$ (the one below). Colors have been employed as a guide to the eye: orange is used when $S_{mix} \approx \log 2$ , green when $S_{mix} < 0.05$ and $\beta > 1/\sqrt{3}$ , yellow when $S_{mix} < 0.05$ and $\beta < 1/\sqrt{3}$ , magenta and blue for all intermediate values, separated by $\beta = 1/3$ . . . . .	82
5.3	Scatter plot of the Location Entropy associated to the ground state for $T = 0.1$ (the one on the top), $T = 0.2$ (the one on the lower left corner), $T = 0.5$ (the one on the lower right corner). Colors have been employed as a guide to the eye: orange is used when $S_{mix} \approx \log 2$ , green otherwise. . . . .	83



# Acronyms

**GS**

Ground State

**BEC**

Bose-Einstein Condensate

**QMC**

Quantum Monte Carlo

**PBC**

Periodic Boundary Conditions

**BH**

Bose Hubbard

**TDVP**

Time-dependent Variational Principle

**CVP**

Continuous Variable Picture

# Chapter 1

## Introduction

*“Logic takes you from A to B, imagination takes you everywhere.”*  
*Albert Einstein*

In this Chapter, we will give a historical and illustrative account of the theoretical aspects and experimental advances in the field of binary mixtures of Bose-Einstein condensates in optical lattices. Furthermore, we will illustrate in details the model used in Condensed Matter Physics to describe a Bose-gas of interacting particles in the presence of external trapping potentials: the Bose-Hubbard Model.

### 1.1 Physics of Ultracold Atoms and Binary Mixtures

#### 1.1.1 Bose-Einstein condensation

Theorized in 1924 by Albert Einstein and Satyendra Nath Bose, a Bose-Einstein condensate (BEC) is a state of matter (also called the fifth state of matter) which is typically formed when a gas of bosons at low densities is cooled to temperatures very close to absolute zero (-273.15 °C). Under such conditions, and thanks to their bosonic quantum statistics, a large fraction of bosons occupy the lowest quantum state (the Ground-State, GS) [8].

The BEC can be formed from gas with a low density of ultra-cold atoms or from some quasiparticles within solids, such as excitons or polaritons.

The basic idea behind this concept is that, at temperatures  $T$  below a certain critical temperature  $T_c$ , the characteristic width of the atomic wave functions approaches the typical inter-particle distance. Consequently, under the temperature  $T_c$ , each

wave packet associated with a single atom begins to overlap the others. At this point, quantum statistics force the atoms to Bose condense and the whole group starts behaving as though it were a single atom [53].

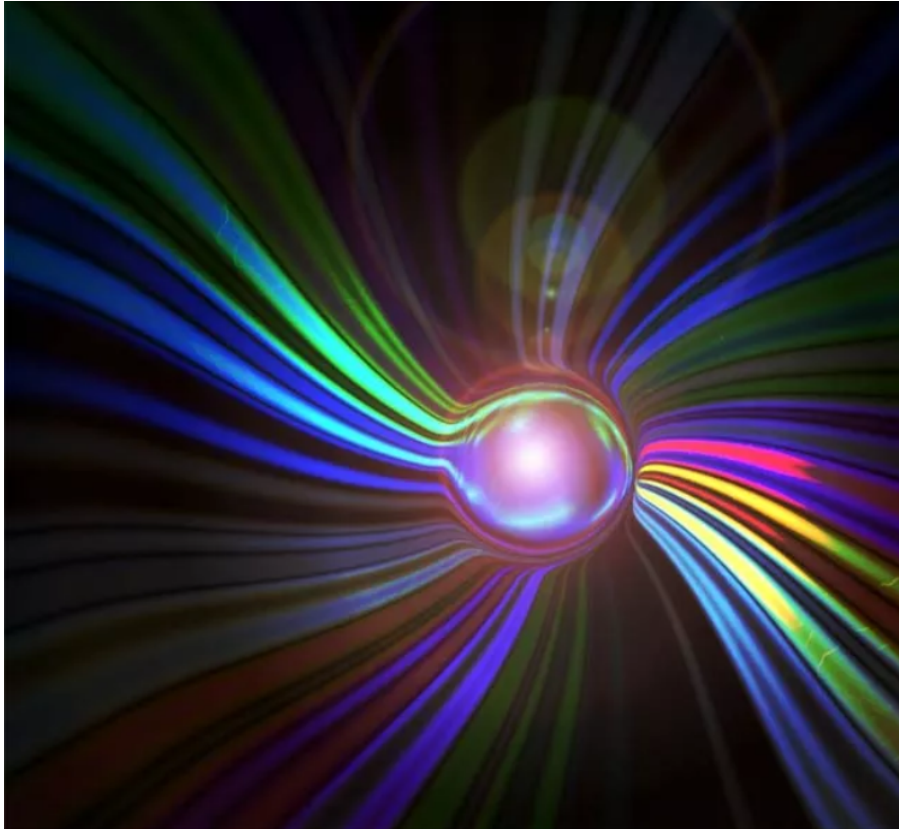


**Figure 1.1:** An illustration of a "super-photon" created when physicists turned photons of light into a state of matter called a Bose-Einstein condensate. (Image: © Jan Klaers, University of Bonn)

For many years, the theory of the existence of BEC had no theoretical relevance or experimental validation, until 1938, when the connection between Superfluidity (just discovered) and Condensates was first hypothesized. Afterwards, a series of papers by Landau, Lifshitz, Penrose and Onsager introduced the concept of nondiagonal long-range order and specified the role of the latter in Bose-Einstein condensates and superfluids [50, 18].

As it often happens, experimental interest in ultracold atomic gases came many years after the first theoretical speculations. In the 1970s, thanks to the advent of new techniques to cool and trap atoms, some groups of physicists began to try to Bose condense some chemical elements [13, 52].

It took a few more years, but finally, in 1995, thanks to powerful and versatile

laser-based cooling techniques, the first Bose-Einstein condensations of  $^{87}\text{Rb}$  and  $^{23}\text{Na}$  gases, respectively, were observed [4] [15]. After that, some other elements were successfully condensed, e.g.  $^7\text{Li}$  [9], spin-polarized hydrogen [24], metastable  $^4\text{He}$  [51, 56], and  $^{41}\text{K}$  [46]. We should consider that, in the conditions of temperature and density normally available in modern experimental equipments, the atomic system would be at equilibrium in the solid phase. Thus, in order to observe Bose-Einstein condensation, one has to keep the system in a metastable gas phase for a sufficiently long time. This is possible, in fact, because three-body losses [63] represents rare events in an ultracold dilute gas, whose typically lifetime is hence long enough to perform experiments.

The experimental results of 1995, celebrated by the award of the Nobel Prize in Physics in 2001 [38], were the first step towards a number of theoretical and experimental studies in the field of quantum gases. Furthermore, thanks to them, new fundamental questions arose and the curiosity of generations of young scientists in this topic grew considerably. Some of these problems have already been addressed and solved: there is now a very rich and renowned literature on Bose-Einstein condensation [53]. However, new questions concerning the Physics of ultracold quantum matter arise every day and remain unanswered, as well as many areas of this research field are still unexplored.

### 1.1.2 Mixtures of Bose-Einstein condensates

Immediately following the achievement of Bose-Einstein condensation in dilute gases, there has been considerable interest in the study of binary mixtures of Bose-Einstein condensates. One of the first examples is represented by a mixture created in 1997, made up of two particular states of the Rubidium atoms. Instead, the first example of a mixture of two different atomic species dates back to 2001 (K and Rb) [46].

Over the last two decades, two species Bose-Einstein condensates have been employed in the exploration of several different phenomena: in addition to the dynamical phase-separation mechanisms, one has modulation instabilities [57, 35, 33, 16], the presence of persistent currents [5, 62] and collective excitations [44].

The situation under which demixing occurs in binary mixtures with inter-species repulsion, has been the focus of a certain number of theoretical investigations, including mean-field treatments at zero [39, 47, 14, 17, 32] and finite temperature [58] as well as Quantum Monte Carlo (QMC) simulations [31].

The separation of the two species is usually characterized in terms of parameters written as a combination of the number of bosons of each species ( $N$  and  $M$  or  $N_a$  and  $N_b$ ), the intra-species repulsion coefficients ( $U_a$  and  $U_b$ ) and the inter-species repulsion coefficient ( $W$ ). This is because the basic rule [60, 54, 37, 41, 12] when

dealing with harmonically-confined BECs in the mean-field approximation is that, if intra- and inter-species scattering lengths  $a_{ij}$  verify the condition

$$a_{12} < \sqrt{a_{11}a_{22}}$$

then the two quantum fluids can be mixed. So, if the inter-species repulsion  $\propto a_{12}$  (that is  $W$ ) gets bigger than the (geometric average of the) intra-species repulsions  $\propto \sqrt{a_{11}a_{22}}$  (that is  $\sqrt{U_a U_b}$ ), then, already in the rather simple case of bosonic binary mixture trapped in a harmonic potential, two phase separation mechanisms are available, depending on the ratio of the atomic masses and of the interaction strengths.

### 1.1.3 Ultracold atoms in optical lattices

The possibility of storing ultracold atoms in artificial periodic potentials of light, enabled by the previously unseen degree of control of matter at the nanoscale, has opened the way to directly plumb the fundamental problems of Condensed Matter Physics[7].

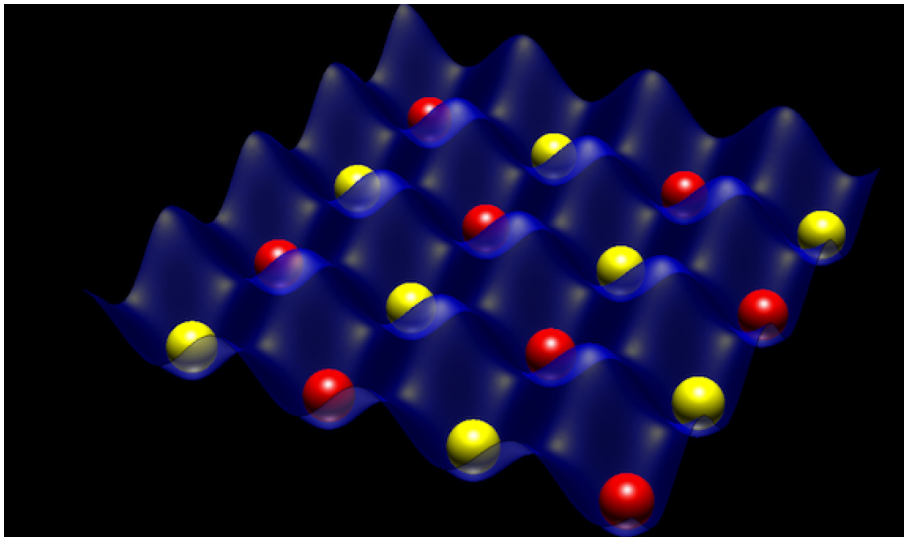


**Figure 1.2:** Illustration of Cold Atoms in an Optical Lattice.

Ultra-cold quantum gases in optical lattices, in fact, could be seen as nothing more than quantum simulators, i.e. quantum systems that have the advantage of being highly controllable and that can be used to mimic and simulate the static or dynamic behavior of other more complex quantum systems. Quantum simulators were proposed by Richard Feynman [20, 21] in 1985, to give particularly clean access to different classes of Hamiltonians (some of which come from solid state

physics, atomic physics, quantum optics or the theory of quantum information) and thus represent almost ideal systems where to test important theoretical concepts and observe quantum many-body effects.

The simplest way in which optical lattices can be created is to superimpose two counter-propagating laser beams, whose interference causes a stationary optical wave to be formed: the latter, in turn, determines a effective periodic potential able to trap the atoms. Based on how many laser beams are used, 1D, 2D or 3D optically-generated periodic potentials can be obtained, the sites of which can be effectively modeled as tight harmonic wells. The fundamental peculiarity of these experimental setups is that the properties of the resulting periodic potential (geometry and depth) are under the complete control of the experimentalists [36]. It is precisely from this last characteristic that the definition of "quantum simulator" is gathered.

### Weakly and strongly interacting regimes

Among the most important peculiarities of ultra-cold atom systems trapped in optical lattices is the possibility of being able to generate and observe strongly correlated quantum regimes (despite the fact that particles are in a ultralow density state). Let's recall, at this point, that a quantum many-body system in which weak interactions are present, can be effectively described by a macroscopic wave function. The temporal evolution of the latter is governed by an ad hoc modified version of the famous Schrödinger equation, i.e. the Gross-Pitaevskii equation, in which there is a nonlinear term that describes the interaction between particles. On the other hand, in the event that strong interactions are present (with respect to kinetic energy), the system cannot be described in terms of a simple single wave function, since it is in an ultraquantistic and strongly correlated state. Not surprisingly, this type of state is one of the most interesting and complicated to analyze, representing, in fact, one of the major challenges of the Physics of Condensed Matter.

An example of such a transition from the weakly to the strongly interacting regime is represented by the quantum phase transition from the Superfluid to Mott-insulator phase, observed for the first time in 2002 by Bloch and his group [28]. This transition can be easily described using the Bose-Hubbard Model [45] and the relevant Hamiltonian:

$$H = -T \sum_{\langle i,j \rangle} (\hat{a}_i^\dagger \hat{a}_j + h.c.) + \frac{U}{2} \sum_i \hat{n}_i (\hat{n}_i - 1) \quad (1.1)$$

The first part constitutes the kinetic energy term, which includes the tunneling coefficient  $T$  between adjacent sites and the  $\hat{a}_i^\dagger$  and  $\hat{a}_i$  operators that, respectively,

create and destroy a particle in the  $i$ -th site. The second term, instead, is nothing but the onsite repulsive energy term  $U$  and includes operator  $\hat{n}_i$ , which counts the number of bosons at the  $i$ -th site. Based on which of the two is the dominant energy term, we can deal with two different types of Ground State:

- if  $\frac{U}{T} \ll 1$  (weakly interacting regime), each atom is delocalized on the entire lattice: we are therefore dealing with a Bose Gas in the Superfluid phase characterized by phase coherence. To describe such a phase of matter we can use a factorized macroscopic state whose components describe, at each site, the local properties of bosons. On-site components are typically coherent states implying that the number of atoms per well follows the Poisson Statistics;
- if  $\frac{U}{T} \gg 1$  (strongly interacting regime), the system is a state called the Mott insulator: a phase of matter where bosons are trapped in single lattice sites and that cannot be described in terms of a macroscopic factorized wavefunction. In this case we are in the presence of a complete correlation in the particle numbers per site, while phase-coherence is completely lost.

Since the first experimental observation of the Superfluid - Mott Insulator transition [28], ultracold atoms have begun to acquire more and more importance in the study of highly interacting quantum systems, to which we can relate problems that are so complex that they cannot be solved in any other way. At the moment, thanks to the ease with which they are controllable, ultra-cold atomic and molecular systems are considered the best basis for studying several important problems of Condensed-Matter Physics, Statistical Physics, High Energy Physics and Quantum Chemistry [29, 6, 42].

### 1.1.4 Binary mixtures in optical lattices

The first experimental realization of a binary mixture in an optical lattice dates back to 2008 and was documented by the Firenze group [11], which worked to produce a degenerate mixture of  $^{87}\text{Rb}$  and  $^{41}\text{K}$  atoms in a 3D optical lattice. After this event, a surprisingly broad scenario of physical phenomena related to bosonic binary mixtures in optical lattices came out. Theoretically, bosonic binary mixtures in optical lattices can be conveniently described by means of the two-species Bose-Hubbard Hamiltonian [30], nothing more than a generalization of the single-species Bose-Hubbard Hamiltonian previously introduced (1.1), which incorporates the inter-species repulsion  $W$  between the two bosonic species:

$$\begin{aligned}
 H = & \frac{1}{2}U_a \sum_i \hat{n}_i (\hat{n}_i - 1) + \frac{1}{2}U_b \sum_i \hat{m}_i (\hat{m}_i - 1) + W \sum_i \hat{m}_i \hat{n}_i + \\
 & -T_a \sum_{\langle i,j \rangle} (\hat{a}_i^\dagger \hat{a}_j + h.c.) - T_b \sum_{\langle i,j \rangle} (\hat{b}_i^\dagger \hat{b}_j + h.c.)
 \end{aligned} \tag{1.2}$$

This Hamiltonian, as well as for the extended lattice case and for another series of interesting problems, has also been used in the study of the mixtures in the two simplest lattice cases: the two-well [19] potential and the three-well [61, 3] potential with the ring geometry. In fact, a lot of attention has been focused on small bosonic lattices since they provide a fertile ground to investigate the quantum-classical correspondence and the role of nonlinear interactions.

## 1.2 The Bose-Hubbard Model

As already mentioned, Hamiltonians (1.1) and (1.2) are respectively the Hamiltonian of the Bose-Hubbard Model and its generalization to the two-species case. This model was created in order to provide a description of the physics of interacting spinless bosons on a lattice. It can be seen as a variant of Hubbard model, which belongs to that class of models of Solid State Physics that deal with describing superconducting systems in an approximate way, as well as the movement of electrons between the atoms of a crystalline solid. The term "Bose", in this case, was introduced for the fact that the particles we are dealing with are bosons.

Firstly introduced by Gersch and Knollman [26] in 1963 in the context of granular superconductors, it became of great interest in the 1980s, after it was found to capture the essence of the Superfluid-Mott insulator transition in a way that was much more mathematically tractable than fermionic metal-insulator models [43, 27, 22]. Speaking of fermions, this model can also be generalized and applied to Bose-Fermi mixtures, in which case the corresponding Hamiltonian is called the Bose-Fermi-Hubbard Hamiltonian.

Now, in order to derive Eq. (1.1), let us start from the second-quantized Hamiltonian describing a Bose-Gas of interacting particles in the presence of external trapping potentials:

$$H = \int d^3r \left[ -\frac{\hbar^2}{2m} \hat{\psi}^\dagger \nabla^2 \hat{\psi} + W(\vec{r}) \hat{\psi}^\dagger \hat{\psi} + \frac{U_0}{2} (\hat{\psi}^\dagger)^2 \hat{\psi}^2 \right] \quad (1.3)$$

where  $W(\vec{r}) = V(\vec{r}) + V_p(\vec{r})$  is the sum of two contributions:

- $V(\vec{r})$  that is a confining harmonic potential

$$V(\vec{r}) = \frac{1}{2} m (\omega_x^2 x^2 + \omega_y^2 y^2 + \omega_z^2 z^2)$$

in which the frequencies  $\omega_x$ ,  $\omega_y$  and  $\omega_z$  determine the spatial distribution of the gas particle;

- $V_p(\vec{r})$  that is the periodic potential responsible for the occurrence of the local minima.

Let us consider the 1D case. The potential  $V_p(\vec{r})$  realized experimentally is periodic and can be represented in the simple form

$$V_p(x) = 2v \sin^2 \left( \frac{\pi x}{a} \right)$$

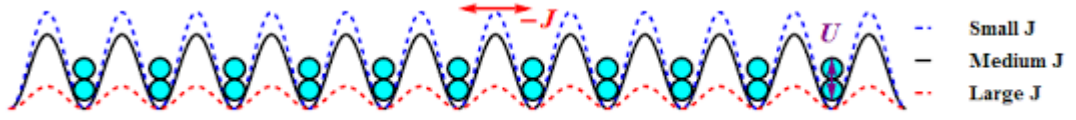


**Figure 1.3:** A schematic representation of the fragmentation in many space components of the condensate in the lattice. Different heights of the wells correspond to different values of the tunneling amplitude  $J$ .

where  $a$  is the distance between two adjacent potential wells, while  $v$  is the optical lattice strength.

Since bosons tend to occupy the positions with the lowest possible energy (potential minima), then  $V_p(x)$  determines the fragmentation in many space components of the condensate (see Fig. (1.3)). So, bosons are trapped and distributed in a periodic sequence of (local) potential wells whose minima are situated at  $x_j = aj$ ,  $j = 1, 2, \dots, L$ .

The fragmentation of the condensate in  $M$  nanoscale subsystems ( $M$  is the number of wells) formed by  $\sim \frac{N}{M}$  bosons (with  $\frac{N}{M} \ll N$ ) trapped in such potential wells shows how the dominating physical process in the resulting many-well system is the creation/destruction of bosons in each well tunneling  $T$  (often labeled with  $J$  too) between adjacent wells takes place.

To describe such a system we are going to use the field picture where the second quantization process allows one to embody the information that the system is formed by many nanoscale components.

Before continuing, let's assume periodic boundary conditions (PBC)

$$f(x + L) = f(x)$$

where  $L = Ma$ . The Hamiltonian becomes:

$$H = \int_0^L dx \left[ \hat{\psi}^\dagger(x) \left( -\frac{\hbar^2}{2m} \frac{\partial^2}{\partial x^2} + V_p(x) \right) \hat{\psi}(x) + \frac{U_0}{2} (\hat{\psi}^\dagger)^2 \hat{\psi}^2 \right] S \quad (1.4)$$

where  $\left( -\frac{\hbar^2}{2m} \frac{\partial^2}{\partial x^2} + V_p(x) \right) = H_0$  and  $S$  is the transverse area of the torus. Furthermore, since we are dealing with a 1D domain  $U_0 = \frac{4\pi\hbar^2 a_s}{m}$  reduces to  $U_0 = \frac{4\pi\hbar^2 a_s}{mS}$ .

### 1.2.1 Derivation of the BH model through the space-mode approximation

Our goal now is to derive the field  $\psi$ . Since the system is at a temperature close to absolute zero, we know that bosons occupy the lowest-energy level of the potential wells localized at  $x = aj$  with  $j \in (1, M)$ . Locally, one has:

$$\begin{aligned} V_p(x) &= V_p [(x - aj) + aj] = 2v \sin^2 \left[ \frac{\pi}{a}(x - aj) + \pi j \right] = \\ &= 2v \sin^2 \left[ \frac{\pi}{a}(x - aj) \right] \simeq 2v \left[ \frac{\pi}{a}(x - aj) - \frac{\pi^3}{6a^3}(x - aj)^3 + \dots \right]^2 \\ &\simeq 2v \frac{\pi^2}{a^2}(x - aj)^2 \end{aligned}$$

so, for  $x \simeq aj$ , potential  $V_p$  reduces to a Harmonic-oscillator potential, then

$$H_0 \simeq -\frac{\hbar^2}{2m} \frac{d^2}{dx^2} + \frac{m\omega^2}{2}(x - aj)^2$$

with  $\omega^2 = \frac{4\pi^2 v}{ma^2}$ . In the absence of interaction  $U_0$ , at  $T \simeq 0$ , the quantum states describing bosons are those involving the minimum energy. Hence, these states are the local Harmonic-oscillator Ground States:

$$W_j(x) \simeq \left( \frac{2\alpha}{\pi} \right)^{\frac{1}{4}} \exp \left[ -\frac{m\omega}{2\hbar}(x - aj)^2 \right] \quad (1.5)$$

where we can easily visualize the Gaussian part  $\exp \left[ -\frac{m\omega}{2\hbar}(x - aj)^2 \right]$ . Now, if we define the following variables

$$\begin{aligned} x_j &= aj \\ \gamma^2 &= \sqrt{\frac{2\alpha}{\pi}} \\ \alpha &= \frac{m\omega}{2\hbar} \end{aligned}$$

we can replace them in Eq. (1.5) in order to obtain a more readable expression

$$W_j(x) \simeq \gamma \exp[-\alpha(x - x_j)^2] \quad (1.6)$$

these are the so-called Wannier functions and satisfy

$$\left[ -\frac{\hbar^2}{2m} \frac{d^2}{dx^2} + \frac{m\omega^2}{2}(x - aj)^2 \right] W_j(x) = E_0 W_j(x)$$

with  $E_0 = \frac{\hbar\omega}{2}$ , i.e. the GS Energy.

The other excited states are never involved due to the fact that no energy is available which allows to create excited states at  $T = 0$ . The Space-Mode Approximation consists in assuming the following field representation

$$\psi(x) \simeq \sum_j a_j W_j(x)$$

meaning that a restricted basis of states  $W_j(x)$  (i.e. the local GSs) is sufficient to describe the behavior of the system at sufficiently low T. They form a basis such that

$$(W_j(x), W_\ell(x)) = \int_0^L dx W_j^*(x) W_\ell(x) \simeq \delta_{j\ell}$$

with  $j, \ell \in [1, M]$ . We exploit the properties of functions  $W_j(x)$  to reduce  $H$  to a simpler form depending only on bosonic modes  $a_j$  and  $a_j^\dagger$ . Let us rewrite  $H$  as  $H = H_0 + U$ , where

$$H_0 = \int_0^L dx \hat{\psi}^\dagger(x) \left( -\frac{\hbar^2}{2m} \frac{\partial^2}{\partial x^2} + V_p(x) \right) \hat{\psi}(x) \quad (1.7)$$

$$U = \frac{U_0}{2} \int_0^L dx \hat{\psi}^{\dagger 2}(x) \hat{\psi}^2(x) \quad (1.8)$$

1. concerning Eq. (1.7) we find

$$\begin{aligned} H_0 &= \sum_j \sum_\ell a_j^\dagger a_\ell \int_0^L dx W_j^*(x) \left( -\frac{\hbar^2}{2m} \frac{\partial^2}{\partial x^2} + V_p(x) \right) W_\ell(x) = \\ &= \sum_j \sum_\ell a_j^\dagger a_\ell \int_0^L dx W_j^*(x) \left[ \left( -\frac{\hbar^2}{2m} \frac{\partial^2}{\partial x^2} + \frac{m\omega^2}{2} (x - a\ell)^2 \right) + \right. \\ &\quad \left. -\frac{m\omega^2}{2} (x - a\ell)^2 + V_p(x) \right] W_\ell(x) \end{aligned}$$

where we added and subtracted the Harmonic-oscillator potential. So, continuing

$$\begin{aligned} H_0 &= \sum_j \sum_\ell a_j^\dagger a_\ell \int_0^L dx W_j^*(x) \left[ E_0 - \frac{m\omega^2}{2} (x - a\ell)^2 + V_p(x) \right] W_\ell(x) = \\ &= \sum_j \sum_\ell a_j^\dagger a_\ell E_0 \int_0^L dx W_j^*(x) W_\ell(x) + \sum_j \sum_\ell a_j^\dagger a_\ell K_{j\ell} = \end{aligned}$$

$$= E_0 \sum_{\ell} a_{\ell}^{\dagger} a_{\ell} + \sum_j \sum_{\ell} a_j^{\dagger} a_{\ell} K_{j\ell}$$

with

$$K_{j\ell} = \int_0^L dx W_j^*(x) \left[ V_p(x) - \frac{m\omega^2}{2}(x - a\ell)^2 \right] W_{\ell}(x)$$

The resulting form of  $H_0$  is

$$H_0 = \sum_{\ell} (E_0 + K_{\ell,\ell}) a_{\ell}^{\dagger} a_{\ell} + \sum_{\ell} a_{\ell+1}^{\dagger} a_{\ell} K_{\ell+1,\ell} + \sum_{\ell} a_{\ell-1}^{\dagger} a_{\ell} K_{\ell-1,\ell} + \dots$$

and it can be shown that

$$K_{j\ell} \simeq v \delta_{j\ell} - v e^{-\alpha a^2 \frac{(\ell-j)^2}{2}} (\pi^2(j-\ell)^2 + (-1)^{j+\ell}) \quad (1.9)$$

This means that in the case  $j = \ell$  we have  $K_{\ell,\ell} = 0$  and, in the case we consider two adjacent minima  $K_{\ell+1,\ell} = K_{\ell-1,\ell}$ . Moreover, we have that

$$|K_{i,\ell}| \ll |K_{\ell+1,\ell}|$$

with  $i = \ell \pm 2, \ell \pm 3, \dots$ . The latter is due to the fact that the Gaussian term in (1.9) becomes stronger and stronger as we get far from the "central well".

In conclusion, Hamiltonian  $H_0$  reduces to the form:

$$H_0 = E_0 \sum_{\ell} a_{\ell}^{\dagger} a_{\ell} - |K_{\ell+1,\ell}| \sum_{\ell} (a_{\ell+1}^{\dagger} a_{\ell} + a_{\ell}^{\dagger} a_{\ell+1}) + \text{negl.} \quad (1.10)$$

Now, noticing that  $a_{\ell}^{\dagger} a_{\ell} = \hat{n}_{\ell}$  is nothing but the boson-number operator and calling  $|K_{\ell+1,\ell}| = T$ , i.e. the hopping amplitude (or tunneling amplitude), we can write

$$\boxed{H_0 = E_0 \sum_{\ell} \hat{n}_{\ell} - T \sum_{\ell} (a_{\ell+1}^{\dagger} a_{\ell} + a_{\ell}^{\dagger} a_{\ell+1})} \quad (1.11)$$

where  $\sum_{\ell} \hat{n}_{\ell}$  represents the total boson number, while the second term represents the exchange of bosons between adjacent wells and is called hopping term. In particular, considering wells  $\ell$  and  $\ell + 1$ :

$$(a_{\ell+1}^{\dagger} a_{\ell} + a_{\ell}^{\dagger} a_{\ell+1})$$

we can see how a boson is created in the state  $\ell + 1$  and destroyed in  $\ell$ , or how it is created in  $\ell$  and destroyed in  $\ell + 1$ , resulting in a perfect Hamiltonian Operator.

**Why tunneling?** Because the effect that brings the boson from  $\ell$  to  $\ell + 1$  (or viceversa) is nothing but the Tunneling Effect.

2. Now let us consider the interaction term (1.8):

$$\begin{aligned} U &= \frac{U_0}{2} \int_0^L dx \psi^{\dagger 2}(x) \psi^2(x) = \\ &= \frac{U_0}{2} \int_0^L dx \sum_i a_i^{\dagger} W_i^*(x) \sum_j a_j^{\dagger} W_j^*(x) \sum_k a_k W_k(x) \sum_l a_l W_l(x) = \\ &= \frac{U_0}{2} \sum_i \sum_j \sum_k \sum_l a_i^{\dagger} a_j^{\dagger} a_k a_l \int_0^L dx W_i(x) W_j(x) W_k(x) W_l(x) \simeq \end{aligned}$$

Remembering that  $W$  is a Gaussian, so we have the main contribution for  $i = j = k = l$ :

$$\begin{aligned} &\simeq \frac{U_0}{2} \sum_i a_i^{\dagger} a_i^{\dagger} a_i a_i \int_0^L dx W_i^4(x) \simeq \\ &\simeq \frac{U_0}{2} K_0 \sum_i \hat{n}_i (\hat{n}_i - 1) \end{aligned}$$

where

$$\begin{aligned} K_0 &= \int_0^L dx W_i^4(x) = \int_0^L dx \gamma^4 e^{-4\alpha(x-x_j)^2} = \\ &\gamma^4 \sqrt{\frac{\pi}{4\alpha}} = \end{aligned}$$

since  $\gamma^2 = \sqrt{\frac{2\alpha}{\pi}}$

$$= \frac{2\alpha}{\pi} \sqrt{\frac{\pi}{4\alpha}} = \sqrt{\frac{\alpha}{\pi}}$$

So, let us now define  $U = U_0 \sqrt{\frac{\alpha}{\pi}}$ ; the interaction term becomes

$$\boxed{U = \frac{U}{2} \sum_i \hat{n}_i (\hat{n}_i - 1)} \quad (1.12)$$

This term is a local energy: it has no zero contribution only if  $\hat{n}_i \geq 2$ . It means that we must have at least two bosons in the well in order to have a contribution from this term.

In conclusion, putting together Eq.s (1.11) and (1.12), the final form of  $H$  is:

$$\boxed{H = E_0 \sum_j a_j^{\dagger} a_j - T \sum_{\ell} (a_{\ell+1}^{\dagger} a_{\ell} + a_{\ell}^{\dagger} a_{\ell+1}) + \frac{U}{2} \sum_i \hat{n}_i (\hat{n}_i - 1)} \quad (1.13)$$

that is the so-called Bose-Hubbard Model Hamiltonian.

## 1.2.2 The BH-Model Phase Diagram

The BH-Model has been hardly studied in the last 30 years owing to the considerable interest raised by the well-known Superfluid - Mott Insulator (SF - MI) phase transition characterizing the system at zero temperature. More recently, the experimental realization of BECs and, in particular, the experimental success in constructing 1D, 2D and 3D (optical) homogeneous lattices where condensed bosons can be trapped, led to the experimental confirmation of the SF-MI transition.

Now, let us take a quite general form of the BH Hamiltonian, including a lattice dimension  $d > 1$  and the presence of external potentials

$$H_{BH} = \frac{U}{2} \sum_j \hat{n}_j(\hat{n}_j - 1) + \sum_i v_i \hat{n}_i - T \sum_{\langle i,j \rangle} (a_i^\dagger a_j + a_j^\dagger a_i) \quad (1.14)$$

where the latter represents a summation between nearest neighbours  $\langle i, j \rangle$ , while term  $\sum_i v_i \hat{n}_i$  allows one to take into account the presence of an external potential  $V(\vec{r})$  (e.g. the parabolic potential confining the condensate) by setting  $v_i = V(\vec{r}_i)$ ,  $i$  being the site at position  $\vec{r}_i$ .

To study the zero-temperature phase diagram of this model one usually refers to the free energy operator  $\hat{F} = \hat{H} - \mu \hat{N}$ , where  $\mu$  is the chemical potential. In particular, it will be the ratio between the latter and U plus the ratio between T and U to be the parameters on the axes of our phase diagram (see Fig. (1.4)).

When these parameters fall within one of the gray domains in the figure (called lobes) the system is in the Mott-Insulator phase. In this state we have the same integer number  $n$  of bosons at each site (integer filling). Notice that the total boson number is given in this case by  $N = M n$ , where  $M$  is the number of lattice sites. A finite energy cost is requested to add (subtract) a single boson to (from) any lattice site. Thus, this phase entails zero compressibility, since, at each site, the number of bosons is frozen. In this case, the dominant contribution to the Ground State is represented by the simple Fock State

$$|\vec{n}\rangle = |n, n, \dots, n\rangle \quad (1.15)$$

while other smaller contributions can be evaluated, for example, in a perturbative way. Instead, outside of the lobes, the fluid has a Superfluid character since it becomes compressible. The filling is no more integer and the expectation value  $\langle \hat{n}_i \rangle$  assumes (almost) continuous values.

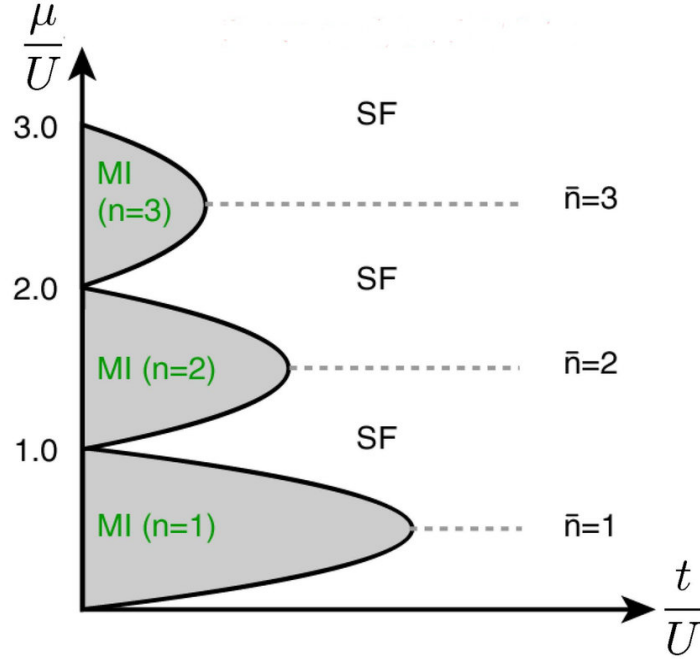


**Figure 1.4:** BH-Model Phase Diagram. The grey domains (lobes) represent the portions of the plane where the system is in the MI-phase. For each lobe, the filling is specified. Outside the domains, the system is in the SF-regime.

### 1.2.3 The Coherent-State Picture of the Bose-Hubbard Model

Let us consider the non-linear BH-Hamiltonian in a 1-dimensional lattice

$$H_{BH} = \frac{U}{2} \sum_j \hat{n}_j(\hat{n}_j - 1) - T \sum_{\langle i,j \rangle} (a_i^\dagger a_j + a_j^\dagger a_i) \quad (1.16)$$

where term  $E_0 \sum_j a_j^\dagger a_j$  has been omitted since it is a conserved quantity. Once we have this Hamiltonian, we can proceed in deriving its effective dynamics by exploiting the method based on the Time-dependent Variational Principle (TDVP) [2, 1].

#### The TDVP method

In order to see how this method works, let us begin with the Schrödinger problem

$$i \hbar \partial_t |\phi_t\rangle = \hat{H} |\phi_t\rangle$$

which we can rewrite as

$$(i \hbar \partial_t - \hat{H}) |\phi_t\rangle = 0 \quad (1.17)$$

What we have in round brackets in Eq. (1.17) is nothing more than an operator: we can therefore calculate its expectation value, that is

$$\langle \phi_t | i \hbar \partial_t - \hat{H} | \phi_t \rangle = 0. \quad (1.18)$$

This new equation is certainly satisfied by the solutions of the original Schrödinger problem, which are, moreover, the best approximation we can obtain. The latter can be shown by the TDVP.

Let us set  $|\phi\rangle = e^{i\frac{S}{\hbar}} |Z\rangle$  where  $|Z\rangle$  is a trial state that depends on the variational parameters  $z_1, z_2, \dots, z_M$ . The next step will be to replace  $|\phi\rangle$  in Eq. (1.18), obtaining

$$\begin{aligned} \langle Z | e^{-i\frac{S}{\hbar}} \left( i \hbar \frac{i}{\hbar} e^{i\frac{S}{\hbar}} S' |Z\rangle + i \hbar e^{i\frac{S}{\hbar}} \partial_t |Z\rangle - e^{i\frac{S}{\hbar}} \hat{H} |Z\rangle \right) &= \\ = -\dot{S} \langle Z | Z \rangle + i \hbar \langle Z | \partial_t | Z \rangle - \langle Z | \hat{H} | Z \rangle &= 0 \end{aligned}$$

Since  $\langle Z | Z \rangle = 1$ , this implies that

$$\dot{S} = i \hbar \langle Z | \partial_t | Z \rangle - \langle Z | \hat{H} | Z \rangle$$

So

$$S = \int_{t_1}^{t_2} dt \left( \hbar \langle Z | \partial_t | Z \rangle - \langle Z | \hat{H} | Z \rangle \right)$$

The term between round brackets can be seen as an effective Lagrangian  $\mathcal{L}(Z) = \mathcal{L}(z_1, z_2, \dots, z_3)$ . This means that  $S$  has the dimension of an Action, while  $\langle Z | \hat{H} | Z \rangle$  can be interpreted as an effective Hamiltonian. So, owing to this semiclassical trick we will be able to find the dynamical evolution of the system.

### Coherent-State Picture and TDVP method

For the  $H_{BH}$  the trial state is assumed to be [40, 48]

$$|\phi\rangle = e^{i\frac{S}{\hbar}} |Z\rangle \quad \text{with} \quad |Z\rangle = \prod_i |z_i\rangle$$

where  $|z_i\rangle$  are the Weyl-Heisenberg (or Harmonic Oscillator) Coherent States such that:

- $a_i |z_i\rangle = z_i |z_i\rangle$ ;
- given  $\Delta x = \sqrt{\langle x^2 \rangle - \langle x \rangle^2}$  and  $\Delta p = \sqrt{\langle p^2 \rangle - \langle p \rangle^2}$ , we have

$$\Delta x \Delta p = \frac{\hbar}{2}$$

i.e. they represent the minimum of the Heisenberg Uncertainty Principle.

Such Coherent States have the form

$$|z_i\rangle = e^{-\frac{|z_i|^2}{2}} \sum_{m=0}^{\infty} \frac{z_i^m}{\sqrt{m!}} |m\rangle$$

but can be expressed in the equivalent form

$$|z_i\rangle = e^{-\frac{|z_i|^2}{2}} e^{z_i a_i^\dagger} |0\rangle \quad (1.19)$$

well reproducing the initial definition

$$\begin{aligned} |z_i\rangle &= e^{-\frac{|z_i|^2}{2}} \sum_{m=0}^{\infty} \frac{z_i^m}{m!} (a_i^\dagger)^m |0\rangle = e^{-\frac{|z_i|^2}{2}} \sum_{m=0}^{\infty} \frac{z_i^m}{m!} \sqrt{m!} |0\rangle = \\ &= e^{-\frac{|z_i|^2}{2}} \sum_{m=0}^{\infty} \frac{z_i^m}{\sqrt{m!}} |m\rangle \end{aligned}$$

Notice that  $\langle\phi|\phi\rangle = \langle Z|Z\rangle = \prod_i \langle z_i|z_i\rangle = 1$  since  $\langle z_i|z_i\rangle = 1$  at each lattice site. Concerning the physical meaning of variables  $z_m$ , the so-called local order parameters, we observe that definitions

$$z_m = \langle z_m | a_m | z_m \rangle \quad z_m^* = \langle z_m | a_m^\dagger | z_m \rangle \quad (1.20)$$

lead to

$$\begin{aligned} n_m &= \langle z_m | n_m | z_m \rangle \simeq |z_m|^2 \\ e^{i\theta_m} &= \frac{z_m}{\sqrt{|z_m|^2}} \end{aligned}$$

where the latter is just the exponential form of  $z_m$  as complex value. Thus, Eqs. (1.20) provide essential informations about the system in that, at each lattice site, both the local average boson number  $n_m$  and the local phase  $\theta_m$  can be evinced from  $z_m$  (and  $z_m^*$ ).

From the Schrödinger equation one obtains

$$\mathcal{S} = \int_0^t d\tau (i \hbar \langle Z | \partial_\tau | Z \rangle - \mathcal{H}(Z)) \quad (1.21)$$

where  $\mathcal{H}(Z) = \langle Z | H | Z \rangle$ .

It can be shown, exploiting definition (1.19), that

$$\langle Z | \partial_\tau | Z \rangle = \frac{1}{2} (\dot{z}_i z_i^* - \dot{z}_i^* z_i) \quad (1.22)$$

$$\langle Z | H | Z \rangle = \frac{U}{2} \sum_j |z_j|^4 - T \sum_j (z_{j+1} z_j^* + z_{j+1}^* z_j) \quad (1.23)$$

The latter is nothing but a semiclassical form of the initial Second Quantized Hamiltonian. Instead, for what concerns the effective Lagrangian, we have

$$\mathcal{L} = \frac{i\hbar}{2} \sum_i (\dot{z}_i z_i^* - z_i^* \dot{z}_i) - \mathcal{H}(Z) \quad (1.24)$$

Then, from the two corresponding Lagrange equations

$$\frac{d}{dt} \frac{\partial \mathcal{L}}{\partial \dot{z}_i^*} - \frac{\partial \mathcal{L}}{\partial z_i^*} = 0$$

$$\frac{d}{dt} \frac{\partial \mathcal{L}}{\partial \dot{z}_i} - \frac{\partial \mathcal{L}}{\partial z_i} = 0$$

we can obtain, respectively

$$\boxed{i\hbar \dot{z}_i = U|z_i|^2 z_i - T(z_{i+1} + z_{i-1})} \quad (1.25)$$

$$i\hbar \dot{z}_i^* = U|z_i|^2 z_i^* - T(z_{i+1}^* + z_{i-1}^*) \quad (1.26)$$

which are one the h.c. of the other.

The new set of equations shows that the initial Schrödinger problem has been reformulated in a different semiclassical form, in which physical information about the system evolution is embodied in the dynamical variables  $z_m$ , the coherent-state parameters.

So, let us take the first of them (Eq. (1.25)) and call it the discrete non-linear Schrödinger equation.

## Chapter 2

# Phase Separation in $L = 2, 3$ Ring Lattices

*“From a certain temperature on, the molecules ‘condense’ without attractive forces; that is, they accumulate at zero velocity. The theory is pretty, but is there some truth in it.”*  
*Albert Einstein*

The purpose of this thesis is to investigate the case of the binary mixture in a lattice with 4 potential wells arranged in a ring. However, it is advisable, before going into the analysis of the latter, to recall the results obtained in the simplest cases (previously studied). As already mentioned in the previous chapter, the simplest cases we are referring to are those of the dimer (2 wells) and the trimer (3 wells). It is important to consider that, while the semiclassical approaches to this kind of systems are generally not problematic, their study at the purely quantum level remains a considerably difficult task and the diagonalization of quantum Hamiltonians mainly relies on the use of numerical techniques. To circumvent these difficulties, an effective analytical method has been developed, which consists in using continuous variables (CVs) to describe the dynamics of bosonic states at low energies. For completeness, we are going to revisit this method in this chapter.

## 2.1 The dimer

Bosons trapped in two potential wells can be described in a good way by the two-mode BH Hamiltonian

$$H_a = \frac{U_a}{2}(a_L^\dagger a_L^\dagger a_L a_L + a_R^\dagger a_R^\dagger a_R a_R) - T_a(a_L^\dagger a_R + a_R^\dagger a_L) \quad (2.1)$$

where  $L$  refers to the left well, while  $R$  to the right one. The boson operators  $a_L, a_L^\dagger, a_R, a_R^\dagger$  satisfy the standard commutator  $[a_k, a_k^\dagger] = 1$  with  $k = L, R$ . Parameters  $U_a$  and  $T_a$  are the boson-boson interaction and the hopping amplitude, respectively.

Therefore, if we are dealing with two species in a 2-well lattice we have to double the bosonic modes and introduce also  $b_L, b_L^\dagger, b_R, b_R^\dagger$  for species B, saying that the previous ones are for species A. In this case the Hamiltonian thus becomes

$$H = H_a + H_b + W(a_L^\dagger a_L b_L^\dagger b_L + a_R^\dagger a_R b_R^\dagger b_R) \quad (2.2)$$

where  $H_a$  and  $H_b$  are the Hamiltonian associated to the single species A and B, respectively. For what concerns  $W$ , instead, it constitutes the inter-species interaction.

The total number of bosons of each species is a conserved quantity (since  $[H, N] = [H, M] = 0$ ), so our system features two dynamical constraints

$$N = n_L + n_R = a_L^\dagger a_L + a_R^\dagger a_R \quad (2.3)$$

$$M = m_L + m_R = b_L^\dagger b_L + b_R^\dagger b_R \quad (2.4)$$

where  $n$  and  $m$  denote both the boson numbers of the two species and their number operators.

### 2.1.1 The Continuous-Variable Picture

When dealing with this kind of bosonic models a useful description can be obtained by observing that physical quantities depending on the local populations  $n_i$  and  $m_i$  (the eigenvalues of number operators  $\hat{n}_i = a_i^\dagger a_i$  and  $\hat{m}_i = b_i^\dagger b_i$ , with  $i = L, R$ ) can be reformulated in terms of continuous variables  $x_i = \frac{n_i}{N}$  representing local densities [59, 23, 34]. Notice that variable  $x_i := n_i/N$  represents a normalized boson population and is regarded as continuous in view of the fact that the total number of bosons  $N$  is assumed to be large.

Thus, for total boson number  $N = \sum_i n_i$  large enough, Fock states

$$|\vec{n}\rangle = |n_1, n_2, \dots, n_L\rangle \equiv |x_1, x_2, \dots, x_L\rangle$$

can be interpreted as functions of variables  $x_i$ , and creation and destruction processes  $n_i \rightarrow n_i \pm 1$  correspond to small variations of the type

$$|x_1, \dots, x_i \pm \epsilon, \dots, x_L\rangle$$

where  $\epsilon = \frac{1}{N} \ll 1$ .

Such an approach, in addition to simplify the energy-eigenvalue problem associated to an Hamiltonian like the one in Eq. (2.2), also leads to a new effective Hamiltonian written as a function of coordinates  $x_i$  and of the corresponding generalized momenta [49]. In particular, if we took a general multimode Hamiltonian  $\hat{H}$ , we can expand up to the second order the quantity  $\hat{H}|E\rangle$  in the corresponding eigenvalue problem

$$\hat{H}|E\rangle = E|E\rangle$$

and rewrite the latter in the CVP form

$$(-D + V)\psi_E(\vec{x}) = E\psi_E(\vec{x}) \quad (2.5)$$

where  $D$  is a generalized Laplacian, while  $V$  is an effective potential. Among the two, we are going to focus on the latter, that can be used to obtain meaningful information about the Ground-State structure as a function of the model parameters.

Notice that, in this picture, constraints such as (2.3) and (2.4) read respectively

$$\sum_{i=1}^2 x_i = 1 \quad (2.6)$$

$$\sum_{i=1}^2 y_i = 1 \quad (2.7)$$

At this point, the minimum-energy configurations can be obtained by imposing the stationarity conditions for the potential  $V$ , expressed by equations  $\frac{\partial V}{\partial x} = 0$  and  $\frac{\partial V}{\partial y} = 0$ .

What has been done in the case of the dimer was the evaluation of the solutions  $(\vec{x}, \vec{y})$  in the CVP approach, followed by the comparison of the obtained results with the exact Ground-State calculated numerically [19]. In particular, there has been a focus on the twin-species case: i.e. the case in which we have equal intra-species interactions  $U_a = U_b = U$ , equal hopping amplitudes  $T_a = T_b = T$  and the same number of bosons of both types  $N = M$  (see Fig. 2.1).

For what concerns the interaction situation, it has been considered the weakly repulsive interaction regime, the strongly repulsive one and even the attractive

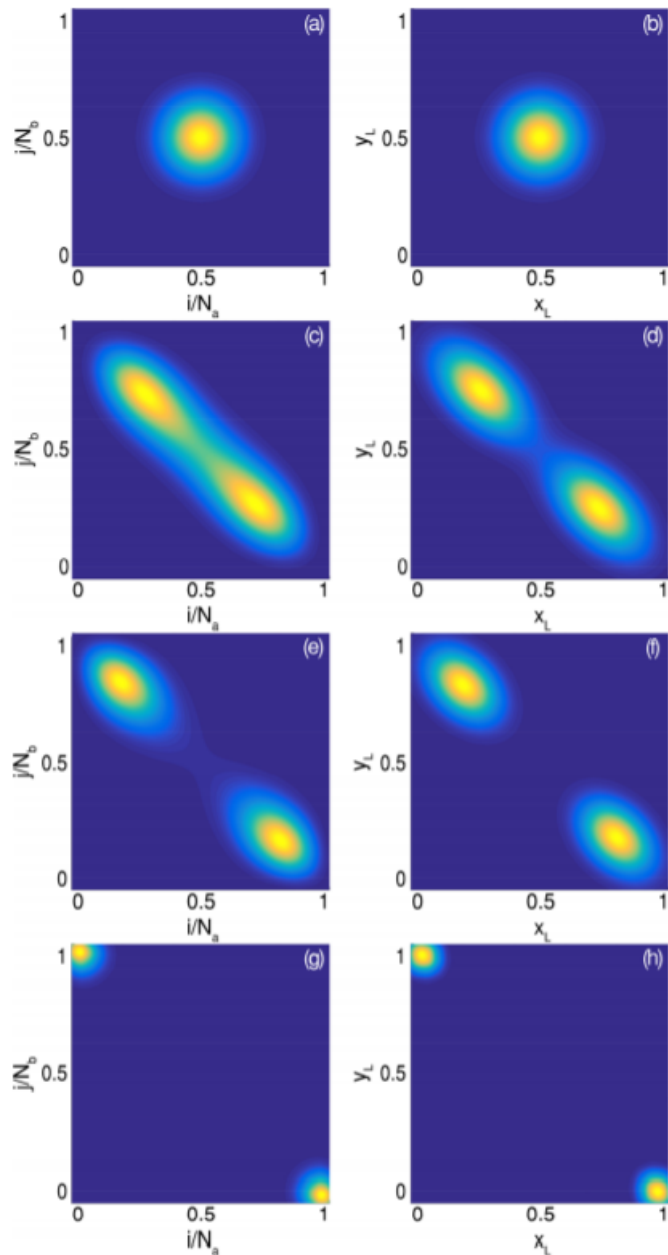


**Figure 2.1:** Probability densities of the ground state for  $U/T = 0.01$ ,  $N = M = 30$ , and (from top to bottom)  $W/T = 0.001, 0.085, 0.093, 0.170$ . Right column: probability density obtained within the CV method. Left column: probability amplitudes for the exact ground state calculated numerically.

interaction regime ( $W$  assumed negative values). It has been observed a definite macroscopic dynamical phase transition to states with localized populations as the inter-species repulsion  $W$  increased, confirmed by the numerical simulations, and a behavior with mirror symmetry in the case of attractive interaction.

In particular, Fig. 2.2 shows how the first fifteen energy levels feature a perfect symmetry between positive and negative values of the inter-species interaction.

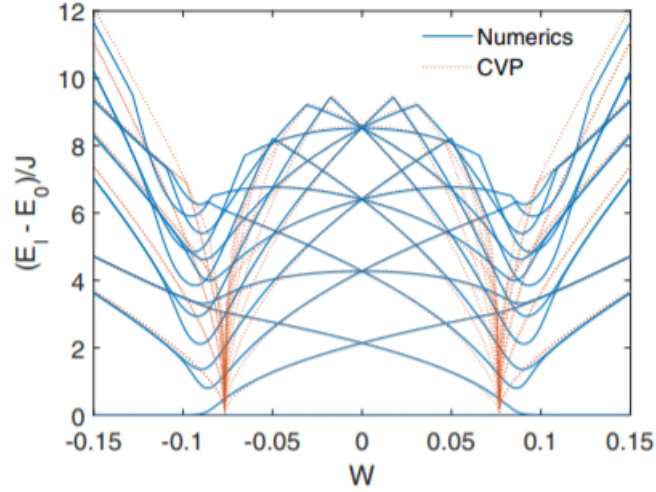


**Figure 2.2:** First 15 energy levels as a function of interspecies interaction  $W$  for intraspecies interaction  $U = 0.01$  (energy units in J ) and total boson number  $N = 60$  with  $N = M$ . The plots compare numerical results (continuous lines) with the analytical eigenvalues (dotted lines) computed within the CV method.

### 2.1.2 The Mixing-Supermixing Phase Diagram in the large populations limit

Particular attention should be paid to the attractive case ( $W < 0$ ) and the related phase diagram [55]. In fact, previous analysis has highlighted the presence of a common phase diagram for systems featuring  $L = 2$  (dimer),  $L = 3$  (trimer), and  $L = 4$  (tetramer, i.e. the case of our interest). Before continuing, however, it must be specified that in this case the analysis was carried out considering heteronuclear species, i.e. the more general case in which  $U_a \neq U_b$  and  $N \neq M$ . Moreover, we are dealing with the large-populations limit, that is when  $\frac{T_a}{U_a N} \rightarrow 0$  and  $\frac{T_b}{U_b M} \rightarrow 0$ . The latter can be regarded as a sort of thermodynamic limit according to the statistical-mechanical approach discussed in [49].

Furthermore, from now on, we are going to recast all the system parameters in only two effective ones, containing all the information about the differences between the two heteronuclear species:

$$\alpha = \frac{W}{\sqrt{U_a U_b}} \quad (2.8)$$

$$\beta = \frac{M}{N} \sqrt{\frac{U_b}{U_a}} \quad (2.9)$$

The former constitutes the ratio between the inter-species attractive coupling and the (geometric average of) the intra-species repulsions, while the latter corresponds to the degree of asymmetry between species A and species B condensates. The introduction of these new effective parameters is particularly useful, since all the important quantities concerning the system can be re-expressed as a function of them only.

So, the attractive-case phase diagram is illustrated in Fig. (2.3) and includes three phases.

1. A completely Mixed phase (labelled with "M"), delimited by  $\alpha > -1$ . The two species are uniformly distributed among the  $L$  wells and feature a perfect mixing;
2. A Partially Localized phase (labelled with "PL"), delimited by  $\alpha < -1$  and  $\beta < -\frac{1}{\alpha}$ . It is characterized by the fact that the minority species (say B) conglomerates in a soliton (that is defined as a self-reinforcing wave packet that maintains its shape while it propagates at a constant velocity), while species A occupy all the available wells, even if in a non-uniform way;
3. A Super-Mixed phase (labelled with "SM"), identified by  $\beta > -\frac{1}{\alpha}$ . In this phase the two species conglomerate in the same well (full localization), giving rise to a single soliton. The other wells remain empty.

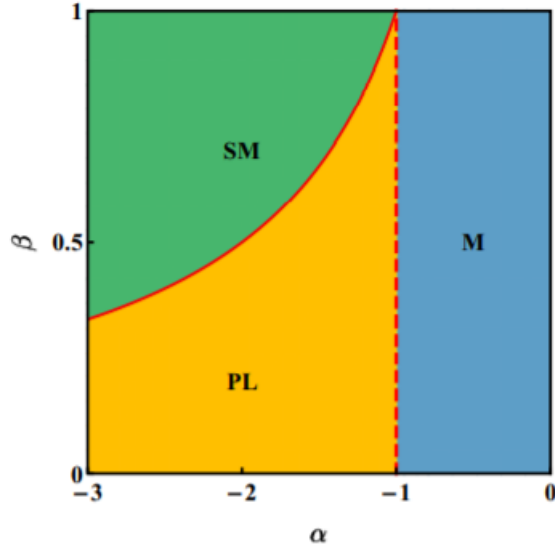


**Figure 2.3:** Phase diagram of a bosonic binary mixture characterized by attractive inter-species interaction and confined in a generic  $L$ -site potential. Phase M is the uniform and mixed one, phase PL features a soliton just in the minority species, while phase SM exhibits the presence of a supermixed soliton. Red dashed (solid) line corresponds to a phase transition where the first (second) derivative of the effective potential of the CVP, associated to this case, with respect to  $\alpha$  is discontinuous.

Thus, these three systems (dimer, trimer and tetramer) have a common path which, as the control parameters  $\alpha$  and  $\beta$  vary, leads from the uniform and mixed configuration (phase M) to the supermixed soliton (phase SM), passing through the intermediate phase (phase PL), which features partial localization. The latter, in particular, gives us the first hint of the soliton generated by the localizing effect of the inter-species attractive coupling. For this reason, we assume that the mechanism of the soliton formation is the same regardless of the value of  $L$  as well as the explicit expression of the GS configurations  $(\vec{x}, \vec{y})$  and of the effective potential  $V$  with respect to  $\alpha$  and  $\beta$  in the three phases. Furthermore, nothing prevents us from thinking that these expressions can also be valid for cases with  $L \geq 5$ . To reinforce this hypothesis, one could observe that, for any  $L$ ,  $V = V(\alpha, \beta)$  is continuous everywhere in the half-plane  $\{(\alpha, \beta) : \alpha \leq 0 \text{ and } 0 \leq \beta \leq 1\}$  and its derivatives present the same discontinuities at the same lines.

### 2.1.3 The Mixing-Demixing Phase Diagram in the large populations limit

As we have seen in Sec. 2.1.1, the repulsive interaction regime has been fully explored, but just in the case of twin species. The case of the heteronuclear species in the large populations limit has never been analyzed for what concerns the dimer. So, we are going to discover this eventuality, trying to produce also this time an outlined phase diagram, just as it has already been done in the attractive regime.

In order to do so, we are going to consider a different approach with respect to the CVP. In fact, as we have seen in Chapter 1, when one deals with a multimode boson model, he can always re-express its dynamics in terms of discrete nonlinear Schrödinger equations. Thus, let us introduce the dimer Hamiltonian derived by combining the TDVP with the coherent-state picture of the BH model:

$$H = \frac{U_a}{2} \left( \sum_{j=1}^2 |a_j|^4 \right) + \frac{U_b}{2} \left( \sum_{j=1}^2 |b_j|^4 \right) + W \left( \sum_{j=1}^2 |a_j|^2 |b_j|^2 \right) \quad (2.10)$$

where the hopping amplitudes  $T_a$  and  $T_b$  have been set equal to 0. Following the Coherent-State Picture, Hamiltonian (2.10) produces the equations of motions given by

$$\begin{aligned} i\hbar \dot{a}_j &= U_a |a_j|^2 a_j + W |b_j|^2 a_j \\ i\hbar \dot{b}_j &= U_b |b_j|^2 b_j + W |a_j|^2 b_j \end{aligned}$$

for  $j = 1, 2$ . Dynamical constraints (2.3) and (2.4) can be rewritten as

$$\begin{aligned} N &= n_1 + n_2 = |a_1|^2 + |a_2|^2 \\ M &= m_1 + m_2 = |b_1|^2 + |b_2|^2 \end{aligned}$$

The ground state belongs to the class of collective-frequency solutions (these can be shown to essentially represent the fixed points of the dynamical equations when the dynamical constraints are taken into account). By setting

$$\begin{aligned} a_j(t) &= a_j e^{\frac{-i\mu_a t}{\hbar}} \\ b_j(t) &= b_j e^{\frac{-i\mu_b t}{\hbar}} \end{aligned}$$

we get

$$\mu_a a_j = U_a |a_j|^2 a_j + W |b_j|^2 a_j \quad (2.11)$$

$$\mu_b b_j = U_b |b_j|^2 b_j + W |a_j|^2 b_j \quad (2.12)$$

for  $j = 1, 2$ .

### Uniform Solution

We start by simply assuming that  $a_j \neq 0$  and  $b_j \neq 0$ . Then the equations reduce to

$$\begin{aligned}\mu_a &= U_a|a_1|^2 + W|b_1|^2, & \mu_a &= U_a|a_2|^2 + W|b_2|^2 \\ \mu_b &= U_b|b_1|^2 + W|a_1|^2, & \mu_b &= U_b|b_2|^2 + W|a_2|^2\end{aligned}$$

which we rewrite in the form

$$\mu_a = U_a n_1 + W m_1, \quad \mu_a = U_a n_2 + W m_2 \quad (2.13)$$

$$\mu_b = U_b m_1 + W n_1, \quad \mu_b = U_b m_2 + W n_2 \quad (2.14)$$

since  $|a_j|^2 = n_j$  and  $|b_j|^2 = m_j$ . Now, combining Eqs. (2.13) and (2.14) with the dynamical constraints, we get

$$n_1 = n_2 = \frac{\mu_a U_b - \mu_b W}{U_a U_b - W^2} \quad (2.15)$$

$$m_1 = m_2 = \frac{\mu_b U_a - \mu_a W}{U_a U_b - W^2} \quad (2.16)$$

showing how this solution features twin populations. Thanks to the constraints  $N = n_1 + n_2$  and  $M = m_1 + m_2$  we discover that  $n_1 = n_2 = N/2$  and  $m_1 = m_2 = M/2$ . By replacing these values in equations (2.13) and (2.14) we are able to determine the values of  $\mu_a$  and  $\mu_b$

$$\begin{aligned}\mu_a &= U_a \frac{N}{2} + W \frac{M}{2} \\ \mu_b &= U_b \frac{M}{2} + W \frac{N}{2}\end{aligned}$$

The substitution of the expressions for  $\mu_a$  and  $\mu_b$  in (2.15) and (2.16) further validate the above results giving, as expected

$$n_j = \frac{\mu_a U_b - \mu_b W}{U_a U_b - W^2} = \frac{1}{2(U_a U_b - W^2)} (U_b(U_a N + W M) - W(U_b M + W N)) = \frac{N}{2}$$

$$m_j = \frac{\mu_b U_a - \mu_a W}{U_a U_b - W^2} = \frac{1}{2(U_a U_b - W^2)} (U_a(U_b M + W N) - W(U_a N + W M)) = \frac{M}{2}$$

for  $j = 1, 2$ .

### Solution with partial separation

In this case we assume  $a_1, a_2, b_2 \neq 0$  and  $b_1 = 0$ . Then we cannot simplify the common factors  $a_j$  and  $b_j$  occurring in the equations (2.11) and (2.12). However, by setting  $b_1 = 0$  these reduce to

$$\begin{aligned}\mu_a a_1 &= U_a |a_1|^2 a_1, & \mu_a a_2 &= U_a |a_2|^2 a_2 + W |b_2|^2 a_2 \\ 0 &= 0, & \mu_b b_2 &= U_b |b_2|^2 b_2 + W |a_2|^2 b_2\end{aligned}$$

showing how only three equations determine the solution. The equations that survive can be reduced to

$$\mu_a = U_a n_1 \tag{2.17}$$

$$\mu_a = U_a n_2 + W m_2 \tag{2.18}$$

$$\mu_b = U_b m_2 + W n_2 \tag{2.19}$$

This example shows how new solutions can emerge by considering the original version of the equation for  $a_j$  and  $b_j$  and introducing the on-site depletion condition  $b_1 = 0$  (other four solutions can be found with this approach, changing the species label or the site one). Let us determine its explicit form. Since  $m_1 = 0$  then  $M = m_1 + m_2 = m_2$ , equations (2.17), (2.18) and (2.19) become

$$\mu_a = U_a n_1 \tag{2.20}$$

$$\mu_a = U_a n_2 + W M \tag{2.21}$$

$$\mu_b = U_b M + W n_2 \tag{2.22}$$

Thanks to the constraint  $N = n_1 + n_2$ , the first two equations give

$$U_a n_1 = U_a n_2 + W M \rightarrow U_a n_1 = U_a (N - n_1) + W M \rightarrow n_1 = \frac{N}{2} + \frac{W M}{2 U_a}$$

Then  $n_2$ ,  $\mu_a$  and  $\mu_b$  are easily found to be

$$n_2 = N - n_1 = \frac{N}{2} - \frac{W M}{2 U_a}$$

$$\mu_a = \frac{N U_a - W M}{2}$$

$$\mu_b = \frac{NW}{2} + MU_b \left( 1 - \frac{W^2}{2U_a U_b} \right)$$

Now, introducing also in this case the effective dimensionless parameters (2.8) and (2.9), we get

$$n_1 = \frac{N}{2} (1 + \alpha\beta) \quad (2.23)$$

$$n_2 = \frac{N}{2} (1 - \alpha\beta) \quad (2.24)$$

and

$$\mu_a = \frac{NU_a}{2} (1 + \alpha\beta) \quad (2.25)$$

$$\mu_b = MU_b \left( \frac{\alpha}{2\beta} + 1 - \frac{\alpha^2}{2} \right) \quad (2.26)$$

Interestingly, due to the fact that necessarily  $n_2 \geq 0$ , then the expression for  $n_2$  is valid only for  $\alpha\beta \leq 1$ , i.e. for  $\beta \leq \frac{1}{\alpha}$ .

### Solution with complete separation

In this case we assume  $a_1, b_2 \neq 0$  and  $a_2 = b_1 = 0$ . Equations (2.11) and (2.12) reduce to

$$\begin{aligned} \mu_a a_1 &= U_a |a_1|^2 a_1, & 0 &= 0 \\ 0 &= 0, & \mu_b b_2 &= U_b |b_2|^2 b_2 \end{aligned}$$

The solution is trivial. The two constraints entail

$$n_1 = N, \quad m_2 = M \quad \text{in addition to} \quad n_2 = m_1 = 0$$

and one has  $\mu_a = U_a N$  and  $\mu_b = U_b M$ . Interestingly, for  $\beta \rightarrow \left(\frac{1}{\alpha}\right)^-$ , the population formulas (2.23) and (2.24) give

$$n_1 = \frac{N}{2} (1 + \alpha\beta) = 1 \quad (2.27)$$

$$n_2 = \frac{N}{2} (1 - \alpha\beta) = 0 \quad (2.28)$$

which perfectly match the solution featuring complete space separation.

### Energy evaluation

Now that the results associated with the various configurations have been found, we can proceed to calculate the value of the Hamiltonian (2.10) as a function of these solutions. We will then proceed to compare these values (also taking into consideration the validity ranges of the solutions on the plane  $(\alpha, \beta)$ ), in order to define where the found configurations actually minimize the energy. Let us start from the uniform configuration; the Hamiltonian evaluated in this case reads

$$H_1 \left( \frac{N}{2}, \frac{N}{2}, \frac{M}{2}, \frac{M}{2} \right) = \frac{N^2 U_a}{4} + \frac{M^2 U_b}{4} + \frac{MNW}{2} \quad (2.29)$$

The latter can be rewritten as a function of  $\alpha$  and  $\beta$  only. Indeed, collecting the factor  $N^2 U_a$ , we get

$$H_1 = N^2 U_a \left( \frac{1}{4} + \frac{1}{4} \frac{M^2 U_b}{N^2 U_a} + \frac{1}{2} \frac{MW}{NU_a} \right)$$

where we can recognize respectively

$$\frac{M^2 U_b}{N^2 U_a} = \beta^2$$

$$\frac{MW}{NU_a} = \alpha\beta$$

So, Eq. (2.29) becomes

$$H_1 = \frac{1}{4} (1 + \beta^2 + 2\alpha\beta) \quad (2.30)$$

where the overall factor  $N^2 U_a$  has been omitted since it is positive for sure and, so, will not affect the sign of  $H_1$ .

Similarly, switching to the energy of the solution with partial delocalization, one can find

$$H_2 \left( \frac{1}{2} N (\alpha\beta + 1), \frac{1}{2} N (1 - \alpha\beta), 0, M \right) = \quad (2.31)$$

$$\frac{1}{4} \left( N^2 (\alpha^2 \beta^2 + 1) U_a + 2M (MU_b + NW(1 - \alpha\beta)) \right)$$

that can be rewritten in term of  $\alpha$  and  $\beta$  as

$$H_2 = \frac{1}{4} \left( -\alpha^2 \beta^2 + 2\alpha\beta + 2\beta^2 + 1 \right) \quad (2.32)$$

Finally, in the fully demixed phase we obtain

$$H_3(N, 0, 0, M) = \frac{N^2 U_a}{2} + \frac{M^2 U_b}{2} \quad (2.33)$$

that, expressed as a function of  $\alpha$  and  $\beta$ , becomes

$$H_3 = \frac{1}{2}(1 + \beta^2) \quad (2.34)$$

At this point, comparing the results we found, we are able to identify the positions of the three phases on the  $(\alpha, \beta)$  plane and find, in such a way, the Mixing-Demixing Phase Diagram of the dimer (see Fig. 2.4)

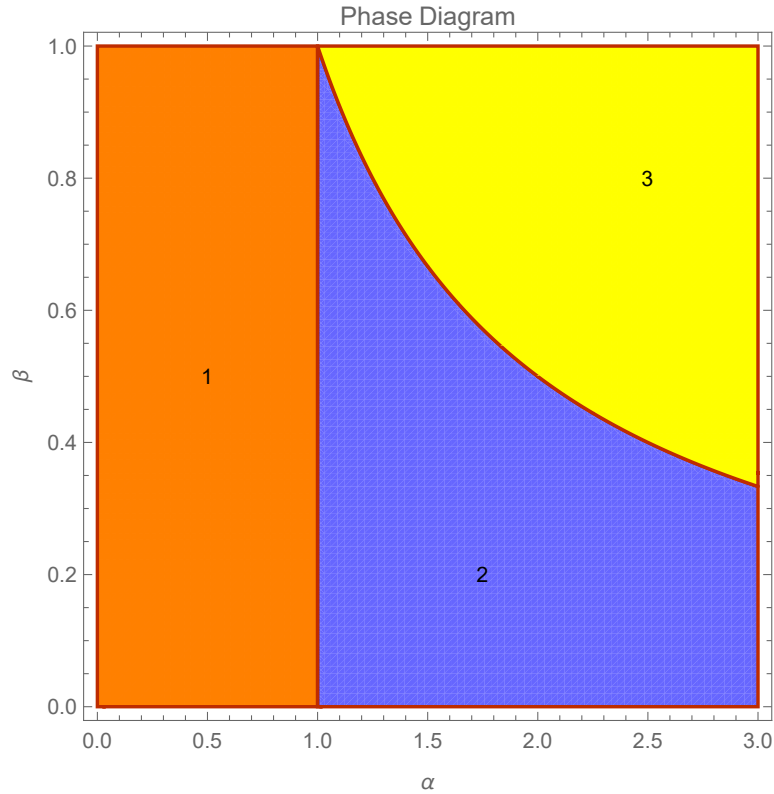


**Figure 2.4:** The Mixing-Demixing Phase Diagram of a binary mixture in a dimer. Each of the three phases corresponds to a different functional relationship between the minimum-energy configuration and the effective model parameters  $\alpha$  and  $\beta$ . Each phase has been labelled with the same number used to label the Hamiltonian in the relevant configuration.

Let us examine how such phases are delimited:

1. Phase 1 (fully mixed) is delimited by  $\alpha < 1$  and it is characterized by a uniform distribution of the two species among the two wells;

2. Phase 2 (partially demixed) is delimited by  $\alpha > 1$  and  $\beta < \frac{1}{\alpha}$ . In this case, the minority species (say B) occupy a single well, while the other one (say A) spreads in both wells, but in different proportion;
3. Phase 3 (fully demixed) is delimited by  $\beta > \frac{1}{\alpha}$ . In this case the two species are completely delocalized: the first in a well and the second in the other well.

It is worth noticing that, for  $\beta = 1$ , that corresponds to the twin species case, phase 2 (the one characterized by partial demixing) reduces to a single point, in perfect agreement for what was found in previous works [19]. It is the increasing asymmetry between the two condensates that lead the creation of an intermediate phase and its subsequent enlargement as  $\beta$  decreases.

Moreover, we can notice also that this phase diagram is the mirror image of the one in Fig. (2.3). Not surprisingly, we had already mentioned the mirror symmetry between the energy levels relevant to positive and negative values of the inter-species interaction  $W$  (so also of  $\alpha$ ), so we could expect this result. However, even if the attractive-case phase diagram was valid for  $L = 2, 3, 4$ , the one we have just found is exclusively related to the dimer and, as we will see, the repulsive interaction regime brings with it more and more unexpected and less trivial phenomena as  $L$  increases.

## 2.2 The trimer

Passing to the case of the trimer (three-well potential equipped with PBC), obviously we are going to consider directly the inter-species repulsive regime ( $W > 0$ ) since the attractive-regime phase diagram (2.3) is valid also for  $L = 3$ . At first, the study of phase-separation mechanism has been extended to the ring-trimer geometry only in the simple case of twin species [61], i.e. species featuring the same Hopping amplitude  $T$ , the same intra-species interaction  $U$ , and the same number of atoms  $N$ . Despite its simplicity, the model that was developed had already shown a non-trivial phenomenology, marked by the presence of an unexpected intermediate phase which is in between a fully mixed and a completely demixed phase. After that, steps forward have been made by introducing asymmetries between species A and species B in the system, i.e. considering different numbers of particles  $N \neq M$ , different on-site interactions  $U_a \neq U_b$  and different Hopping parameters  $T_a \neq T_b$ .

The system, also in this case, can be described by the Bose-Hubbard Hamiltonian

$$H = \frac{U_a}{2} \sum_{j=1}^3 n_j (n_j - 1) + \frac{U_b}{2} \sum_{j=1}^3 m_j (m_j - 1) + W \sum_{j=1}^3 n_j m_j + \quad (2.35)$$

$$-T_a \sum_{j=1}^3 (a_{j+1}^\dagger a_j + a_j^\dagger a_{j+1}) - T_b \sum_{j=1}^3 (b_{j+1}^\dagger b_j + b_j^\dagger b_{j+1})$$

where operators  $a_j, a_j^\dagger, b_j, b_j^\dagger$  destroy and create bosons of species A or B, respectively, in site  $j \in [1,2,3]$ . The bosonic character of these operators, as we have already seen in the case of the dimer, is enforced by standard commutation relations, i.e.

$$\begin{aligned} [a_i, a_j^\dagger] &= \delta_{ij} = [b_i, b_j^\dagger] \\ [a_i, b_j^\dagger] &= 0 \end{aligned}$$

After introducing number operators  $n_j = a_j^\dagger a_j$  and  $m_j = b_j^\dagger b_j$ , one can observe that the total numbers of bosons of each species ( $N = \sum_j n_j$  and  $M = \sum_j m_j$  respectively) constitute two independent conserved quantities, namely  $[N, H] = [M, H] = 0$ . Also in this case, has been exploited the CVP method, resorting to the replacement of the inherently discrete quantum numbers associated to the Fock-state basis with continuous variables. As we observed in subsection 2.1.1, this semi-classical approximation scheme allows one to derive an effective semi-classical Hamiltonian  $H_{eff}$  which well reproduces the low-energy physics of the original quantum model. As we have already seen, for the search of the GS we need only one of the two elements that make up  $H_{eff}$ : the effective potential  $V$ , that in the case of the trimer reads

$$\begin{aligned} V &= -2NT_a (\sqrt{x_1 x_2} + \sqrt{x_2 x_3} + \sqrt{x_3 x_1}) - 2MT_b (\sqrt{y_1 y_2} + \sqrt{y_2 y_3} + \sqrt{y_3 y_1}) + \\ &+ \frac{U_a N^2}{2} (x_1^2 + x_2^2 + x_3^2) + \frac{U_b M^2}{2} (y_1^2 + y_2^2 + y_3^2) + WMN(x_1 y_1 + x_2 y_2 + x_3 y_3) \end{aligned} \quad (2.36)$$

For what concerns the two constraints, in this approach they become

$$\sum_{j=1}^3 x_j = 1 \quad (2.37)$$

$$\sum_{j=1}^3 y_j = 1. \quad (2.38)$$

We discover that, once again, the Ground-State properties of a bosonic binary mixture in a L-ring lattice (in this case with  $L = 3$ ) can be conveniently represented by means of a two-dimensional phase diagram which is, in turn, spanned by the two specific effective variables  $\alpha$  and  $\beta$ , representing functions of the original-model parameters (see Eqs. (2.8) and (2.9)). As usual, each phase features a characteristic boson-population distribution, which results in a different degree of mixing and in a different expression of the GS energy.

### 2.2.1 Phase Diagram in the large population limit

Placing ourselves within the limit of large population, i.e. considering  $\frac{T_a}{U_a N} \rightarrow 0$  and  $\frac{T_b}{U_b M} \rightarrow 0$  (so we can regard the hopping amplitudes as negligible), four well-defined phases come to light (see Fig. (2.5)). More specifically, in this limit the effective potential (2.36) reduces to

$$V = \frac{U_a N^2}{2}(x_1^2 + x_2^2 + x_3^2) + \frac{U_b M^2}{2}(y_1^2 + y_2^2 + y_3^2) + WMN(x_1 y_1 + x_2 y_2 + x_3 y_3) \quad (2.39)$$

that can be rescaled as

$$V = \frac{1}{2}(x_1^2 + x_2^2 + x_3^2) + \frac{U_b M^2}{2U_a N^2}(y_1^2 + y_2^2 + y_3^2) + \frac{WM}{U_a N}(x_1 y_1 + x_2 y_2 + x_3 y_3). \quad (2.40)$$

The last expression can be further simplified if one notices that

$$\frac{U_b M^2}{U_a N^2} = \beta^2$$

$$\frac{WM}{U_a N} = \alpha\beta.$$

Thus, finally, we obtain

$$V = \frac{1}{2}(x_1^2 + x_2^2 + x_3^2) + \frac{\beta^2}{2}(y_1^2 + y_2^2 + y_3^2) + \alpha\beta(x_1 y_1 + x_2 y_2 + x_3 y_3) \quad (2.41)$$

In each phase, the minimum-energy configuration is the one that minimizes effective potential (2.41). The latter has been found by means of an exhaustive exploration of the polytope-like domain of such function (for a clear explanation of how this method works see [61]) and can be presented as:

- Phase 1: (colored in blue) is characterized by a uniform distribution among the three wells, i.e.  $x_j = y_j = 1/3$  for  $j = 1, 2, 3$ . In this phase, being  $\alpha < 1$ , the inter-species repulsion is too small to cause spatial separation;
- Phase 2: (colored in orange) is delimited by  $1 < \alpha < 2\beta$ . It occurs for intermediate values of  $\alpha$  and not-too asymmetric species. In this region, one has complete demixing in two wells and mixing in the remaining one;
- Phase 3: (colored in purple) is delimited by  $\frac{1}{2\alpha} < \beta < \frac{\alpha}{2}$ . It occurs for high values of  $\alpha$  and not-too asymmetric species. The characteristic of this phase is that one species clots in one site, while the other spreads the remaining two, causing the complete demixing of the two condensates;

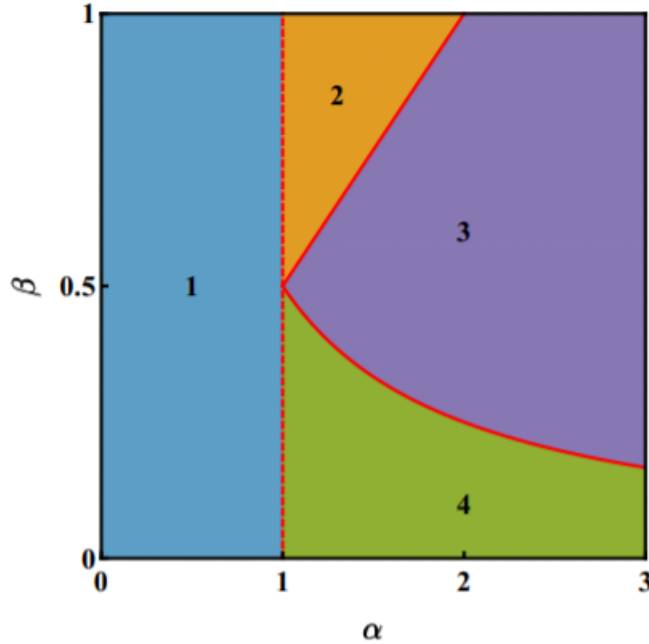


**Figure 2.5:** Phase diagram of a binary mixture in a ring trimer. Each of the four phases is related to a different functional relationship between the minimum-energy configuration and effective model parameters  $\alpha$  and  $\beta$ . This behaviour has a direct impact on the mixing properties of the system and on its GS energy. Red dashed (solid) line represents a mixing-demixing transition across which the components  $x_j$  and  $y_j$  of the minimum-energy configuration feature a jump discontinuity (are continuous). The plot has been obtained by means of a fully-analytic minimization of potential (2.41) under the constraints (2.37) and (2.38).

- Phase 4: (colored in green) is delimited by  $\alpha > 1$  and  $\beta < \frac{1}{2\alpha}$ . It occurs for high values of  $\alpha$  and sufficiently asymmetric species. The characteristic of this phase is that one species clots in one site (the one in the minority), while the other spreads in all three sites, even if in different proportions.

Concerning phases 2, 3 and 4, we remark that, due to the  $Z_3$  symmetry of the system, they are not unique and that other isoenergetic configurations can be obtained by cyclic permutations of site indexes. The nature of the mixing-demixing transitions has been highlighted in diagram (2.5) with red dashed lines in the case of jump discontinuities, while with solid red lines in the case of continuous transitions.

## 2.2.2 Phases and Degree of Mixing

A good indicator for the investigation of the criticalities of the system, without resorting to the representation of the overall minimizing configuration  $(\vec{x}, \vec{y})$ , turned out to be the Entropy of Mixing. The latter is able to quantify the degree of mixing of two different species in discretized domains. At first, it was introduced in the context of macromolecular simulations [10], while recently it has been introduced in the world of ultracold atoms in order to investigate the link between chaotic dynamical regimes and mixing properties of a bosonic binary mixture in a ring trimer [61].

Therefore, given a certain minimum-energy configuration, the Mixing Entropy associated with it is defined as

$$S_{mix} = -\frac{1}{2} \sum_{j=1}^3 \left( x_j \ln \frac{x_j}{x_j + y_j} + y_j \ln \frac{y_j}{x_j + y_j} \right) \quad (2.42)$$

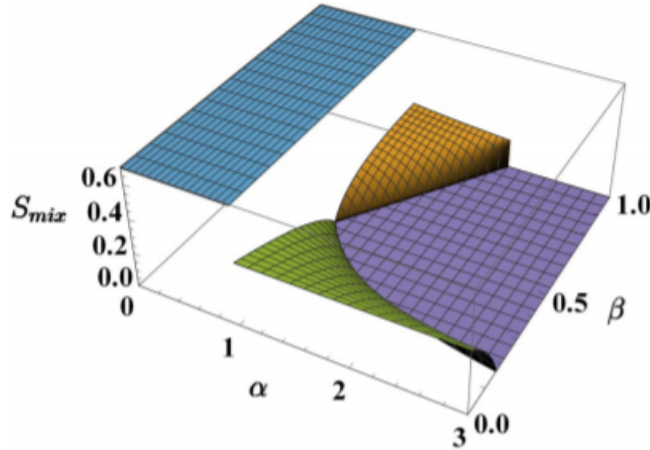


**Figure 2.6:** Entropy of mixing,  $S_{mix}$ , in the four phases. Phase 1 (in blue) features perfect mixing and  $S_{mix}$  takes the biggest possible value, i.e.  $\log 2 \approx 0.69$ . Conversely, phase 3 (in purple) features perfect demixing and  $S_{mix}$  is therefore zero.

As we can see in Fig. (2.6),  $S_{mix}$  is zero in phase 3 (complete demixing) while achieves the maximum possible value,  $\log 2 \approx 0.69$  in phase 1 (perfect mixing). It is in this figure of  $S_{mix}$ , plotted as a function of model parameters  $\alpha$  and  $\beta$ , that all the criticalities exhibited by the minimum-energy configuration are clearly visible; in fact, it is discontinuous at transition 1-2 and 1-3 while it is continuous at transitions 2-3 (apart from the special case  $\beta = 1$ ) and 3-4. The special case is due to the fact that, in the case of perfectly symmetric species,  $\beta = 1$ , the system gains

an additional symmetry (consisting in the interchangeability of species' labels in Eq. (2.42) and a further discontinuity at transition 2–3 appears. The twin-species limit, widely discussed in [61], therefore features a qualitatively different critical behavior. For all these reason, it constitutes a valid indicator to capture the occurrence of mixing-demixing transitions.

Such an indicator can also be used to investigate the effects of moving away from the limit of large populations, i.e. when one goes to consider ratios  $\frac{T_a}{U_a N}$  and  $\frac{T_b}{U_b M}$  as finite. This is equivalent to deal with systems with limited numbers of atoms and featuring non-vanishing hopping terms. In this regime, all the phases previously found are still recognizable, even if they get hazy and deformed.

The effects of non-negligible hopping terms can be summarized as follows:

- The minimum-energy configuration  $(\vec{x}, \vec{y})$ , regarded as a function of model parameters  $\alpha \in (0, 3)$  and  $\beta \in (0, 1)$ , is continuous and, consequently, so is the entropy  $S_{mix}$  (comparing Figs (2.6) and (2.7), one can notice that the jump discontinuities are replaced by smooth junctions);
- The completely-mixed phase is favored by the presence of non-negligible hopping amplitudes, its boundary being given by the inequality

$$\alpha < \sqrt{\left(1 + \frac{9}{2} \frac{T_a}{U_a N}\right) \left(1 + \frac{9}{2} \frac{T_b}{U_b M}\right)} \quad (2.43)$$

The latter corresponds to the condition under which the Hessian matrix associated to effective potential (2.41) (and evaluated for  $x_j = y_j = 1/3$ , with  $j = 1, 2, 3$ ) is positive definite. Moving away from the large-populations limit, the right-hand side of Eq. (2.43) rises above the value 1, thus determining an enlargement of phase 1 at the expenses of the phases next to it (see the expansion of the blue region in Fig. (2.7) moving from the panel at left to the panel at right);

- As one can intuitively imagine, the perfectly demixed phase is hindered by the presence of hopping processes between the wells and therefore tends to occur for higher values of  $\alpha$  (see the constriction of the purple region in Fig. (2.7) moving from the left panel to the right panel);
- Remarkably, increasing the hopping amplitudes, phase 4 not only enlarges, but overruns the  $\beta > 1/2$  region, squashing and shrinking phases 2 and 3 (moving from the left to the right panel of Fig. (2.7), one can see that the green phase expands at the expenses of the regions colored in purple and orange).

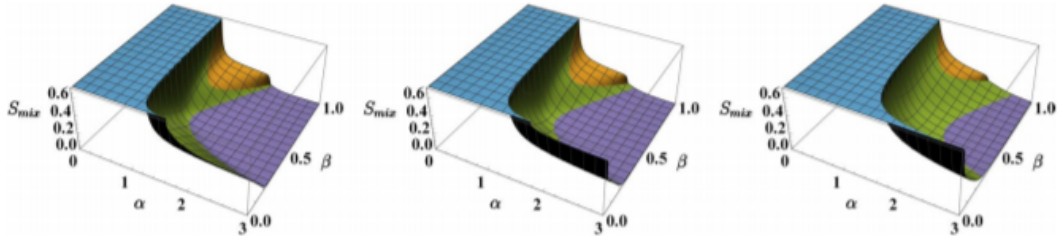


**Figure 2.7:** Mixing Entropy associated to the configurations  $(\vec{x}, \vec{y})$  which minimize effective potential (2.41) sweeping model parameters  $\alpha$  and  $\beta$ . The following values/intervals have been chosen:  $U_a = U_b = 1$ ,  $N = 15$ ,  $M \in [0, 15] \rightarrow \beta \in [0, 1]$ ,  $W \in [0, 3] \rightarrow \alpha \in [0, 3]$ ,  $T_a = T_b = T$ , where  $T = 0.1, 0.2, 0.5$  in the left, central and right panel respectively. Colors have been employed as a guide to the eye: blue is used when  $S_{mix} = \log 2$ , purple when  $S_{mix} < 0.05$ , green for all intermediate values except the domain corresponding to phase 2 and therefore colored in orange.

## Chapter 3

# The Ground State in the large-population limit

*“Physics is really nothing more than a search for ultimate simplicity, but so far all we have is a kind of elegant messiness.”*  
Bill Bryson

The time has now come to get to the heart of the purpose of this thesis: the 4-well ring. In this chapter we are going to delve into hitherto unexplored waters, facing something completely new. In fact, as regards the binary mixture in 4 potential wells, equipped with PBC, only forecasts had been made up to now and only in the case of twin species ( $U_a = U_b = U$ ,  $T_a = T_b = T$ ,  $N = M$ ) [61]. The CVP approach has been applied to a generalization of effective potential (2.36) which, in the case of vanishing tunnelling and at the transition point  $W/U = 1$  (that is,  $\alpha = 1$ ), can be shown to be minimized by any macroscopic configuration of the type  $y_j = \frac{1}{2} - x_j$ , with  $j = 1, 2, 3, 4$  (four of them are shown in Fig. (3.1)). As soon as  $W/U$  gets larger than 1, the degeneracy of these solutions disappear and just one of them survives.

What we are going to do now is to investigate not only what happens next, but we will directly deal with the asymmetric-species case. To this end, we are not going to use the CVP anymore; instead we will approach the 4-well Hamiltonian in the Coherent-State Variational Picture (see subsection 1.2.3). This analysis constitutes a first answer to the question of what happens to the phase separation mechanism in rings having an even or an odd number of sites: does the parity of  $L$  influence the behaviour of these kind of systems? Should we expect that the case with  $L = 4$  is more similar to the dimer, than to the trimer? So let's go into the chapter, trying to answer these questions.

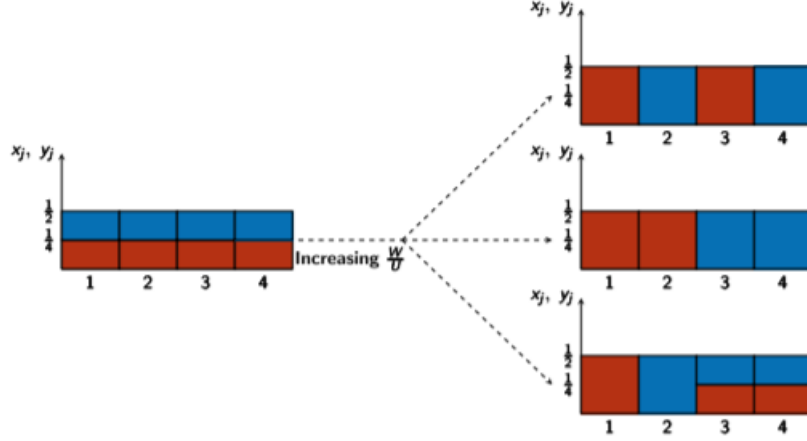


**Figure 3.1:** Possible phase-separation mechanisms for a binary mixture in a 4-well potential with PBC. Blue (red) color corresponds to species A (B). On the left, the fully mixed configurations is depicted. On the right, some examples of demixed configurations (from top to bottom: complete demixing with emulsion-like structure, complete demixing with well separated structure, and partial demixing). Left panel corresponds to  $W/U < 1$ , right panels to  $W/U = 1$ .  $T/U = 0$  has been chosen for all plots.

### 3.1 The Coherent-State Variational Picture

Let us start to deal with the case with four potential wells (to which we can refer also as "tetramer"): the model Hamiltonian of the tetramer derived by combining the TDVP with the coherent-state picture of the BH model reads

$$\begin{aligned}
 H = & \frac{U_a}{2} \left( \sum_j |a_j|^4 \right) + \frac{U_b}{2} \left( \sum_j |b_j|^4 \right) + W \left( \sum_j |a_j|^2 |b_j|^2 \right) \\
 & - T_a \left( \sum_{j=1}^4 a_j a_{j+1}^* + a_{j+1} a_j^* \right) - T_b \left( \sum_{j=1}^4 b_j b_{j+1}^* + b_{j+1} b_j^* \right)
 \end{aligned} \tag{3.1}$$

so, finding the corresponding effective Lagrangian, we can write the discrete non-linear Schrodinger equations related to the problem:

$$i\hbar \dot{a}_j = U_a |a_j|^2 a_j + W |b_j|^2 a_j - T_a (a_{j+1} + a_{j-1})$$

$$i\hbar \dot{b}_j = U_b |b_j|^2 b_j + W |a_j|^2 b_j - T_b (b_{j+1} + b_{j-1})$$

for  $j = 1, 2, 3, 4$ .

Since the number of particles of both species is fixed and

$$\begin{aligned} n_j &= |a_j|^2 \\ m_j &= |b_j|^2 \end{aligned}$$

the system features the following dynamical constraints

$$N_a = N = n_1 + n_2 + n_3 + n_4 = |a_1|^2 + |a_2|^2 + |a_3|^2 + |a_4|^2 \quad (3.2)$$

$$N_b = M = m_1 + m_2 + m_3 + m_4 = |b_1|^2 + |b_2|^2 + |b_3|^2 + |b_4|^2 \quad (3.3)$$

The ground state belongs to the class of collective-frequency solutions (these can be shown to essentially represent the fixed points of the dynamical equations when the dynamical constraints (3.2) and (3.3) are taken into account). By setting

$$\begin{aligned} a_j(t) &= a_j e^{\frac{-i\mu_a t}{\hbar}} \\ b_j(t) &= b_j e^{\frac{-i\mu_b t}{\hbar}} \end{aligned}$$

we can write

$$\begin{aligned} \mu_a a_j &= U_a |a_j|^2 a_j + W |b_j|^2 a_j - T_a (a_{j+1} + a_{j-1}) \\ \mu_b b_j &= U_b |b_j|^2 b_j + W |a_j|^2 b_j - T_b (b_{j+1} + b_{j-1}) \end{aligned}$$

for  $j = 1, 2, 3, 4$ .

### 3.1.1 Solutions for $T_a = T_b = 0$

First of all, let us place ourselves in the case in which the hopping parameters ( $T_a, T_b$ ) are set equal to zero. Obviously, the last terms of our equations disappear and we get

$$\begin{aligned} \mu_a a_j &= U_a |a_j|^2 a_j + W |b_j|^2 a_j \\ \mu_b b_j &= U_b |b_j|^2 b_j + W |a_j|^2 b_j \end{aligned}$$

for  $j = 1, 2, 3, 4$ . Considering the presence of the four potential wells, we can try to guess which are the most probable configurations, as well as the most trivial ones: the completely mixed configuration and the completely demixed one. To do this, the partially demixed phases already found in the case of the dimer and trimer can be useful (check out Chapter 2): we can take inspiration from the latter in order to create our hypotheses for the possible intermediate phases of the tetramer. In the next pages, all the most reasonable configurations taken into account are represented, starting from the mixed one, then all the hypotheses for the partially demixed ones and, finally, two hypotheses for the completely demixed phase. Unlike the cases with  $L = 2, 3$ , the lattice with four wells provides the first case where more than one completely demixed phase can be guessed. Bosons of species A and B are represented in Cyan and Pink respectively.

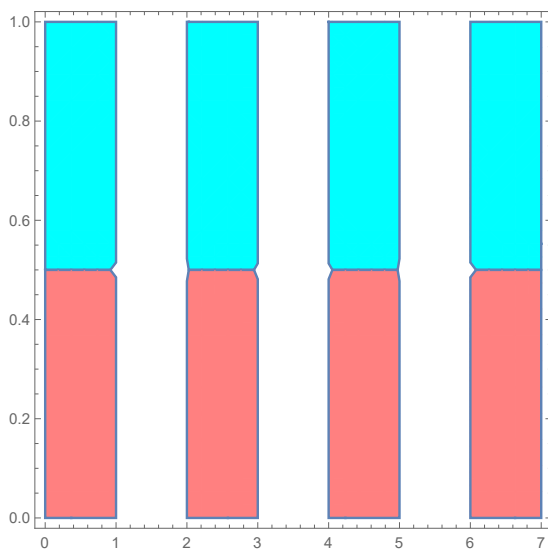


**Figure 3.2:** Case 1: Mixed (Uniform) phase.

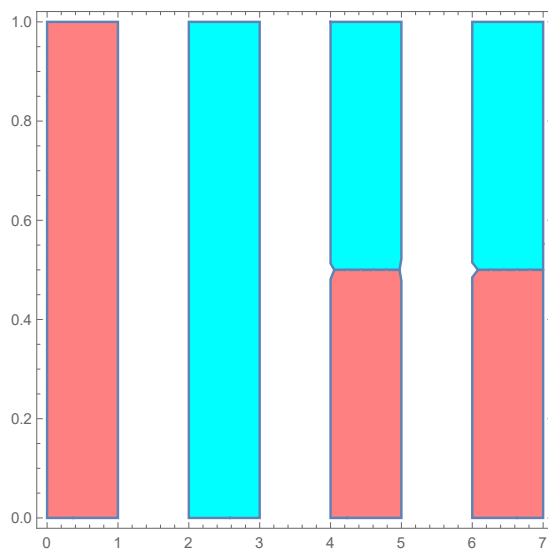


**Figure 3.3:** Case 2: Partially demixed phase that recalls the trimer's phase 2. We can call this one the "half-demixed phase".

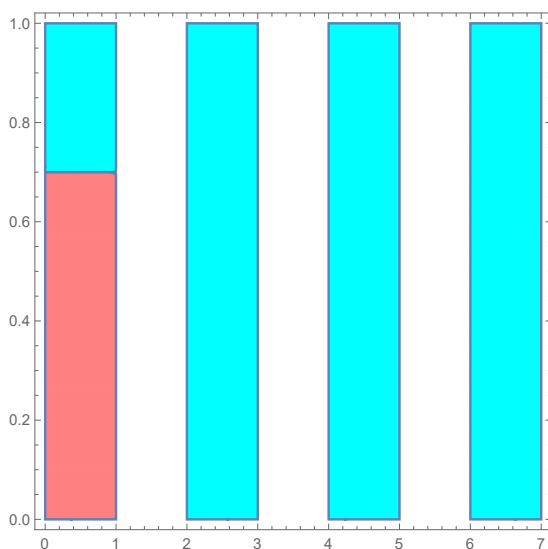


**Figure 3.4:** Case 3: Partially demixed phase that recalls the trimer's phase 4. We can call this one "phase with mixing in a single well".

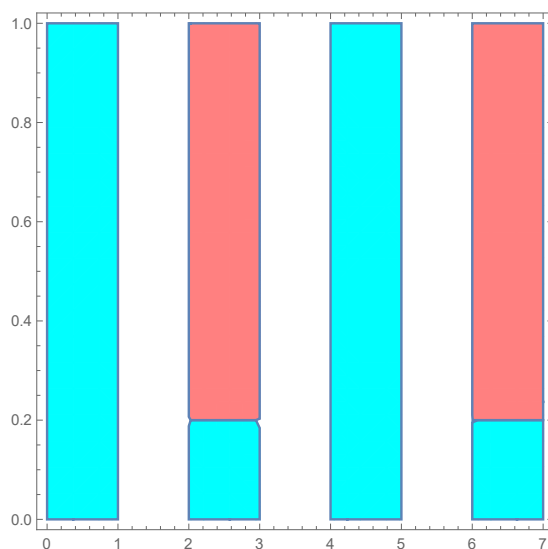


**Figure 3.5:** Case 4: Partially demixed phase that recalls the dimer's phase 2; let's call it the "partially demixed double dimer".

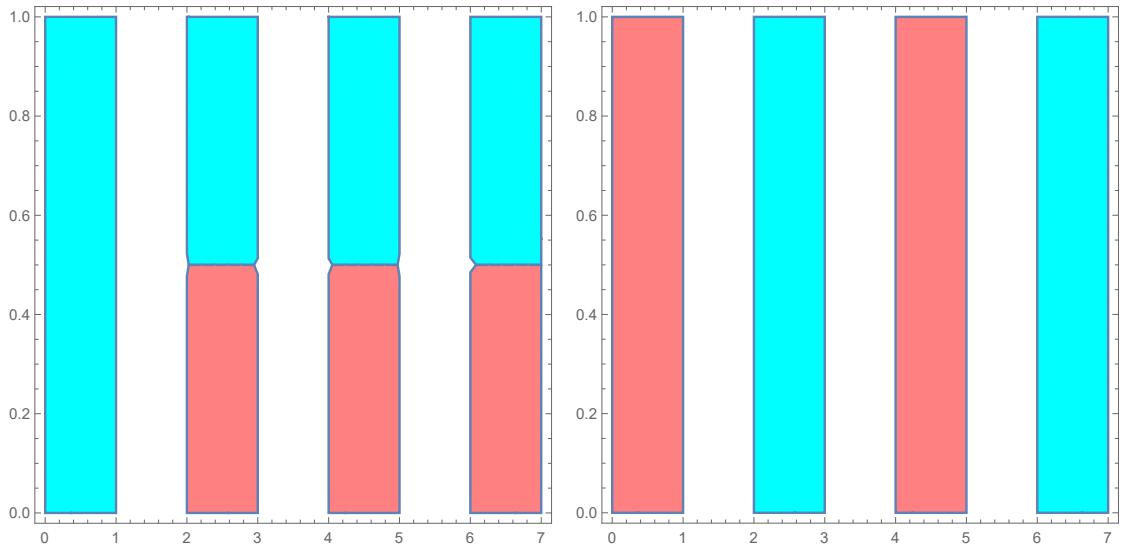


**Figure 3.6:** Case 5: Partially demixed phase consisting in the union of a filled well and a trimer in uniform configuration: a totally new guess. We can call this one the "quasi-uniform phase".

**Figure 3.7:** Case 6: Completely demixed phase that recalls the dimer one. Let's call it "dimer-like".

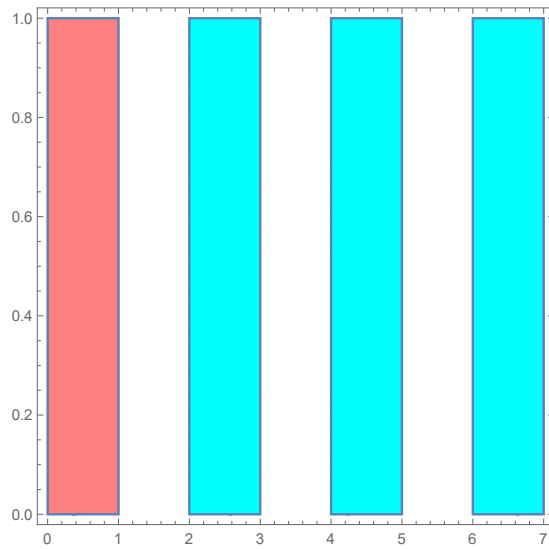


**Figure 3.8:** Case 7: Completely demixed phase that recalls the trimer one. Let's call it "trimer-like".

**Case 1: mixed (uniform) phase**

In order to find the uniform solution, We start by simply assuming that we must have  $a_j \neq 0$  and  $b_j \neq 0$ . Then the equations reduce to

$$\mu_a = U_a |a_j|^2 + W |b_j|^2$$

$$\mu_b = U_b |b_j|^2 + W |a_j|^2$$

for  $j = 1, 2, 3, 4$ .

which we can rewrite in the form

$$\mu_a = U_a n_j + W m_j \tag{3.4}$$

$$\mu_b = U_b m_j + W n_j \tag{3.5}$$

There are eight unknown populations  $n_j$  and  $m_j$  with two constraints  $N = n_1 + n_2 + n_3 + n_4$  and  $M = m_1 + m_2 + m_3 + m_4$ . Imposing the latter leads to determine  $\mu_a$  and  $\mu_b$ . The derivation of  $n_1, n_2, n_3, n_4, m_1, m_2, m_3$  and  $m_4$  gives

$$n_1 = n_2 = n_3 = n_4 = \frac{\mu_a U_b - \mu_b W}{U_a U_b - W^2} \tag{3.6}$$

$$m_1 = m_2 = m_3 = m_4 = \frac{\mu_b U_a - \mu_a W}{U_a U_b - W^2} \tag{3.7}$$

showing how this solution features twin populations. Thanks to the constraints  $N = n_1 + n_2 + n_3 + n_4$  and  $M = m_1 + m_2 + m_3 + m_4$  we discover that  $n_1 = n_2 = n_3 = n_4 = \frac{N}{4}$  and  $m_1 = m_2 = m_3 = m_4 = \frac{M}{4}$ . Substituting these values in equations (3.4) and (3.5), we are able to find  $\mu_a$  and  $\mu_b$

$$\mu_a = U_a \frac{N}{4} + W \frac{M}{4}$$

$$\mu_b = U_b \frac{M}{4} + W \frac{N}{4}$$

Now, replacing the values founded for  $\mu_a$  and  $\mu_b$  in equations (3.6) and (3.7), we have further validation of the previous results, in fact:

$$n_j = \frac{\mu_a U_b - \mu_b W}{U_a U_b - W^2} = \frac{1}{4(U_a U_b - W^2)} (U_b(U_a N + W M) - W(U_b M + W N)) = \frac{N}{4}$$

$$m_j = \frac{\mu_b U_a - \mu_a W}{U_a U_b - W^2} = \frac{1}{4(U_a U_b - W^2)} (U_a(U_b M + W N) - W(U_a N + W M)) = \frac{M}{4}$$

**Case 2: half-demixed phase**

Let's assume that  $b_1 = a_2 = 0$ : a situation that recalls one of the intermediate phases of the trimer. The first well is filled with bosons of species A, while the second is filled with bosons of species B. In the other two wells we still have a complete mixing (see Fig. (3.3)). So  $m_1 = n_2 = 0$  e  $N = n_1 + n_3 + n_4$ ,  $M = m_2 + m_3 + m_4$ . Our eight equations boil down to

$$\begin{aligned}\mu_a &= U_a n_1 \\ 0 &= 0 \\ \mu_a &= U_a n_3 + W m_3 \\ \mu_a &= U_a n_4 + W m_4 \\ 0 &= 0 \\ \mu_b &= U_b m_2 \\ \mu_b &= U_b m_3 + W n_3 \\ \mu_b &= U_b m_4 + W n_4\end{aligned}$$

By observing this system, we can see that, putting together the third and seventh equations, or the fourth and eighth, two systems with two equations and two unknowns come out. By solving them, we find the following solutions as a function of  $\mu_a$  and  $\mu_b$

$$\begin{aligned}n_3 &= \frac{\mu_a W - \mu_b U_a}{W^2 - U_a U_b} \\ m_3 &= \frac{\mu_b W - \mu_a U_b}{W^2 - U_a U_b} \\ n_4 &= \frac{\mu_a W - \mu_b U_a}{W^2 - U_a U_b} \\ m_4 &= \frac{\mu_b W - \mu_a U_b}{W^2 - U_a U_b}\end{aligned}$$

i.e. we find that

$$\begin{aligned}n_3 &= n_4 \\ m_3 &= m_4\end{aligned}$$

With this new information, we can rewrite the constraints as

$$\begin{aligned}n_1 &= N - 2n_3 \\ m_2 &= M - 2m_3\end{aligned}$$

in this way our problem is reduced to a system with two equations and two unknowns

$$N - 2n_3 = n_3 + \frac{W}{U_a}m_3$$

$$M - 2m_3 = m_3 + \frac{W}{U_b}n_3$$

from which we obtain

$$n_3 = n_4 = \frac{3U_aU_bM - U_bWN}{9U_aU_b - W^2}$$

$$m_3 = m_4 = \frac{3U_aU_bN - U_aWM}{9U_aU_b - W^2}$$

Furthermore, introducing the two parameters

$$\alpha = \frac{W}{\sqrt{U_aU_b}} \tag{3.8}$$

and

$$\beta = \frac{M}{N} \sqrt{\frac{U_b}{U_a}} \tag{3.9}$$

we can rewrite the last two results as

$$n_3 = n_4 = \frac{(3 - \alpha\beta)N}{9 - \alpha^2}$$

$$m_3 = m_4 = \frac{(3 - \frac{\alpha}{\beta})M}{9 - \alpha^2}$$

At this point, we are also able to evaluate  $n_1$  and  $m_2$ :

$$n_1 = \frac{N(\alpha^2 - 3 - 2\alpha\beta)}{\alpha^2 - 9}$$

$$m_2 = \frac{M(-2\alpha - 3\beta + \alpha^2\beta)}{(\alpha^2 - 9)\beta}$$

**Validity range of the previous solutions** Of course, we need to verify that all of the above solutions are non-negative. In order to do this, let's continue in order:

1.

$$n_3 = \frac{(3 - \alpha\beta)N}{9 - \alpha^2} \geq 0$$

we have two possibilities

- positive numerator and denominator

$$3 - \alpha\beta \geq 0 \rightarrow \beta \leq \frac{3}{\alpha}$$

$$9 - \alpha^2 > 0 \rightarrow \alpha < 3$$

- negative numerator and denominator

$$3 - \alpha\beta \leq 0 \rightarrow \beta \geq \frac{3}{\alpha}$$

$$9 - \alpha^2 < 0 \rightarrow \alpha > 3$$

2.

$$m_3 = \frac{(3 - \alpha/\beta)M}{9 - \alpha^2} \geq 0$$

- positive numerator and denominator

$$3 - \alpha/\beta \geq 0 \rightarrow \beta \geq \frac{\alpha}{3}$$

$$9 - \alpha^2 > 0 \rightarrow \alpha < 3$$

- negative numerator and denominator

$$3 - \alpha/\beta \leq 0 \rightarrow \beta \leq \frac{\alpha}{3}$$

$$9 - \alpha^2 < 0 \rightarrow \alpha > 3$$

3.

$$n_1 = \frac{N(\alpha^2 - 3 - 2\alpha\beta)}{\alpha^2 - 9} \geq 0$$

- positive numerator and denominator

$$\alpha^2 - 3 - 2\alpha\beta \geq 0 \rightarrow \beta \leq \frac{\alpha^2 - 3}{2\alpha}$$

$$\alpha^2 - 9 > 0 \rightarrow \alpha > 3$$

- negative numerator and denominator

$$\alpha^2 - 3 - 2\alpha\beta \leq 0 \rightarrow \beta \geq \frac{\alpha^2 - 3}{2\alpha}$$

$$\alpha^2 - 9 < 0 \rightarrow \alpha < 3$$

4.

$$m_2 = \frac{M(-2\alpha - 3\beta + \alpha^2\beta)}{(\alpha^2 - 9)\beta} \geq 0$$

- positive numerator and denominator

$$-2\alpha - 3\beta + \alpha^2\beta \geq 0 \rightarrow \beta \geq \frac{2\alpha}{\alpha^2 - 3}$$

$$\alpha^2 - 9 > 0 \rightarrow \alpha > 3$$

- negative numerator and denominator

$$-2\alpha - 3\beta + \alpha^2\beta \leq 0 \rightarrow \beta \leq \frac{2\alpha}{\alpha^2 - 3}$$

$$\alpha^2 - 9 < 0 \rightarrow \alpha < 3$$

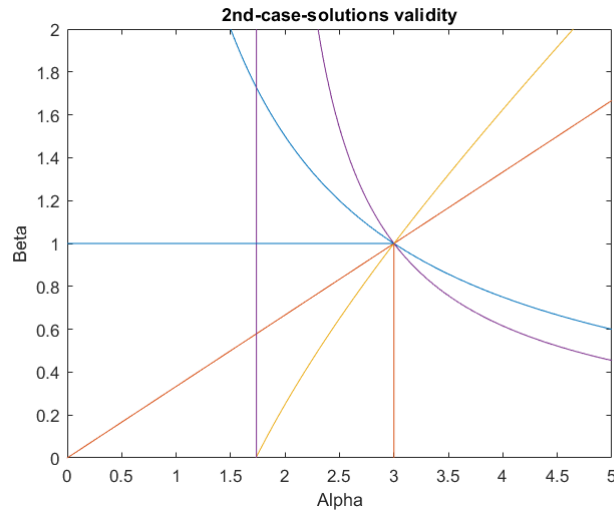


**Figure 3.9:** Case 2 solutions: Range of validity.

In Figure (3.9) there are all the curves found by studying the validity conditions. Following what we have found, we will have that the solutions are valid only within the triangle identified by the purple asymptote, the orange line starting at (0,0) and the segment starting from (0,1) and ending in (3,1).

**Case 3: phase with mixing in a single well**

In this case we assume  $b_2 = b_3 = b_4 = 0$ , which implies

$$m_2 = m_3 = m_4 = 0$$

$$M = m_1$$

it is reasonable to assume such a behavior when  $M \ll N$ , or in general, when one of the two bosonic populations is much greater than the other, in analogy with what has already been seen in the case of one of the trimer's intermediate phases (see Fig. (3.4)).

Our eight equations boil down to

$$\mu_a = U_a n_1 + W m_1$$

$$\mu_a = U_a n_2$$

$$\mu_a = U_a n_3$$

$$\mu_a = U_a n_4$$

$$\mu_b = U_b m_1 + W n_1$$

$$0 = 0$$

$$0 = 0$$

$$0 = 0$$

From the second, third and fourth equation it is evident that  $n_2 = n_3 = n_4 = n$  and  $N = n_1 + 3n$ . The solutions of the system are then

$$n = \frac{N}{4} + \frac{WM}{4U_a} = \frac{N}{4}(1 + \alpha\beta)$$

$$n_1 = \frac{N}{4}(1 - 3\alpha\beta)$$

Since we must have  $n_1 \geq 0$ , we find  $\beta \leq \frac{1}{3\alpha}$ . We can identify with the latter the range of validity of the solution.

**Case 4: partially demixed double-dimer**

Let's take  $b_1 = b_3 = 0$ . This configuration can be seen as the union of two dimers' intermediate phases. From (Fig. (3.5)) it is easy to see how the system can be split in two dimers, each one with a completely filled well and mixing in the other one. In this sense we can call this configuration the "double dimer". Our equations become

$$\mu_a = U_a n_1$$

$$\mu_a = U_a n_2 + W m_2$$

$$\mu_a = U_a n_3$$

$$\mu_a = U_a n_4 + W m_4$$

$$0 = 0$$

$$\mu_b = U_b m_2 + W n_2$$

$$0 = 0$$

$$\mu_b = U_b m_4 + W m_4$$

From the first and third equations we have that  $n_1 = n_3 = n$ . Furthermore, suppose that the remaining bosons are distributed equally in the remaining wells:  $n_2 = n_4 = n_0$  e  $m_2 = m_4 = m_0$ . Constraints therefore become

$$N = 2n + 2n_0$$

$$M = 2m_0$$

At this point it is very easy to find solutions

$$m_0 = \frac{M}{2}$$

$$n = \frac{N}{4} + \frac{MW}{4U_a} = \frac{N}{4}(1 + \alpha\beta)$$

$$n_0 = \frac{N}{4} - \frac{MW}{4U_a} = \frac{N}{4}(1 - \alpha\beta)$$

which, just as in the case of two-wells ring, are valid for  $\beta \leq \frac{1}{\alpha}$ .

**Case 5: quasi-uniform phase**

The configuration of this case is a totally new guess; in the sense that it is not inspired from anything that has been found previously (see Fig. (3.6)). Let's simply say  $b_1 = 0$  ( $m_1 = 0$ ). So our system of equations will become

$$\begin{aligned}\mu_a &= U_a n_1 \\ \mu_a &= U_a n_2 + W m_2 \\ \mu_a &= U_a n_3 + W m_3 \\ \mu_a &= U_a n_4 + W m_4 \\ 0 &= 0 \\ \mu_b &= U_b m_2 + W n_2 \\ \mu_b &= U_b m_3 + W n_3 \\ \mu_b &= U_b m_4 + W n_4\end{aligned}$$

Now, strengthened by the fact that in the previous case (the "double dimer"), equally distributed populations were found, we can assume that this is also the case and therefore  $m_2 = m_3 = m_4 = m$  and  $n_2 = n_3 = n_4 = n$ . Our constraints become

$$\begin{aligned}N &= n_1 + 3n \rightarrow n = \frac{N - n_1}{3} \\ M &= 3m \rightarrow m = \frac{M}{3}\end{aligned}$$

So, we obtain the equation for  $n_1$ :

$$U_a n_1 = U_a n + W m = U_a \frac{N - n_1}{3} + W \frac{M}{3}$$

Solving it, we find

$$\begin{aligned}n_1 &= \frac{N}{4}(1 + \alpha\beta) \\ n &= \frac{N}{4} \left(1 - \frac{\alpha\beta}{3}\right)\end{aligned}$$

Therefore, in order to have  $n \geq 0$  we have to impose the condition  $\beta \leq \frac{3}{\alpha}$ , but since  $\beta$  can be at least equal to 1, it follows that  $\alpha$  must be greater than 3. The validity interval of this solution seems to fall completely in the zone in which we expect the demixed phase to be stable. Already from this simple reasoning, it seems difficult that it could be the GS.

**Case 6 and 7: fully demixed phases**

The configurations associated to the two possible demixed states are trivial (see Figures (3.7) and (3.8)).

# Chapter 4

## Phase Diagram

*“Not only is the Universe stranger than we think, it is stranger than we can think.”*  
Werner Heisenberg

Now that we have the analytical form of all the hypothesized solutions as a function of the model parameters  $\alpha$  and  $\beta$ , we can continue to look for which of them are part of the minimum-energy configuration. First of all, one has to compute the Hamiltonian's value associated to each of these solutions; then, it will be the turn of the comparisons between these values, in order to determine which is the minimizing one and - above all - where.

The purpose is to find a Phase Diagram like the ones that has been found in all previous cases (see Figs. (2.3), (2.4) and (2.5)), where phases are clearly distinguishable. After that, we will try to find an effective indicator, able to capture the criticalities of the transitions (as has already been done in the case of the trimer with the Mixing Entropy; see subsection 2.2.2).

### 4.1 Evaluation of the energy associated to the found solutions

Now that we have computed the values of  $(\vec{n}, \vec{m}) = (n_1, n_2, n_3, n_4, m_1, m_2, m_3, m_4)$ , we can evaluate the values of the Hamiltonian at  $T = 0$  (where  $T$  is the hopping amplitude)

$$H(\vec{n}, \vec{m}) = \frac{U_a}{2}(n_1^2 + n_2^2 + n_3^2 + n_4^2) + \frac{U_b}{2}(m_1^2 + m_2^2 + m_3^2 + m_4^2) + W(n_1m_1 + n_2m_2 + n_3m_3 + n_4m_4) \quad (4.1)$$

in the various configurations. We will then continue with comparing the results found in order to understand how many and which phases there are.

A phase associated with a specific configuration is identified where the energy associated with the same configuration is minimal compared to all the others. Later, putting together the intervals found in this way with the validity intervals of the various solutions, we will be able to construct the phase diagram of the system.

#### 4.1.1 Case 1: completely mixed phase

Let's start with the case corresponding to the mixed phase: in this situation the two populations are equally distributed in the four wells, therefore

$$H_1 \left( \frac{N}{4}, \frac{N}{4}, \frac{N}{4}, \frac{N}{4}, \frac{M}{4}, \frac{M}{4}, \frac{M}{4}, \frac{M}{4} \right) = \frac{N^2 U_a}{8} + \frac{M^2 U_b}{8} + \frac{MNW}{4} \quad (4.2)$$

Now, remembering the definitions of the model parameters  $\alpha$  (3.8) and  $\beta$  (3.9), we can rewrite this expression as

$$H_1 = \frac{\alpha\beta}{4} + \frac{\beta^2}{8} + \frac{1}{8} \quad (4.3)$$

Where an overall factor  $N^2 U_a$  has been omitted since it is always positive (so, it does not affect the energy-confrontations) and will be also the collected factor in front of every other energy function, in this section, written in terms of  $\alpha$  and  $\beta$ .

#### 4.1.2 Case 2: half-demixed phase

Let's now move on to the hypotheses for any intermediate stages. First, let's see the energy of the configuration mimicking phase 2 of the trimer:

$$H = \frac{-4MNU_a U_b (3(U_a + U_b) + W) + M^2 U_b (6U_a^2 + 9U_a U_b + 4U_a W - W^2)}{18U_a U_b - 2W^2} +$$

$$+ \frac{N^2 U_a (9U_a U_b + 6U_b^2 + 4U_b W - W^2)}{18U_a U_b - 2W^2}$$

However, the solution written in this way is very difficult to deal with. So let's try to proceed in an alternative way to find the energy in this case: instead of replacing in the Hamiltonian the solutions expressed as a function of  $U_a$ ,  $U_b$  and  $W$ , we directly replace those expressed as a function of  $\alpha$  and  $\beta$ , obtaining:

$$H = \frac{4MNW(\alpha - 3\beta)\beta(-3 + \alpha\beta) + M^2 U_b (6\alpha^2 - 4\alpha^3\beta + (27 - 6\alpha^2 + \alpha^4)\beta^2)}{2(-9 + \alpha^2)^2\beta^2} +$$

$$+ \frac{N^2 U_a \beta^2 (27 + \alpha^2 (-6 + \alpha^2 - 4\alpha\beta + 6\beta^2))}{2(-9 + \alpha^2)^2 \beta^2}$$

Let's focus on the numerator. Collect  $N^2 U_a$ :

$$N^2 U_a \left[ 4 \frac{MW}{NU_a} (\alpha - 3\beta) \beta (-3 + \alpha\beta) + \frac{M^2 U_b}{N^2 U_a} (6\alpha^2 - 4\alpha^3 \beta + (27 - 6\alpha^2 + \alpha^4) \beta^2) + \right. \\ \left. + \beta^2 (27 + \alpha^2 (-6 + \alpha^2 - 4\alpha\beta + 6\beta^2)) \right]$$

dove  $\frac{MW}{NU_a} = \alpha\beta$  e  $\frac{M^2 U_b}{N^2 U_a} = \beta^2$ .

Fortunately, the term in square brackets can be simplified and factorized, obtaining for the energy:

$$H = \frac{N^2 U_a (-9 + \alpha^2) \beta^2 (-3 + \alpha^2 - 4\alpha\beta - 3\beta^2 + \alpha^2 \beta^2)}{2(-9 + \alpha^2)^2 \beta^2}$$

Simplifying

$$H = \frac{N^2 U_a (-3 + \alpha^2 - 4\alpha\beta - 3\beta^2 + \alpha^2 \beta^2)}{2(-9 + \alpha^2)} \quad (4.4)$$

### 4.1.3 Case 3: phase with mixing in a single well

In this case

$$H = \frac{N^2 U_a^2 + 2MNU_a W + M^2 (4U_a U_b - 3W^2)}{8U_a} \quad (4.5)$$

The latter can be rewritten as a function of model parameters as:

$$H_3 = \frac{1}{8} \left( (4 - 3\alpha^2) \beta^2 + 2\alpha\beta + 1 \right) \quad (4.6)$$

### 4.1.4 Case 4: partially demixed double-dimer

In this case

$$H = \frac{N^2 U_a^2 + 2MNU_a W + M^2 (2U_a U_b - W^2)}{8U_a} \quad (4.7)$$

The latter can be rewritten as a function of model parameters as:

$$H_4 = \frac{1}{8} \left( (2 - \alpha^2) \beta^2 + 2\alpha\beta + 1 \right) \quad (4.8)$$

### 4.1.5 Case 5: quasi-uniform phase

In this case

$$H = \frac{1}{24} \left( 3N^2U_a + 6MNW + \frac{M^2(4U_aU_b - W^2)}{U_a} \right) \quad (4.9)$$

The latter can be rewritten as a function of model parameters as:

$$H = \frac{1}{24} (3 + 6\alpha\beta + \beta^2(4 - \alpha^2)) \quad (4.10)$$

### 4.1.6 Case 6: dimer-like demixed phase

For what concerns the demixed phase, it is worth remembering how the latter was characterized for the dimer and for the trimer:

- in the dimer we observed a perfect division: one species in one well and the other species in the second well;
- in the trimer one species went to concentrate in one well, while the other split into the remaining two.

In both cases, there was no other way to have complete separation. When we consider the four-wells ring, however, two ways to reach it appear for the first time: a dimer-like way, a species in two wells and the other in the other two (with all the possible cyclic permutations of the site labels), and a trimer-like way, with a species concentrated in a single well and the other scattered over the remaining three.

In the dimer-like case, energy is

$$H_{dd} \left( \frac{N}{2}, 0, \frac{N}{2}, 0, 0, \frac{M}{2}, 0, \frac{M}{2} \right) = \frac{N^2U_a}{4} + \frac{M^2U_b}{4} \quad (4.11)$$

The latter can be rewritten as a function of model parameters as:

$$H_{dd} = \frac{1}{4} (\beta^2 + 1) \quad (4.12)$$

### 4.1.7 Case 7: trimer-like demixed phase

In the event that complete separation occurs as in the trimer, the energy is

$$H_{dt} \left( 0, \frac{N}{3}, \frac{N}{3}, \frac{N}{3}, M, 0, 0, 0 \right) = \frac{N^2U_a}{6} + \frac{M^2U_b}{2} \quad (4.13)$$

The latter can be rewritten as a function of model parameters as:

$$H_{dt} = \frac{\beta^2}{2} + \frac{1}{6} \quad (4.14)$$

## 4.2 Comparison between the values of the energy in the different configurations

We will now proceed with the comparison of the results we found, as anticipated at the beginning of this chapter.

### 4.2.1 Comparison between case 1 and case 6

Let's begin with the mixed phase and one of the demixed phases: the dimer-like one. We wonder what parameter values it applies to

$$\frac{N^2 U_a}{8} + \frac{M^2 U_b}{8} + \frac{M N W}{4} \leq \frac{N^2 U_a}{4} + \frac{M^2 U_b}{4}$$

Bringing all the factors into the r.h.s. of the inequality we find

$$N^2 U_a \left( 1 + \frac{M^2 U_b}{N^2 U_a} - 2 \frac{M W}{N U_a} \right) \geq 0$$

Now, since  $N$  and  $U_a$  are definitely both greater than 0 and remembering the definitions of  $\alpha$  and  $\beta$ , we can further simplify our expression

$$1 + \beta^2 - 2\alpha\beta \geq 0$$

and therefore the mixed configuration is actually more advantageous than the demixed one for

$$\alpha \leq \frac{1}{2\beta} + \frac{1}{2}\beta$$

**Remark:** setting  $\beta = 1$  and thus bringing us back to the symmetric case (that is the case with twin species, identified by  $U_a = U_b$  e  $M = N$  and so also by  $\beta = 1$ ), we find that the mixed phase is the advantageous one for  $\alpha \leq \frac{1}{2} + \frac{1}{2} = 1$ , i.e.

$$\frac{W}{U} \leq 1$$

in perfect agreement with what we already know [61].

### 4.2.2 Comparison between case 1 and case 7

We wonder what parameter values it applies to

$$\frac{N^2 U_a}{8} + \frac{M^2 U_b}{8} + \frac{M N W}{4} \leq \frac{N^2 U_a}{6} + \frac{M^2 U_b}{2}$$

that is, when the energy of the mixed configuration is less than that of the trimer-like demixed case. Bringing all the factors into the r.h.s. of the inequality we find

$$N^2 U_a \left( 1 + 9 \frac{M^2 U_b}{N^2 U_a} - 6 \frac{M W}{N U_a} \right) \geq 0$$

Now, since  $N$  and  $U_a$  are definitely both greater than 0 and remembering the definitions of  $\alpha$  and  $\beta$ , we can simplify our expression again

$$1 + 9\beta^2 - 6\alpha\beta \geq 0$$

and therefore the mixed configuration is actually more advantageous than the demixed one for

$$\alpha \leq \frac{1}{6\beta} + \frac{3}{2}\beta$$

### 4.2.3 Comparison between case 6 and case 7

At this point one question arises: which of the two demixed phases is the "right" one? Or are they both, but in different areas of the phase diagram? And it is precisely here that the peculiarity of the tetramer comes out. So let's proceed with the comparison of the two energies:

$$\frac{N^2 U_a}{4} + \frac{M^2 U_b}{4} \leq \frac{N^2 U_a}{6} + \frac{M^2 U_b}{2}$$

that leads to

$$\frac{M^2 U_b}{N^2 U_a} \geq \frac{1}{3}$$

that is, the dimer-like demixed phase is more advantageous than the trimer-like phase for

$$\boxed{\beta \geq \frac{1}{\sqrt{3}} \approx 0.58} \tag{4.15}$$

Now we just have to identify and place the intermediate phases between the mixed and demixed ones.

### 4.2.4 Comparison with case 2 in the symmetrical case

To continue with the research of the intermediate phases, we can first try to bring ourselves back to a simpler case, namely the one in which  $\beta = 1$  (i.e. when one deals with twin-species). Given the previous result, we will have that in this regime

it will be the dimer-like phase to "be the leader" between the two demixed phases. Comparing the mixed phase

$$H_{sym} \left( \frac{N}{4}, \frac{N}{4}, \frac{N}{4}, \frac{N}{4}, \frac{N}{4}, \frac{N}{4}, \frac{N}{4}, \frac{N}{4} \right) = \frac{N^2(U + W)}{4}$$

with the demixed dimer-like

$$H_{sym} \left( \frac{N}{2}, 0, \frac{N}{2}, 0, 0, \frac{N}{2}, 0, \frac{N}{2} \right) = \frac{N^2U}{2}$$

both in the symmetrical case, it is quite trivial to verify that the latter is more advantageous for  $\alpha \geq 1$ . Therefore, in order to find the possible intermediate phases that could occur for  $\alpha \geq 1$ , it makes sense to compare the energies of the various partially demixed configuration hypotheses (previously found) with that of the demixed dimer-like case.

Furthermore, among the four hypotheses presented above, only one is likely to be (in some range) the Ground State: the one we called "half-demixed phase". In fact, it is the only one which does not show the numerical predominance of one species over the other. Moreover, the other hypotheses are probable as Ground State only in the case of asymmetric populations, thus when  $\beta$  differs from 1. So let's proceed with the comparison of the two energies:

$$\frac{N^2U}{2} - \frac{N^2U(U + W)}{3U + W} \leq 0$$

Simplifying, we find

$$\frac{N^2U(1 - \alpha)}{3 + \alpha} \leq 0$$

So we have two possibilities:

- **1<sup>st</sup> possibility:**

$$1 - \alpha \geq 0 \rightarrow \alpha \leq 1$$

$$3 + \alpha \leq 0 \rightarrow \alpha \leq -3$$

- **2<sup>nd</sup> possibility:**

$$1 - \alpha \leq 0 \rightarrow \alpha \geq 1$$

$$3 + \alpha \geq 0 \rightarrow \alpha \geq -3$$

Obviously, the first possibility is to be discarded. We therefore find that the dimer-like completely demixed phase comes out as soon as we reach  $\alpha = 1$  and we cross it, going towards higher values of the effective parameter. Only for  $\alpha$  exactly equal to 1, the two energies coincide, showing the existence of a degeneration for

the GS at this point, as had already been seen with the polytope method in [61] and pointed out at the beginning of Chapter 3 (see Fig. (3.1)).

We therefore conclude that for  $\beta = 1$ , four wells behave as two: we have a single phase transition for  $\alpha = 1$ , which separates a completely mixed phase from a completely demixed (dimer-like, to be precise).

### 4.2.5 Comparisons in the asymmetrical cases for the partially demixed phases

As one has probably noticed, we introduced a certain notation in order to label the Hamiltonian-functions associated to each phase. For the sack of clarity, we will report it in the following list, before continuing:

- $H_{unif}$  =Hamiltonian in the mixed case (case (4.3));
- $H_{dt}$  =Hamiltonian in the trimer-like demixed phase (case (4.14));
- $H_{dd}$  =Hamiltonian in the dimer-like demixed phase (case (4.12));
- $H_i$  (for  $i=2,3,4,5$ ) = Hamiltonian associated with the corresponding partially demixed phase case.

#### Case 3: single mixed-well phase

First of all, let's compare the partially demixed phase hypothesis of case 3 with the trimer-like totally demixed phase (it makes no sense to compare it with the dimer-like phase, as the solutions for this case are valid only for  $\beta \leq \frac{1}{3\alpha}$ ). Imposing the comparison, we will get:

$$H_{dt} - H_3 \leq 0 \rightarrow \frac{(NU_a - 3MW)^2}{24U_a} \leq 0$$

It is immediately evident that the condition is never verified. We therefore may think that the solution of case 3 is more advantageous than the trimer-like phase everywhere. However, we must remember once again that the solutions are only valid for  $\beta \leq \frac{1}{3\alpha}$ ; thus, this hyperbole will be the line of separation between the two phases.

With respect to the comparison with the other partially demixed phase hypotheses, let's proceed with seeing where case 3 is more advantageous than case 4:

$$H_3 - H_4 \leq 0 \rightarrow \frac{M^2(U_a U_b - W^2)}{4U_a}$$

Collecting  $U_a U_b$  at the numerator, we notice that what we just need to solve is

$$1 - \alpha^2 \leq 0 \rightarrow \alpha \leq -1 \cup \alpha \geq 1$$

Therefore, for  $\alpha \geq 1$  the energy of case 3 is more advantageous than that of case 4, always below the validity line.

There is nothing left to do now, but to compare case 3 with case 5:

$$H_3 - H_5 \leq 0 \rightarrow \frac{M^2(U_a U_b - W^2)}{3U_a}$$

that is, also in this case, for  $\alpha \geq 1$ , case 3 always "wins" over case 5.

#### Case 4: double-dimer

We have already seen that, below  $\beta = \frac{1}{3\alpha}$ , case 3 always wins over case 4. But let's see, now, how the latter behaves when compared with the remaining hypotheses.

Let's start as usual with the totally demixed phases.

- dimer-like:

$$H_{dd} - H_4 \leq 0 \rightarrow \frac{(NU_a - MW)^2}{8U_a} \leq 0$$

that is, the configuration of case 4 (blue in (Fig. (4.1))) always seems to be advantageous compared to the demixed one we are considering (green). However, even in this case, remember that the solutions associated with  $H_4$  are valid only below  $\beta = \frac{1}{\alpha}$ . Furthermore, in correspondence with this hyperbola, the two energies are equivalent, thus giving rise to degenerate states.

- trimer-like:

$$H_{dt} - H_4 \leq 0$$

that is

$$\frac{N^2 U_a^2 - 6MNU_a W + 3M^2(2U_a U_b + W^2)}{24U_a} \leq 0$$

Collecting  $U_a U_b$  from the last parenthesis of the numerator:

$$\frac{N^2 U_a^2 - 6MNU_a W + 3M^2 U_a U_b (2 + \alpha^2)}{24U_a} \leq 0$$

It is easy to notice that we can simplify  $U_a$  everywhere. Collecting  $MNW$  now, we get:

$$MNW \left[ \frac{1}{\alpha\beta} - 6 + 3\frac{\beta}{\alpha}(2 + \alpha^2) \right] \leq 0$$

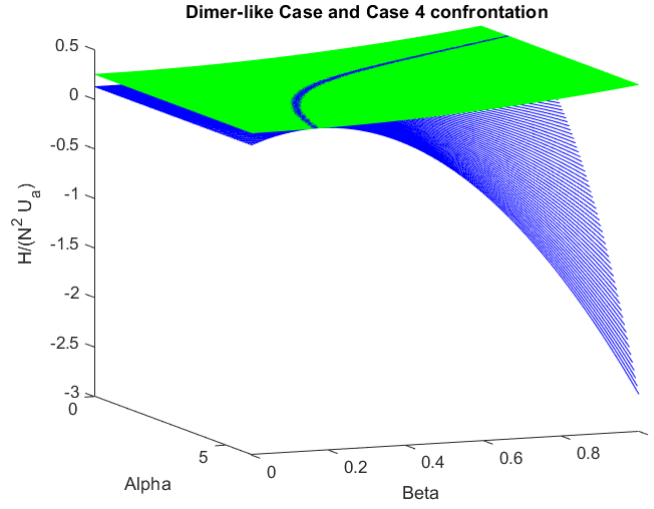


**Figure 4.1:** Comparison between case 4 partially demixed phase and the dimer-like totally demixed phase.

Observing that  $M$ ,  $N$  and  $W$  are greater than 0, we can proceed by considering only what we have in square brackets, and finally obtain

$$3(2 + \alpha^2)\beta^2 - 6\alpha\beta + 1 \leq 0$$

Solving with respect to  $\beta$ :

$$\frac{3\alpha - \sqrt{6\alpha^2 - 6}}{3(2 + \alpha^2)} \leq \beta \leq \frac{3\alpha + \sqrt{6\alpha^2 - 6}}{3(2 + \alpha^2)}$$

This range can be seen highlighted in blue in Figures (4.2) and (4.3). Since the hyperbola  $\beta = \frac{1}{\alpha}$  cuts this blue region, and that solutions 4 are valid only below it, we will have that the only remaining yellow portion is the lower right corner indicated by the two straight lines in Fig. (4.3).

### Case 5: quasi-uniform case

First of all, we must verify if case 5 is advantageous with respect to the demixed phases:

- dimer-like:

$$H_{dd} - H_5 \leq 0$$

and the result of the previous inequality is

$$\frac{3\alpha - \sqrt{8\alpha^2 - 2}}{2 + \alpha^2} \leq \beta \leq \frac{3\alpha + \sqrt{8\alpha^2 - 2}}{2 + \alpha^2}$$

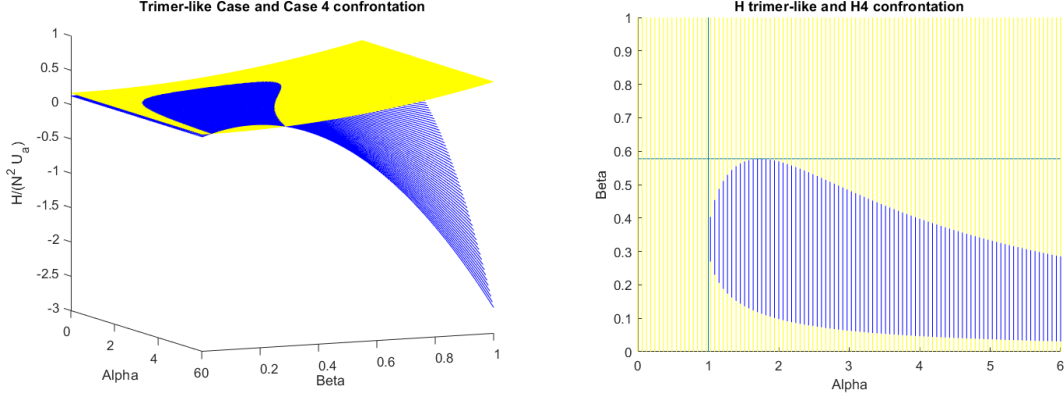


**Figure 4.2:** Comparison between case 4 partially demixed phase and the trimer-like totally demixed phase.

**Figure 4.3:** This is nothing but the graph of figure (3.2) seen from above. The two straight lines are put there in order to highlight the small surviving yellow corner, where the energy of case 4 is smaller than the one of the demixed phase.

- trimer-like

$$H_{dt} - H_5 \leq 0 \rightarrow 1 - 6\alpha\beta + \beta^2(8 + \alpha^2) \leq 0$$

and the result of the previous inequality is

$$\frac{3\alpha - \sqrt{8(\alpha^2 - 1)}}{8 + \alpha^2} \leq \beta \leq \frac{3\alpha + \sqrt{8(\alpha^2 - 1)}}{8 + \alpha^2}$$

We can now proceed with the comparison with the other partially demixed states:

- Comparison with case 4

$$H_4 - H_5 \leq 0 \rightarrow \frac{M^2(U_a U_b - W^2)}{12U_a} \leq 0$$

so, trivially, for  $\alpha \geq 1$  case 4 is the most advantageous;

- Comparison with case 3

$$H_3 - H_5 \leq 0$$

also in this situation, it is trivial to demonstrate that case 5 is not minimal compared to the others.

**Case 2: half-demixed phase**

Case 2 was placed last not by chance; in fact, attention must be paid to the very particular conditions of validity of the solutions. Indeed, the "triangle" of validity of these solutions falls completely within the zone in which the minimum energy is that of the completely dimer-like demixed configuration (see Fig. (4.4)). Therefore, it only makes sense to make the following comparison:

$$H_{dd} - H_2 \leq 0$$

that is

$$\frac{-3 - \alpha^2 + 8\alpha\beta - (3 + \alpha^2)\beta^2}{4(\alpha^2 - 9)} \leq 0$$

Let's start with the case with a positive numerator

$$-3 - \alpha^2 + 8\alpha\beta - (3 + \alpha^2)\beta^2 \geq 0$$

$$3 + \alpha^2 - 8\alpha\beta + (3 + \alpha^2)\beta^2 \leq 0$$

$$\frac{4\alpha - \sqrt{16\alpha^2 - (3 + \alpha^2)^2}}{3 + \alpha^2} \leq \beta \leq \frac{4\alpha + \sqrt{16\alpha^2 - (3 + \alpha^2)^2}}{3 + \alpha^2}$$

and negative denominator:

$$\alpha^2 - 9 \leq 0 \rightarrow -3 \leq \alpha \leq +3$$

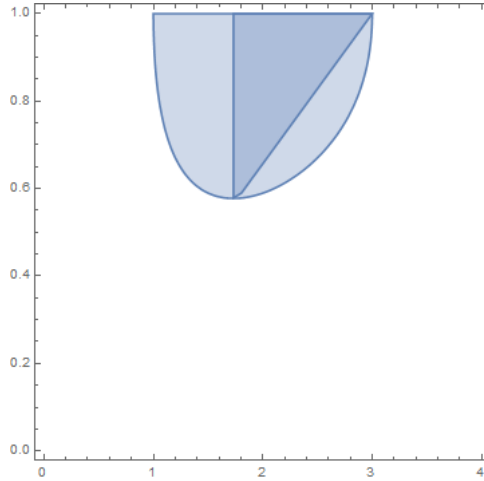


**Figure 4.4:** The interval of validity of the case 2 solutions (represented by the triangle) lays entirely in the region where  $H_{dd}$  is the minimal (the outer curve).

In the intervals of  $\alpha$  and  $\beta$  that interest us, the area in which  $H_{dd}$  is less than  $H_2$  completely encompasses the triangle in which are valid the solutions of case 2

(as it is possible to see in Fig. (4.4)). We conclude, therefore, by asserting that this last case does not appear in the phase diagram and it makes no sense to check the case with negative numerator and negative denominator, since we have already found the answer with the alternative.

### 4.3 Phase Diagram

After making all the comparisons, we can proceed by putting together the results and plotting the phase diagram in the large-populations limit in the domain  $\mathcal{D} = \{(\alpha, \beta) : 0 \leq \alpha \leq 4, 0 \leq \beta \leq 1\}$ :

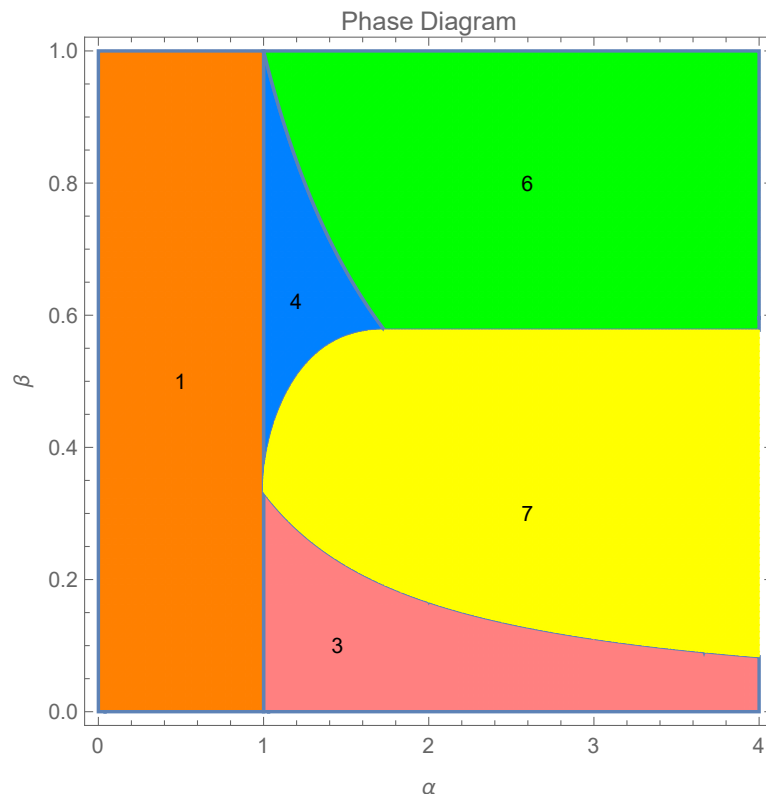


**Figure 4.5:** Phase diagram of a binary mixture in a ring tetramer. Each of the five phases corresponds to a different functional relationship between the minimum-energy configuration and effective model parameters  $\alpha$  and  $\beta$ . This circumstance has a direct impact on the mixing properties of the system and on its GS energy. The labels of each phase are the numbers corresponding to the name of the cases which were "winners" of the comparisons referred to in the previous paragraphs.

This domain has been chosen since in the given range of parameters the diagram exhibits all the five phases (notice, in fact, that if  $\beta > 1$ , one can swap species

labels A and B and, so, we come back to region  $\mathcal{D}$ ). At this point, it is appropriate to summarize the characteristics of each phase and the boundaries by which they are delimited

- in Phase 1 (colored in orange in Fig. (4.5), its schematic representation is reported in panel (a) of Fig. (4.6)), inter-species repulsion  $W$  is too small to allow phase separation; therefore, the species are evenly distributed among the four wells and completely mixed, i.e.  $n_j = \frac{N}{4}$  and  $m_j = \frac{M}{4}$ , for  $j = 1,2,3,4$ ;
- Phase 4 (colored in blue in Fig. (4.5), its schematic representation is reported in panel (b) of Fig. (4.6)), is delimited by  $\alpha > 1$  and

$$\frac{3\alpha + \sqrt{6\alpha^2 - 6}}{3(2 + \alpha^2)} < \beta < \frac{1}{\alpha}$$

that is, we are considering intermediate  $\alpha$  values and fairly symmetrical species. This phase is characterized by two wells filled with the same species (say A) and mixing in the other two (with a clear prevalence of the other species, say B);

- Phase 3 (colored in pink in Fig. (4.5), its schematic representation is reported in panel (c) of Fig. (4.6)) occurs for sufficiently high values of  $\alpha$  and sufficiently asymmetric species. It is delimited by  $\alpha > 1$  and  $\beta < \frac{1}{3\alpha}$ . This phase occurs when one species is definitely a minority compared to the other. The bosons of this species, therefore, will concentrate in a single well, while those of the other species will scatter, with different proportions, in all four well;
- Phase 6 (colored in green in Fig. (4.5), its schematic representation is reported in panel (d) of Fig. (4.6)) corresponds to the dimer-like demixed phase. It occurs for high values of  $\alpha$ , but for not too much asymmetrical species. In particular, it is delimited by  $\beta > \frac{1}{\alpha}$  for  $\alpha < \sqrt{3}$  and  $\beta > \frac{1}{\sqrt{3}}$  for  $\alpha > \sqrt{3}$ . This phase is characterized by two wells filled with one species, while the other two filled with the other species;
- Phase 7 (colored in yellow in Fig. (4.5), its schematic representation is reported in panel (e) of Fig. (4.6)) corresponds to the trimer-like demixed phase. It occurs when we are dealing with asymmetrical species. In particular, it is delimited by  $\beta > \frac{1}{3\alpha}$ ,  $\beta < \frac{1}{\sqrt{3}}$  for  $\alpha > \sqrt{3}$  and

$$\beta < \frac{3\alpha + \sqrt{6\alpha^2 - 6}}{3(2 + \alpha^2)}$$

for  $\alpha < \sqrt{3}$ . This phase is characterized by three wells filled with one species, while the other one filled with the other species;

In conclusion, the great peculiarity of this phase diagram should be underlined: one half of it strongly recalls the phase diagram of the dimer, while the other half exhibits a behavior similar to that of the trimer [3]. This division corresponds to the value of (Eq. 3.9):

$$\beta = \frac{1}{\sqrt{3}}$$

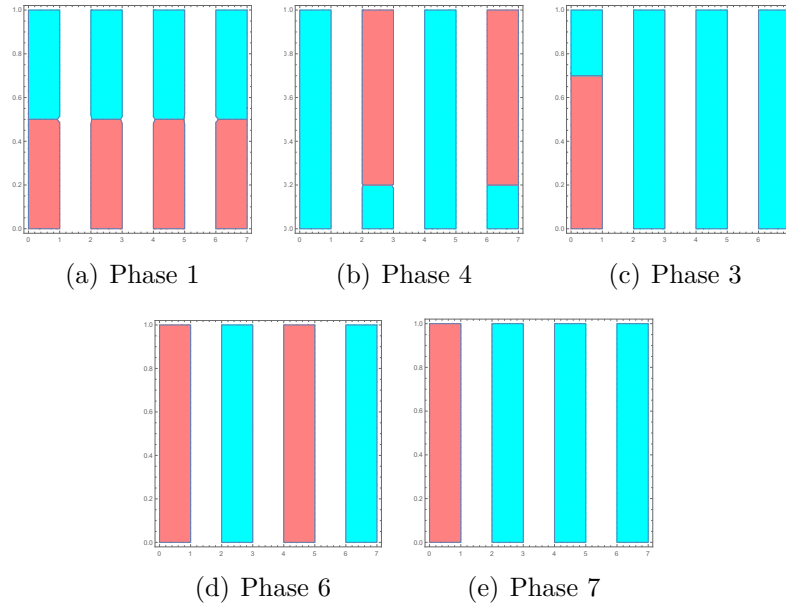


**Figure 4.6:** For convenience, we report here the schematic representations of the configurations that have become part of the Phase Diagram in Fig. (4.5)

Two critical points can be identified:

$$(\alpha, \beta) = \left( \sqrt{3}, \frac{1}{\sqrt{3}} \right)$$

$$(\alpha, \beta) = \left( 1, \frac{1}{3} \right)$$

in correspondence of which many phases' boundary lines meet.

### 4.3.1 Behaviour of minimum-energy configuration $(\vec{n}, \vec{m})$

Among the phases we found, one has both continuous and discontinuous mixing-demixing transitions for the population components  $n_j$  and  $m_j$ . In particular, there is a jump discontinuity in correspondence with the passage from phase one to the

others confining with it; while another jump is present at the transition from phases 4 and 6 to phases 3 and 7. Instead, transitions from phase 4 to 6, and the one from phase 3 to 7, are continuous.

The behaviour of the two populations in the different wells are represented in Figures (4.7), (4.8), (4.9), (4.10), (4.11), (4.12), (4.13) and (4.14).

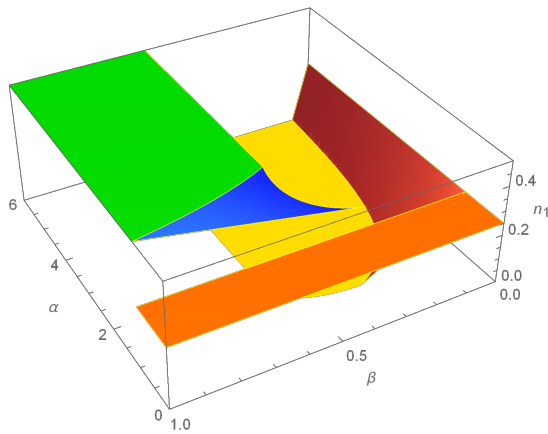


**Figure 4.7:** Behaviour of species A in the 1<sup>st</sup> well.

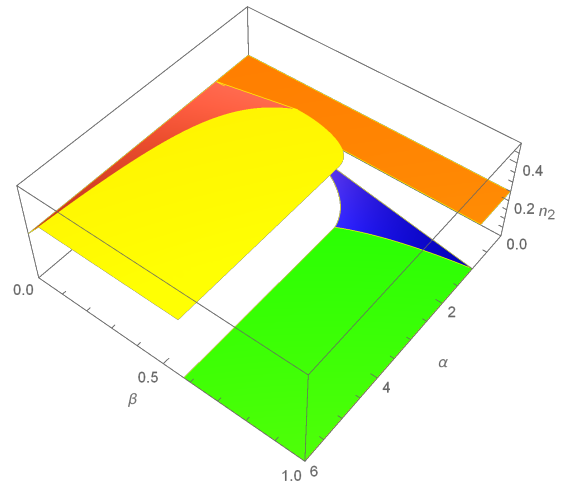


**Figure 4.8:** Behaviour of species A in the 2<sup>nd</sup> well.

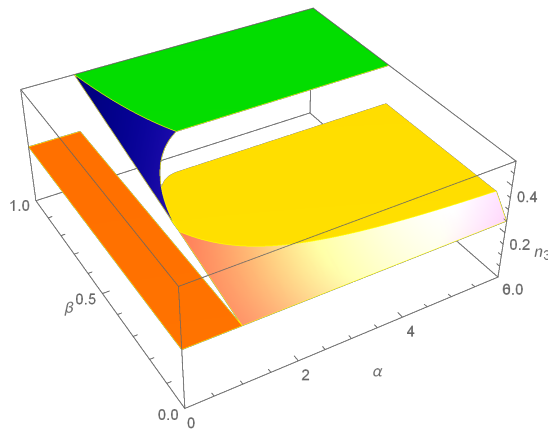


**Figure 4.9:** Behaviour of species A in the 3<sup>rd</sup> well.

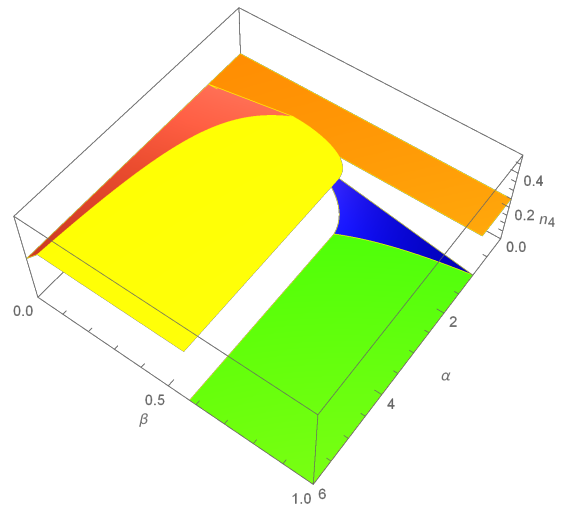


**Figure 4.10:** Behaviour of species A in the 4<sup>th</sup> well.

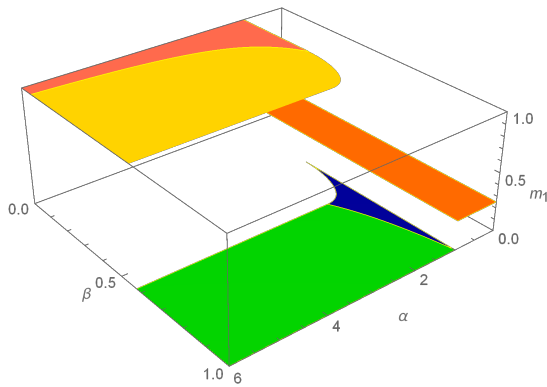


**Figure 4.11:** Behaviour of species B in the 1<sup>st</sup> well.

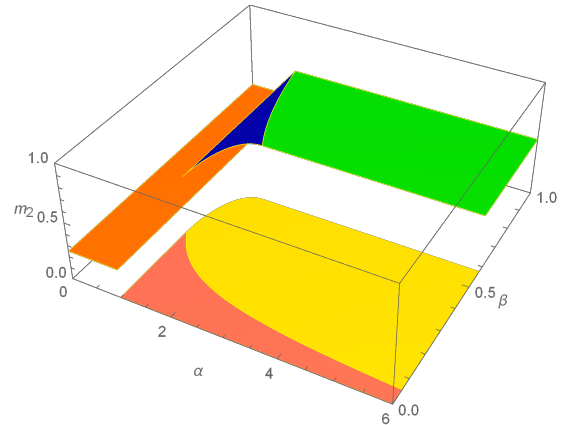


**Figure 4.12:** Behaviour of species B in the 2<sup>nd</sup> well.

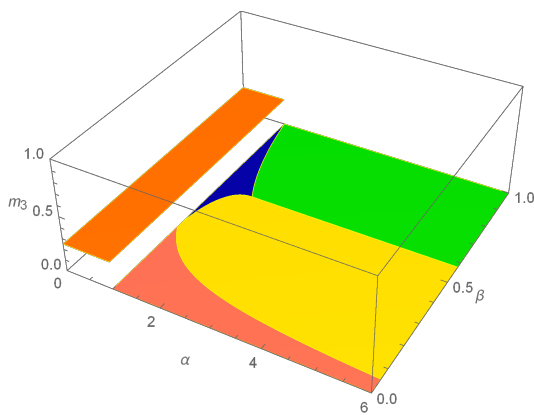


**Figure 4.13:** Behaviour of species B in the 3<sup>rd</sup> well.

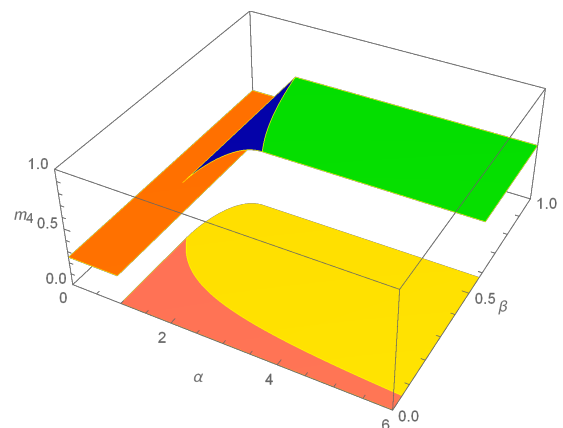


**Figure 4.14:** Behaviour of species B in the 4<sup>th</sup> well.

The fact that each graph is represented from a different angle is to emphasize the discontinuous transitions from time to time. The same angle for all graphics would certainly have been more elegant, but it would have failed to show all the mixing-demixing transitions.

Let us remember that, thanks to the symmetry of the system, the minimum energy configurations shown in the figures are not unique: other isoenergetic configurations can be obtained through cyclic permutations of the site indices.

### 4.3.2 Phases and degree of mixing

When dealing with two different species in discretized domains, an effective indicator for quantifying the degree of mixing is the Entropy of Mixing  $S_{mix}$ . This indicator comes from the field of macromolecular simulations; only recently it has been introduced in the world of ultracold atoms as a useful tool for the investigation of the properties of a bosonic binary mixture. According to the definition given in [10], the entropy of mixing associated to a certain minimum-energy configuration  $(\vec{x}, \vec{y})$  reads

$$S_{mix} = -\frac{1}{2} \sum_{j=1}^4 \left( x_j \ln \frac{x_j}{x_j + y_j} + y_j \ln \frac{y_j}{x_j + y_j} \right) \quad (4.16)$$

Where we based this formula on normalized populations  $x_j = n_j/N$  and  $y_j = m_j/M$ , instead of  $n_j$  and  $m_j$ , as we did in Eq. (2.42). Note that the contribution of each site  $j$  to the total mixing entropy is not fixed; it is weighted by the number of particles present in it. As shown in Fig. (4.15),  $S_{mix}$  is zero in the two completely demixed phases (phase 6 and 7) while achieves the maximum possible value,  $\log 2 \approx 0.69$  in phase 1 (perfect mixing).

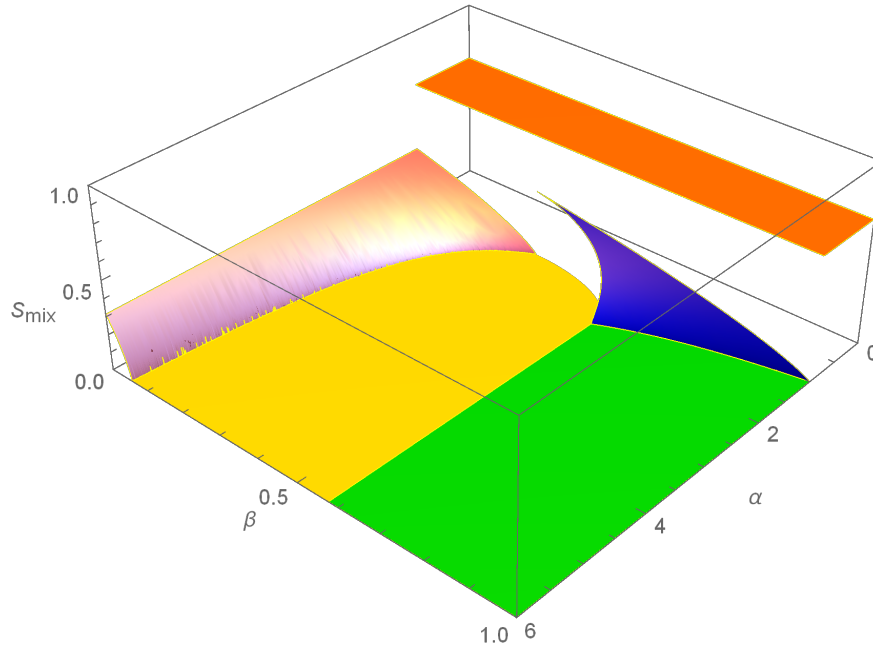


**Figure 4.15:** Entropy of mixing,  $S_{mix}$ , in the five phases. Phase 1 (in orange) features perfect mixing and  $S_{mix}$  takes the biggest possible value, i.e.  $\log 2 \approx 0.69$ . Conversely, phase 6 and 7 (in green and yellow) features perfect demixing and  $S_{mix}$  is therefore zero.

One of the most useful aspects of mixing entropy is that it reports the same

criticalities (jump discontinuities) as the minimum energy configuration, but without the need to investigate all 8 populations,  $n_j$  and  $m_j$ , one at a time. However, in the case of the 4 wells, one of the jumps is not present between the two demixed phases: both equal to zero from the point of view of this indicator. The latter, therefore, at this juncture, is not an excellent measure as it was for the dimer and the trimer. Anyway, it does not fail to capture the jump from phase 1 to the others and the jump at the transition 4-7 (blue-yellow).

### 4.3.3 Phases and Free Energy

Since our system is at zero temperature, the free energy  $F = E - TS$  coincides with the internal energy  $E$ , i.e. the GS energy. We have already computed the values of the Hamiltonian (4.1) in the various phases in (sec. 4.1). Let us now recall how Eqs. (4.3), (4.12), (4.14), (4.8) and (4.6) can be written in term of model parameters  $\alpha$  and  $\beta$ , respectively:

$$H_1 = \frac{\alpha\beta}{4} + \frac{\beta^2}{8} + \frac{1}{8} \quad (4.17)$$

$$H_{dd} = \frac{1}{4} (\beta^2 + 1) \quad (4.18)$$

$$H_{dt} = \frac{\beta^2}{2} + \frac{1}{6} \quad (4.19)$$

$$H_4 = \frac{1}{8} \left( (2 - \alpha^2) \beta^2 + 2\alpha\beta + 1 \right) \quad (4.20)$$

$$H_3 = \frac{1}{8} \left( (4 - 3\alpha^2) \beta^2 + 2\alpha\beta + 1 \right) \quad (4.21)$$

The graphic representation of these expressions (see Fig. (4.16)), shows that  $H$  is indeed continuous everywhere and, in particular, across the transitions.

However, exactly as in the case of mixing entropy, also thanks to energy, we have a proof of the non-analytic behavior of the system at transitions 1-3, 1-4, and 4-7. These evidences can be found by computing the first and second derivatives of the Hamiltonian with respect to  $\alpha$  (seen as a control parameter). But, unfortunately, even in this case we fail to capture the jump at the transition 6-7 (see Figures (4.17), (4.18) and (4.19)).

The expressions of the first derivatives are, respectively

$$\frac{\partial H_1}{\partial \alpha} = \frac{\beta}{4} \quad (4.22)$$

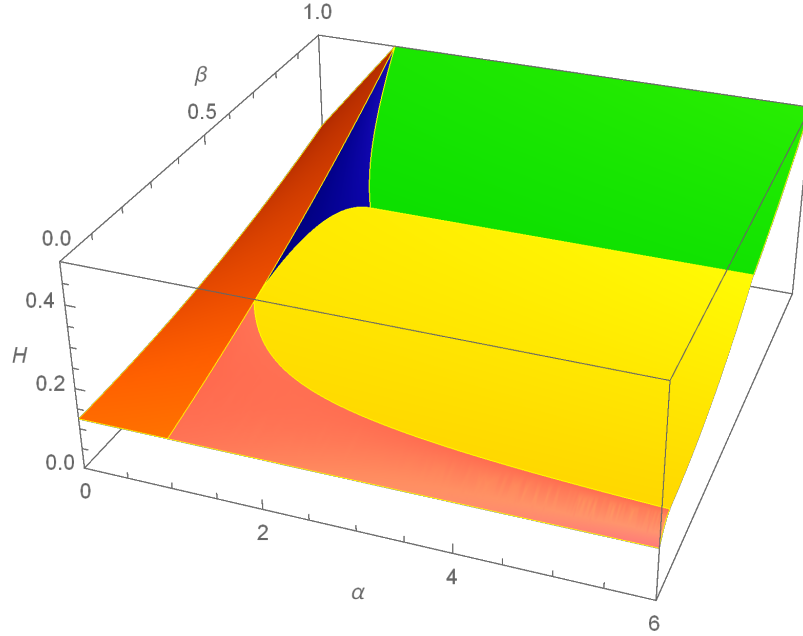


**Figure 4.16:** Hamiltonian relevant to the minimum-energy configuration as a function of the model parameters  $\alpha$  and  $\beta$ .

$$\frac{\partial H_{dd}}{\partial \alpha} = 0 \quad (4.23)$$

$$\frac{\partial H_{dt}}{\partial \alpha} = 0 \quad (4.24)$$

$$\frac{\partial H_4}{\partial \alpha} = \frac{1}{8} (2\beta - 2\alpha\beta^2) \quad (4.25)$$

$$\frac{\partial H_3}{\partial \alpha} = \frac{1}{8} (2\beta - 6\alpha\beta^2) \quad (4.26)$$

In the graph of the first derivative we can observe a peculiar behavior, never observed before. We can see, in fact, that the transitions from phase 1 are discontinuous everywhere, except at the point  $(1, \frac{1}{3})$ .

Instead, for what concerns the second derivatives (obviously excluding the trivial ones):

$$\frac{\partial^2 H_1}{\partial \alpha^2} = 0 \quad (4.27)$$

$$\frac{\partial^2 H_4}{\partial \alpha^2} = -\frac{\beta^2}{4} \quad (4.28)$$

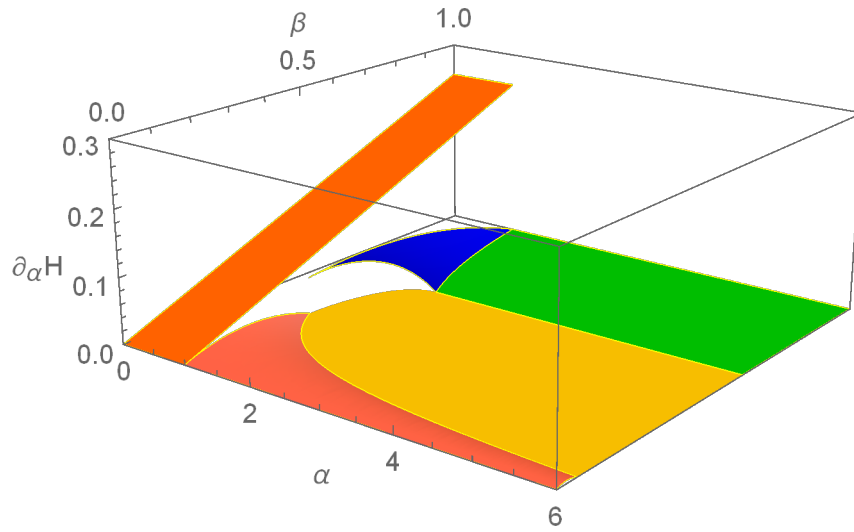


**Figure 4.17:** First derivative with respect to  $\alpha$  of the Hamiltonian relevant to the minimum-energy configuration, as a function of the model parameters  $\alpha$  and  $\beta$ .

$$\frac{\partial^2 H_3}{\partial \alpha^2} = -\frac{1}{4} (3\beta^2) \quad (4.29)$$

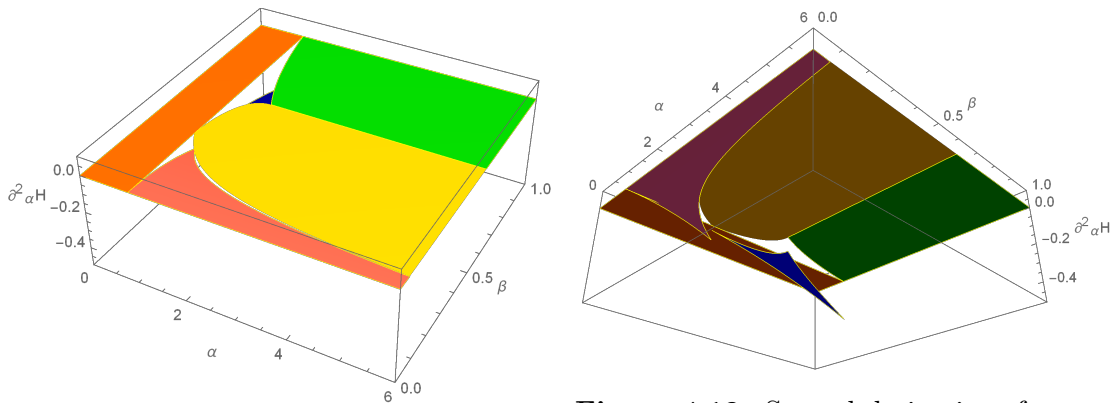


**Figure 4.18:** Second derivative with respect to  $\alpha$  of the Hamiltonian relevant to the minimum-energy configuration, as a function of the model parameters  $\alpha$  and  $\beta$ .

**Figure 4.19:** Second derivative of energy seen from below. This different point of view is presented with the intention of emphasizing the new jumps present at the transitions 4-6 and 3-7.

What we can see, in the graph of the second derivative, the occurrence of jumps at transitions 4-6 and 3-7, at which, instead, the first derivative was continuous.

Once again, we failed to capture the non-analyticity of the transition 6-7, between the two demixed phases. In order to do that, we are going to introduce a new indicator in the next subsection.

#### 4.3.4 Phases and Location Entropy

Since it has not been possible to visualize the complete analytical behaviour at the transitions plotting the Mixing Entropy, the Hamiltonian and its derivatives, we need to introduce a different critical indicator: the Location Entropy.

The use of this physical quantity had already become necessary in the case of attractive inter-species interaction ( $W < 0$ ), previously discussed in Chapter 2 [55], and is well known in statistical thermodynamics and physical chemistry [10, 25]. The difference with respect to the Mixing Entropy is that they provide complementary information: while it describes the degree of mixing between the two species, the Location Entropy measures the spatial localization of the particles regardless of their species.

The expression of the Location Entropy is given by

$$S_{loc} = - \sum_{j=1}^4 \frac{x_j + y_j}{2} \ln \frac{x_j + y_j}{2} \quad (4.30)$$

Inserting the expressions found previously for the  $x_j$ 's and the  $y_j$ 's in the various phases in Eq. (4.30) (remembering that  $x_j = n_j/N$  and  $y_j = m_j/M$ ), we can calculate the value that  $S_{loc}$  assumes in the latter. The results can be seen in Fig (4.20).

It is immediately clear how necessary the introduction of this different critical indicator was, given its ability to capture both the criticalities that had already emerged thanks to the Mixing Entropy (Fig. (4.15)), and the fateful jump at transition 6-7, which the latter had not been able to represent. Indeed, Phase 6 and Phase 7 are characterized by the same degree of mixing (the two species are completely separated in both cases, even if in different ways), but the delocalization of particles among the four wells is completely different.

In conclusion, it is the combined use of  $S_{mix}$  (4.16) and  $S_{loc}$  (4.30) that allows us to appreciate the profound differences between the five phases of the tetramer and to have a clear and complete view of their critical behavior.

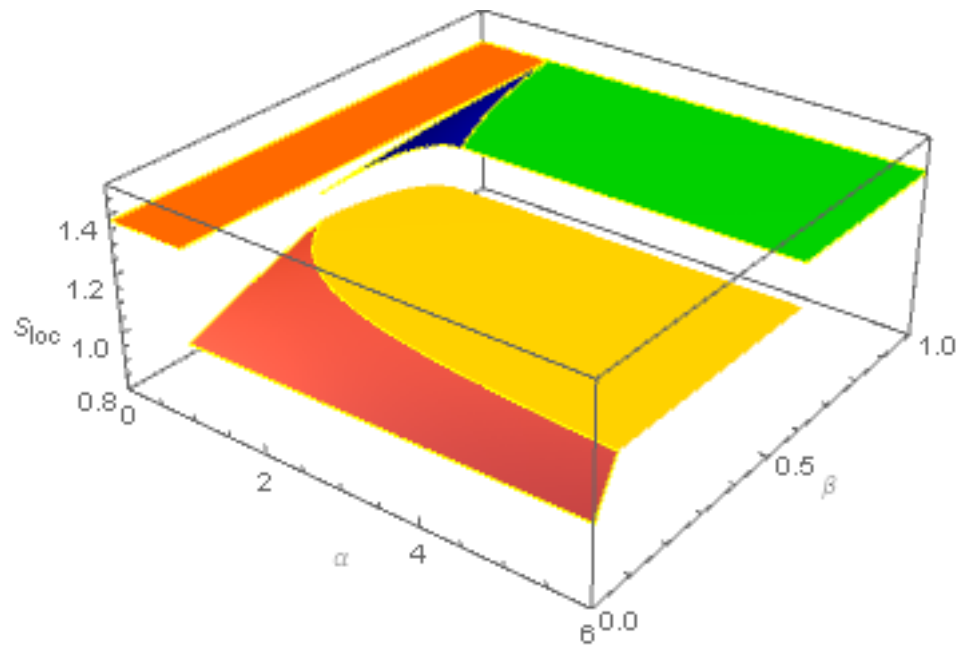


**Figure 4.20:** Location Entropy,  $S_{loc}$ , in the five phases. Thanks to the use of this indicator, one can finally observe the critical behavior at transition 6-7, between the two demixed phases, as well as at the transitions 1-4, 4-7 and 1-3 already observed in the Entropy of Mixing.

## Chapter 5

# Finite-Size Effects on the Mixing-Demixing Transitions

*“Knowing is not enough; we must apply. Willing is not enough; we must do.”  
Johann Wolfgang von Goethe*

As we have seen in the previous chapters, the emergence of the five phases is completely clear and computable in an analytical way only in the Large Population Limit, i.e. for  $\frac{T_a}{U_a N} \rightarrow 0$  and  $\frac{T_b}{U_b M} \rightarrow 0$ . Such phases are still recognizable also in the more realistic case of finite-size systems (i.e. systems with limited numbers of particles and featuring non-vanishing hopping amplitudes). In this Chapter we are going to explore the effects of setting  $T_a \neq 0$  and  $T_b \neq 0$ .

### 5.1 GS configuration with non-vanishing hopping terms

In the Phase Diagram (4.5) it is possible to visualize the five phases separated by boundaries that can be found in an analytical way, as well as, the values of the GS-state configuration  $(\vec{n}, \vec{m})$ , the values of the Energy and its derivatives and, finally, the ones of the Mixing Entropy and the Location Entropy. Instead, in the finite-size regime, even if we can still observe the occurrence of five different phases, the phase diagram gets blurred and deformed.

The minimum-energy configuration  $(\vec{n}, \vec{m})$ , regarded as a function of model parameters  $\alpha \in (0,3)$  and  $\beta \in (0,1)$ , cannot be evaluated analytically and one has to resort to numerical techniques. In order to do that, we have to pass from the Coherent-State Picture, used till now, to the Continuous Variable Picture (see subsection 2.1.1 and Appendix B for clarifications). In fact, it results simpler to search numerically the minima of the effective potential  $V$  (see Eq. (2.5)), than the ones of Hamiltonian (3.1).

In the case of the tetramer, such effective potential reads

$$V = \frac{U_a N^2}{2} \sum_{i=1}^4 x_i^2 + \frac{U_b M^2}{2} \sum_{i=1}^4 y_i^2 + W M N \sum_{i=1}^4 x_i y_i +$$

$$-2NT_a \sum_{i=1}^4 \sqrt{x_i x_{i+1}} - 2MT_b \sum_{i=1}^4 \sqrt{y_i y_{i+1}} \quad (5.1)$$

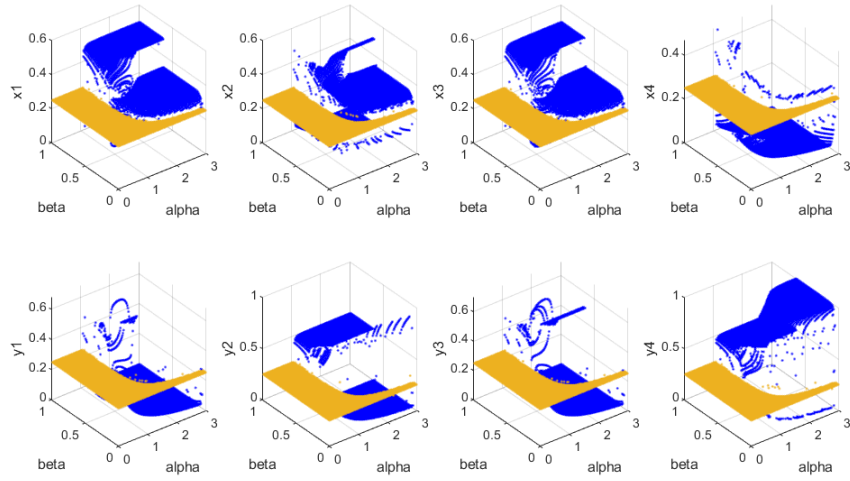
which comes with the two constraints  $\sum_i x_i = 1$  and  $\sum_i y_i = 1$ , and where variables  $x_i \equiv n_i/N$  and  $y_i \equiv m_i/M$  represent normalized boson populations and are regarded as continuous in view of the fact that the total numbers of bosons  $N$  and  $M$  are assumed to be large. Thus, the research of the minimum configuration  $(\vec{n}, \vec{m})$  becomes the one of the configuration  $(\vec{x}, \vec{y})$  that minimizes effective potential (5.1).

Therefore, using the Matlab function 'fmincon', that finds numerically the minimum points of a constrained nonlinear multivariable function (see Appendix A), we have been able to see what happens when finite-size effects matter. For this purpose, the following values/intervals have been chosen (and maintained also for the Mixing and Location Entropy plots):

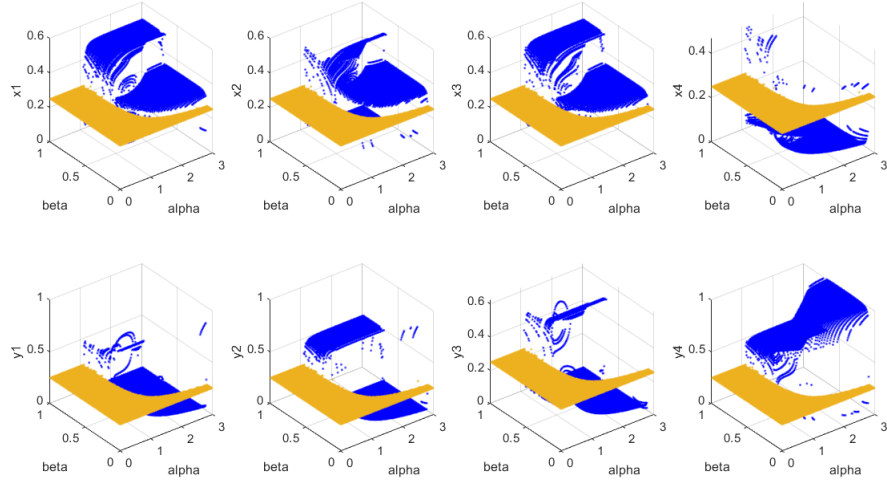
- $U_a = U_b = 1$ ;
- $N = 15$ ;
- $M \in [0,15] \rightarrow \beta \in [0,1]$ ;
- $W \in [0,3] \rightarrow \alpha \in [0,3]$ ;
- $T_a = T_b = T$  where  $T$  takes the values 0.1, 0.2 and 0.5.

Observing Fig. (5.1), we can notice that the minimum-energy configuration, regarded as a function of model parameters becomes smoother at the jump discontinuities as the hopping parameter  $T$  increases. Moreover, we have a confirmation

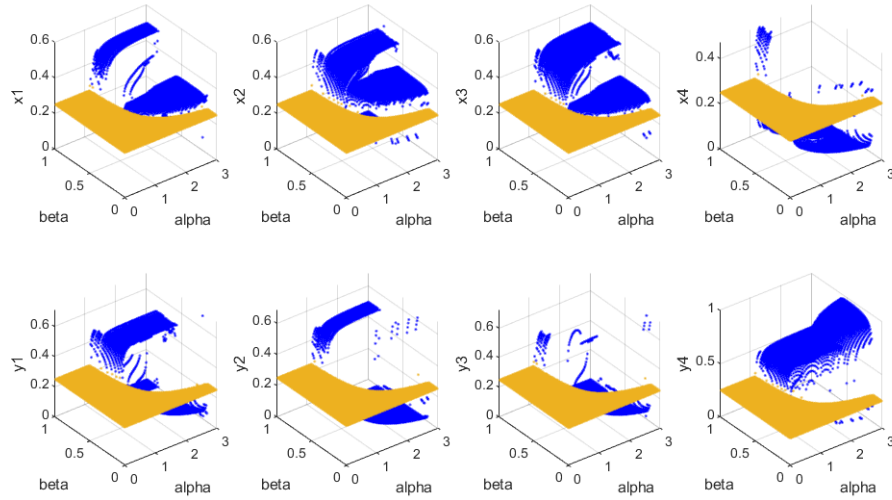
of the behavior of the system analytically predicted in the previous chapters and of the progress of the 5 phases.



[ $T = 0.1$ ]



[T = 0.2]



[T = 0.5]

**Figure 5.1:** Scatter plot of the minimum-energy configuration  $(\vec{x}, \vec{y})$  for  $T = 0.1, 0.2, 0.5$  (going from top to bottom). The orange color has been chosen to mark the region in which the mixed phase persists. All the other phases are colored in blue. The occurrence of a phase transition at  $\beta = 1/\sqrt{3}$  is clearly recognizable and still discontinuous for the lowest value of the hopping amplitude  $T$  (first panel), but it starts to become smoother as  $T$  increases (second and third panels).

In particular, the presence of the abrupt transition from the mixed phase (represented in orange in the figures) to the others (colored in blue) stands out, as well as, the one that occurs at  $\beta = 1/\sqrt{3}$ . Confirmation that will become even more visible if one goes to observe the behaviour of  $S_{mix}$  and  $S_{loc}$  as  $T$  increases.

One can also notice that the region occupied by the fully-mixed phase enlarges going from the first panel of Fig. (5.1) to the last one. This is because the uniform distribution of the two species among the four wells is favored by the presence of non-negligible hopping terms. The border of this region can be found analytically, and will be the object of the next section.

## 5.2 The border of the fully-mixed phase

In order to find the analytic expression of the mixed-phase border we have to resort to the Hessian matrix associated to effective potential (5.1). This boundary, in fact, corresponds to the condition under which the Hessian matrix (evaluated at point  $x_j = \frac{1}{4}$  and  $y_j = \frac{1}{4}$ , with  $j = 1, 2, 3, 4$ ) is positive definite. Thus, the first step is to find the matrix, that is given by

$$\begin{pmatrix} N^2 U_a + 4 N T_a & -2 N T_a & 0 & -2 N T_a & M N W & 0 & 0 & 0 \\ -2 N T_a & N^2 U_a + 4 N T_a & -2 N T_a & 0 & 0 & M N W & 0 & 0 \\ 0 & -2 N T_a & N^2 U_a + 4 N T_a & -2 N T_a & 0 & 0 & M N W & 0 \\ -2 N T_a & 0 & -2 N T_a & N^2 U_a + 4 N T_a & 0 & 0 & 0 & M N W \\ M N W & 0 & 0 & 0 & M^2 U_b + 4 M T_b & -2 M T_b & 0 & -2 M T_b \\ 0 & M N W & 0 & 0 & -2 M T_b & M^2 U_b + 4 M T_b & -2 M T_b & 0 \\ 0 & 0 & M N W & 0 & 0 & -2 M T_b & M^2 U_b + 4 M T_b & -2 M T_b \\ 0 & 0 & 0 & M N W & -2 M T_b & 0 & -2 M T_b & M^2 U_b + 4 M T_b \end{pmatrix}$$

and, subsequently, diagonalize it in order to find its eight eigenvalues and verify that they are positive. The latter can be listed as

$$E_1 = \frac{1}{2} \left( -\sqrt{-2M^2N^2U_aU_b + N^4U_a^2 + M^4U_b^2 + 4M^2N^2W^2} + N^2U_a + M^2U_b \right) \quad (5.2)$$

$$E_2 = \frac{1}{2} \left( \sqrt{-2M^2N^2U_aU_b + N^4U_a^2 + M^4U_b^2 + 4M^2N^2W^2} + N^2U_a + M^2U_b \right) \quad (5.3)$$

$$E_3 = E_4 = \frac{1}{2} \left( -\sqrt{(N^2U_a + 4NT_a - M(MU_b + 4T_b))^2 + 4M^2N^2W^2} + \right. \\ \left. + N^2U_a + 4NT_a + M^2U_b + 4MT_b \right) \quad (5.4)$$

$$E_5 = E_6 = \frac{1}{2} \left( +\sqrt{(N^2U_a + 4NT_a - M(MU_b + 4T_b))^2 + 4M^2N^2W^2} + \right. \\ \left. (N^2U_a + 4NT_a - M(MU_b + 4T_b))^2 + 4M^2N^2W^2 \right) \quad (5.5)$$

$$E_7 = \frac{1}{2} \left( -\sqrt{(N^2U_a + 8NT_a - M(MU_b + 8T_b))^2 + 4M^2N^2W^2} + \right. \\ \left. + N^2U_a + 8NT_a + M^2U_b + 8MT_b \right) \quad (5.6)$$

$$E_8 = \frac{1}{2} \left( +\sqrt{(N^2U_a + 8NT_a - M(MU_b + 8T_b))^2 + 4M^2N^2W^2} + \right.$$

$$+N^2U_a + 8NT_a + M^2U_b + 8MT_b) \quad (5.7)$$

and one can notice that Eqs. (5.2) and (5.3) are equal among them, except for the sign in front of the term under square root. The same can be said about Eqs. (5.4) and (5.5), and Eqs. (5.6) and (5.7). In particular, the first two eigenvalues do not depend on the hopping amplitudes  $T_a$  and  $T_b$ , so they are not relevant for the purpose to find a boundary that is an effect of the presence of non-vanishing hopping terms. Instead, comparing the last two with the remaining four, we can notice that they have the same form, but with different numerical prefactors. Obviously, we will choose the one that will probably give us the smallest possible value (that is Eq. (5.4)) and verify its positivity. After some calculations, we get the condition

$$\alpha < \sqrt{\left(1 + 4\frac{T_a}{U_a N}\right) \left(1 + 4\frac{T_b}{U_b M}\right)} \quad (5.8)$$

that has the same form as in the case of the three-well potential (see Eq. (2.43)), but with a different numerical factor in front of  $\frac{T_a}{U_a N}$  and  $\frac{T_b}{U_b M}$  [3].

One can observe that, walking away from the large-populations limit, the right-hand term rises above the value 1, thus determining an enlargement of the mixed phase at the expenses of the neighboring ones (see the enlargement of the orange region in Fig. (5.1), moving from the first panel to the last). This boundary is a clear example of how the form of the phases gets deformed in this regime and how strong is the influence of the hopping terms.

### 5.3 Mixing and Location Entropy

One can easily guess that the fully demixed phases are mined by the presence of hopping processes between the wells and therefore occurs for higher values of  $\alpha$ . This effect can be visualized, in particular, in the behaviour of the Mixing Entropy, in Fig. (5.2), and it reminds, to a certain extent, the messy action of the hopping amplitude in the Superfluid-to-Mott-insulator transition, which increases the mobility of bosons and makes the spatial fragmentation characteristic of the insulating phase increasingly difficult (see subsection 1.2.2). In the figures, we can observe that, as  $T$  increases the two demixed phases (green and yellow) move more and more towards higher values of  $\alpha$ , while the intermediate phases expand their areas and make the transition from uniform configuration less and less abrupt.

Colors have been chosen in a non-rigorous way, just to remember where the old phases (for  $T = 0$ ) were located. For example, the separation line between the green and the yellow phases has always been put at  $\beta = 1/\sqrt{3}$ , even if it is obvious that it occurs for higher values of  $\beta$  as  $T$  grows up (see the end of the "tip" of the

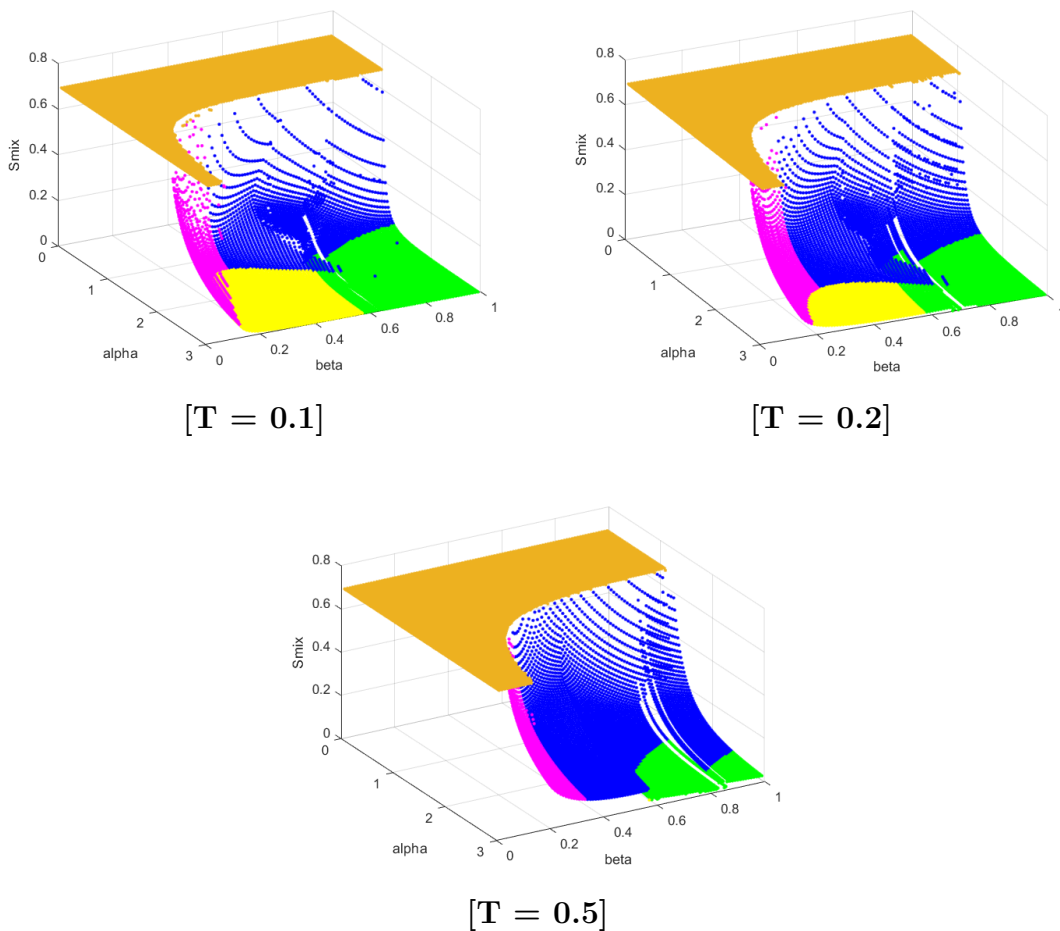


**Figure 5.2:** Scatter plot of the Mixing Entropy associated to the ground state for  $T = 0.1$  (the one on the upper left corner),  $T = 0.2$  (the one on the upper right corner),  $T = 0.5$  (the one below). Colors have been employed as a guide to the eye: orange is used when  $S_{mix} \approx \log 2$ , green when  $S_{mix} < 0.05$  and  $\beta > 1/\sqrt{3}$ , yellow when  $S_{mix} < 0.05$  and  $\beta < 1/\sqrt{3}$ , magenta and blue for all intermediate values, separated by  $\beta = 1/3$ .

blue phase in Fig. (5.2)). This phenomenon is even more visible in the scatter plots of the Location Entropy for different values of  $T$  (see Fig. (5.3)). For what concerns the latter, in fact, the jump from phase 6 to phase 7 (the two demixed phases; see section 4.3 for explanation) occurs around the value of  $\beta = 0.8$  and more, for lowest values of  $T$ . Instead, for  $T = 0.5$ , the trimer-like demixed phase (the one represented in yellow in previous chapters) appears to have been pushed completely out of the plot range. Moreover, one can notice the narrowing of the green band at the top (always referring to Fig. (5.3)) and the respective widening of the one at the

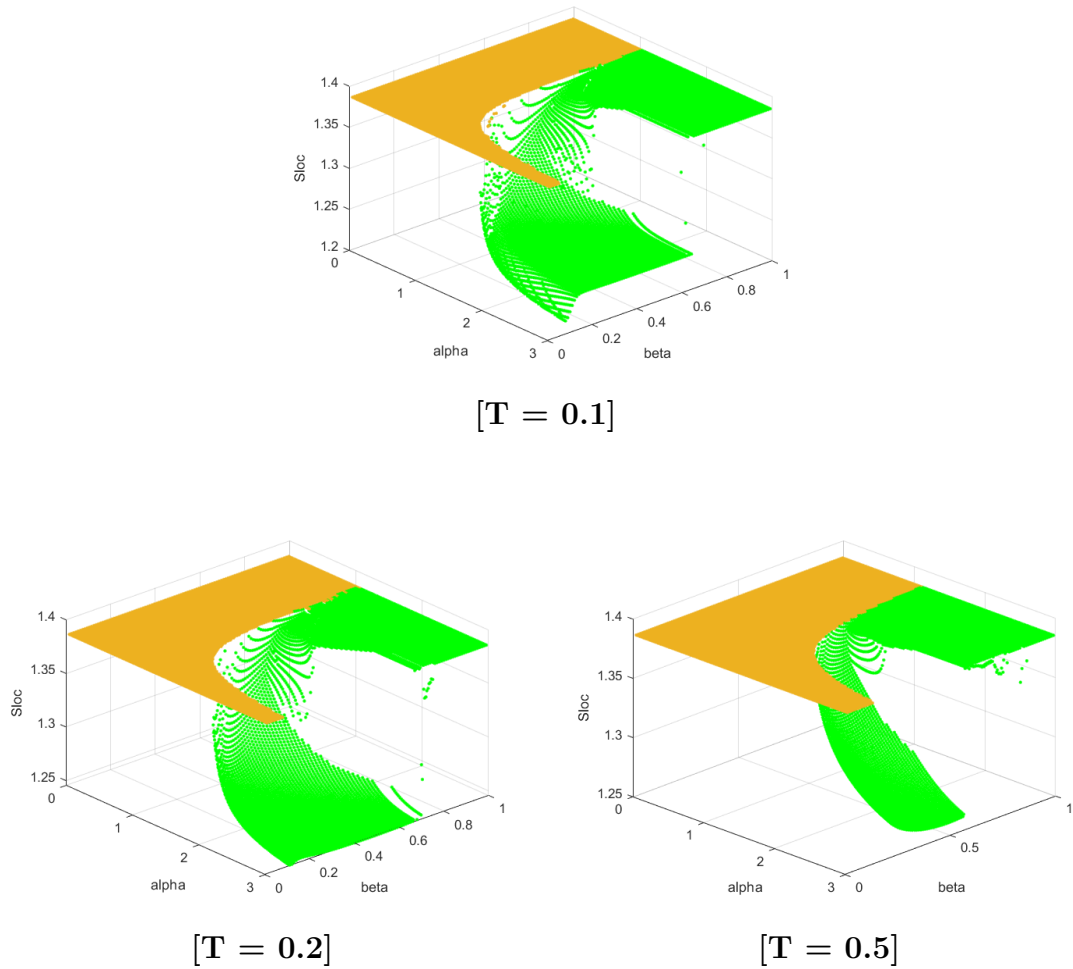


**Figure 5.3:** Scatter plot of the Location Entropy associated to the ground state for  $T = 0.1$  (the one on the top),  $T = 0.2$  (the one on the lower left corner),  $T = 0.5$  (the one on the lower right corner). Colors have been employed as a guide to the eye: orange is used when  $S_{mix} \approx \log 2$ , green otherwise.

bottom: further evidence of the shift of the transition line towards higher values of  $\beta$ .

In conclusion, we can assert that the behaviour of  $S_{mix}$  (5.2) and  $S_{loc}$  (5.3) is perfectly coherent with what has already been seen in the case of the trimer. The results obtained coincide with what was expected by inserting the presence of non-negligible hopping terms.



# Appendix A

## The finding-minima Numerical Algorithm

In this Appendix we report the complete Matlab code of the iterative algorithm developed and employed for the search for the minima of the effective potential (5.1). For completeness, the graphic representation commands have also been reported, as well as the implementation of the Colormaps (which collect the criteria on the colors with which it was chosen to mark the different phases).

The main Matlab-function used is 'fmincon', i.e. a tool that finds the minima of constrained nonlinear multivariable function. More specifically, it is a nonlinear programming solver that finds the minimum of a problem specified by

$$\min_x f(x) \text{ such that } \begin{cases} c(x) \leq 0 \\ ceq(x) = 0 \\ A \cdot x \leq b \\ Aeq \cdot x = beq \\ lb \leq x \leq ub, \end{cases}$$

where  $b$  and  $beq$  are vectors,  $A$  and  $Aeq$  are matrices,  $c(x)$  and  $ceq(x)$  are functions that return vectors, and  $f(x)$  is a function that returns a scalar.  $f(x)$ ,  $c(x)$ , and  $ceq(x)$  can be nonlinear functions. For what concerns  $x$ ,  $lb$ , and  $ub$ , they can be passed as vectors or matrices. The meaning of all these elements can be listed as follow:

- $f(x)$  is the function of which we are looking for the minimum, while  $x$  is the minimum, i.e. the solution of our problem;

- $A$  and  $b$  can be passed to the function 'fmincon' if the solution has to respect a condition of the form  $A \cdot x \leq b$ ;
- $Aeq$  and  $beq$  can be passed to the function 'fmincon' if the solution has to respect a condition of the form  $Aeq \cdot x = beq$ ;
- $c(x)$  and  $ceq(x)$  can be passed to the function 'fmincon' if the solution has to respect conditions of the form  $c(x) \leq 0$  or  $ceq(x) = 0$ , respectively;
- $lb$  and  $ub$  represent the lower and the upper bounds, respectively, that the solution has to satisfy. They can be set to infinity or minus infinity if the solution is not bounded.

Moreover, it is necessary to pass to the 'fmincon' function also a starting point  $x_0$ , from which it starts to find a minimizer. In our case, of crucial importance has been the choice of the starting point and its variation once one crosses the transition line  $\beta = 1/\sqrt{3} \approx 0.58$ .

To express the constraints, on the other hand, among the various opportunities listed above, the use of  $lb$ ,  $ub$ ,  $Aeq$  and  $beq$  has been chosen. Since populations  $x_j$  and  $y_j$  must assume values between 0 and 1, the lower bound has been set to  $[0,0,0,0,0,0,0,0]$ , while the upper bound to  $[1,1,1,1,1,1,1,1]$ . For what concern the constraints  $\sum_{i=1}^4 x_j = 1$  and  $\sum_{i=1}^4 y_j = 1$ , instead, we set

$$Aeq = \begin{pmatrix} 1 & 1 & 1 & 1 & 0 & 0 & 0 & 0 \\ 0 & 0 & 0 & 0 & 1 & 1 & 1 & 1 \end{pmatrix}$$

and  $beq = [1,1]$ . This choice proved to be particularly effective and, overall, using this algorithm allowed us to find all the results we were looking for.

```

1 basis_point = [0.5,0,0.5,0,0,0.5,0,0.5]; %we start from the demixed
  phase
2 basis_point_start = [0.5,0,0.5,0,0,0.5,0,0.5];
3
4 t = 0.033;
5 lb= [0,0,0,0,0,0,0,0]; %lower bound
6 ub= [1,1,1,1,1,1,1,1]; %upper bound
7 AA=[];
8 bb=[];
9 Aeq=[1,1,1,1,0,0,0,0;0,0,0,0,1,1,1,1]; %Aeq x = beq
10 beq=[1,1];
11 options = optimoptions(@fmincon,'FunctionTolerance',1e-15,'
  ConstraintTolerance',1e-15,'MaxFunctionEvaluations',10000);
12
13 i=1;
14 for B=0.99:-0.01:0.01

```

```

15     for A=3:-0.02:0.01
16
17         f = @(x) (1/2)*(x(1)^2 + x(2)^2+x(3)^2 + x(4)^2) + ((B^2)/2)*(x
18             (5)^2 + x(6)^2+x(7)^2 + x(8)^2) + A*B*(x(1)*x(5)+ x(2)*x(6)+x(3)*x
19             (7)+ x(4)*x(8)) - 2*t*(sqrt(x(5)*x(6)) + sqrt(x(7)*x(6)) + sqrt(x
20             (7)*x(8)) + sqrt(x(8)*x(5))) - 2*t*(sqrt(x(1)*x(2)) + sqrt(x(2)*x
21             (3)) + sqrt(x(3)*x(4)) + sqrt(x(4)*x(1)));
22
23         if A==3
24             x = fmincon(f, basis_point_start,AA,bb,Aeq,beq,lb,ub,[],
25             options);
26         else
27             x = fmincon(f, basis_point,AA,bb,Aeq,beq,lb,ub,[], options);
28         end
29
30         Vstar = (1/2)*(x(1)^2 + x(2)^2+x(3)^2 + x(4)^2) + ((B^2)/2)*(x(5)
31             ^2 + x(6)^2+x(7)^2 + x(8)^2) + A*B*(x(1)*x(5)+ x(2)*x(6)+x(3)*x(7)
32             + x(4)*x(8)) - 2*t*(sqrt(x(5)*x(6)) + sqrt(x(7)*x(6)) + sqrt(x(7)*
33             x(8)) + sqrt(x(8)*x(5))) - 2*t*(sqrt(x(1)*x(2)) + sqrt(x(2)*x(3))
34             + sqrt(x(3)*x(4)) + sqrt(x(4)*x(1)));
35
36         S_mix = -1/2*( x(1)*log(x(1)/(x(1)+x(5))) + x(5)*log(x(5)/(x
37             (1)+x(5))) + x(2)*log(x(2)/(x(2)+x(6))) + x(6)*log(x(6)/(x(2)
38             +x(6))) + x(3)*log(x(3)/(x(3)+x(7))) + x(7)*log(x(7)/(x(3)+x(7))
39             ) + x(4)*log(x(4)/(x(4)+x(8))) + x(8)*log(x(8)/(x(4)+x(8))));
40
41         S_loc = -((x(1)+x(5))/2*log((x(1)+x(5))/2) + (x(2)+x
42             (6))/2 *log((x(2)+x(6))/2) + (x(3)+x(7))/2 *log((x(3)+x(7))/2) +
43             (x(4)+x(8))/2 *log((x(4)+x(8))/2));
44
45         if A==3 && B>(0.58)
46             basis_point_start = [0.5,0,0.49,0.01,0,0.5,0.1,0.49];
47             basis_point = [0.5,0,0.49,0.01,0,0.5,0.1,0.49];
48
49         elseif A==3 && B<(0.58)
50             basis_point_start =
51             [0.32,0.33,0.31,0.02,0.01,0.01,0.01,0.97];
52             basis_point = [0.32,0.33,0.31,0.02,0.01,0.01,0.01,0.97];
53
54         else
55             basis_point = [x(1), x(2), x(3), x(4), x(5), x(6), x(7), x(8)
56             ];
57         end
58
59         vx1(i,:)=[A,B,x(1)];
60         vx2(i,:)=[A,B,x(2)];
61         vx3(i,:)=[A,B,x(3)];
62         vx4(i,:)=[A,B,x(4)];
63         vy1(i,:)=[A,B,x(5)];

```

```

48     vy2(i,:)=[A,B,x(6)];
49     vy3(i,:)=[A,B,x(7)];
50     vy4(i,:)=[A,B,x(8)];
51     vVst(i,:)=[A,B,Vstar];
52     vSmix(i,:)=[A,B,S_mix];
53     vSloc(i,:)=[A,B,S_loc];
54
55     i=i+1;
56     end
57 end
58
59 len=length(vx1(:,1));
60 C=ones(len,3); % Mixing Entropy Colormap
61 K=ones(len,3); % Location Entropy Colormap
62 Q=ones(len,3); % configuration Colormap
63
64 for i=1:len
65     if vSmix(i,3)>=0.68
66         C(i,:)=[0.9290, 0.6940, 0.1250]; %orange
67     elseif vSmix(i,3)<=0.05 && vSmix(i,2)<=0.57735
68         C(i,:)=[1,1,0]; %yellow
69     elseif vSmix(i,3)<=0.05 && vSmix(i,2)>=0.57735
70         C(i,:)=[0,1,0]; %green
71     elseif vSmix(i,1)>1 && vSmix(i,2)<=(1/3)
72         C(i,:)=[1,0,1]; %magenta
73     else
74         C(i,:)=[0,0,1]; %blue
75     end
76
77 end
78
79 for i=1:len
80     if vSmix(i,3)>=0.68
81         Q(i,:)=[0.9290, 0.6940, 0.1250]; %orange
82     else
83         Q(i,:)=[0,0,1]; %blue
84     end
85 end
86
87 for i=1:len
88     if vSmix(i,3)>=0.68
89         K(i,:)=[0.9290, 0.6940, 0.1250];
90     else
91         K(i,:)=[0,1,0];
92     end
93 end
94
95 subplot(2,4,1)
96 scatter3(vx1(:,1),vx1(:,2),vx1(:,3),10,Q,'.')
```

```
97 xlabel( 'alpha' );
98 ylabel( 'beta' );
99 zlabel( 'x1' );
100
101 subplot(2,4,2)
102 scatter3(vx2(:,1),vx2(:,2),vx2(:,3),10,Q, 'r. ')
103 xlabel( 'alpha' );
104 ylabel( 'beta' );
105 zlabel( 'x2' )
106
107 subplot(2,4,3)
108 scatter3(vx3(:,1),vx3(:,2),vx3(:,3),10,Q, 'r. ')
109 xlabel( 'alpha' );
110 ylabel( 'beta' );
111 zlabel( 'x3' );
112
113 subplot(2,4,4)
114 scatter3(vx4(:,1),vx4(:,2),vx4(:,3),10,Q, 'r. ')
115 xlabel( 'alpha' );
116 ylabel( 'beta' );
117 zlabel( 'x4' );
118
119 subplot(2,4,5)
120 scatter3(vy1(:,1),vy1(:,2),vy1(:,3),10,Q, 'r. ')
121 xlabel( 'alpha' );
122 ylabel( 'beta' );
123 zlabel( 'y1' );
124
125 subplot(2,4,6)
126 scatter3(vy2(:,1),vy2(:,2),vy2(:,3),10,Q, 'r. ')
127 xlabel( 'alpha' );
128 ylabel( 'beta' );
129 zlabel( 'y2' )
130
131 subplot(2,4,7)
132 scatter3(vy3(:,1),vy3(:,2),vy3(:,3),10,Q, 'r. ')
133 xlabel( 'alpha' );
134 ylabel( 'beta' );
135 zlabel( 'y3' );
136
137 subplot(2,4,8)
138 scatter3(vy4(:,1),vy4(:,2),vy4(:,3),10,Q, 'r. ')
139 xlabel( 'alpha' );
140 ylabel( 'beta' );
141 zlabel( 'y4' );
142
143 scatter3(vSmix(:,1),vSmix(:,2),vSmix(:,3),50,C, 'r. ')
144 xlabel( 'alpha' );
145 ylabel( 'beta' );
```

```
146 zlabel('Smix');  
147  
148 scatter3(vSloc(:,1),vSloc(:,2),vSloc(:,3),50,K, '. ')  
149 xlabel('alpha');  
150 ylabel('beta');  
151 zlabel('Sloc');
```

# Appendix B

## The link between the CVP and the Coherent-State method

It is interesting to highlight the link between the two pictures exploited for the purpose of this work, i.e. the link of the two-component Bose-Hubbard Hamiltonian reduced to the form (2.5) (let us take the case of the dimer as an example) with its semiclassical version which exhibits, as the most part of multimode boson models, a dynamics typically described by discrete nonlinear Schrödinger equations (see Eq. (2.10) in the case of the dimer with negligible hopping amplitudes). The semiclassical picture applied to the BH model, in which boson operators are replaced by local order parameters, is discussed in subsection 1.2.3.

The derivation of the generalized version of Eq. (2.10) (i.e. with non-negligible hopping amplitudes) can be performed by means of the coherent-state variational method where operators become classical variables within a sort of generalized Bogoliubov scheme. The semiclassical Hamiltonian associated to

$$H = \frac{U_a}{2} \sum_{j=1}^2 a_j^\dagger a_j^\dagger a_j a_j + \frac{U_b}{2} \sum_{j=1}^2 b_j^\dagger b_j^\dagger b_j b_j + W \sum_{j=1}^2 a_j^\dagger a_j b_j^\dagger b_j +$$
$$-T_a \sum_{j=1}^2 a_j^\dagger a_{j+1} - T_b \sum_{j=1}^2 b_j^\dagger b_{j+1} \quad (\text{B.1})$$

is easily found to be

$$H_s = \frac{U_a}{2} \sum_j |a_j|^4 + \frac{U_b}{2} \sum_j |b_j|^4 + W \sum_j |a_j|^2 |b_j|^2 +$$

$$-T_a \sum_j a_j^* a_{j+1} - T_b \sum_j b_j^* b_{j+1} \quad (\text{B.2})$$

where symbols  $a$  and  $b$  represents now local order parameters. Moreover, we have already seen how dynamical constraints (2.3) and (2.4) can be rewritten as

$$N = n_1 + n_2 = |a_1|^2 + |a_2|^2$$

$$M = m_1 + m_2 = |b_1|^2 + |b_2|^2$$

within this scheme. Now, by using the classical version  $x = (|a_1|^2 - |a_2|^2)/N$  and  $y = (|b_1|^2 - |b_2|^2)/M$  of the operators leading to the CVP-form of the Hamiltonian (see Eq. (2.5)), one obtains, up to a constant term

$$H_s = \frac{u_a}{4} (1 + x^2) + \frac{u_b}{4} (1 + y^2) + \frac{w}{2} (1 + xy) +$$

$$- \left[ \tau_a \sqrt{1 - x^2} \cos(2\theta_x) + \tau_b \sqrt{1 - y^2} \cos(2\theta_y) \right] \quad (\text{B.3})$$

where  $\theta_x = (\phi_1 - \phi_2)/2$  and  $\theta_y = (\nu_1 - \nu_2)/2$  are angle variables canonically conjugate with the action variables  $x$  and  $y$  satisfying the Poisson brackets

$$\{x, \theta_x\} = \frac{1}{\hbar N}$$

$$\{y, \theta_y\} = \frac{1}{\hbar M}$$

Variables  $\phi_j$  and  $\nu_j$  are the phases of the local order parameters

$$a_j = |a_j| e^{i\phi_j}$$

$$b_j = |b_j| e^{i\nu_j}$$

The Poisson brackets of  $|a_j|^2$ ,  $|b_j|^2$  with  $\phi_j$ ,  $\nu_j$  can be easily inferred from the canonical ones  $\{a_j, a_j^*\} = 1/(i\hbar)$ ,  $\{b_j, b_j^*\} = 1/(i\hbar)$  given by the coherent-state variational method.

Thus, now that we have (B.3), we can find the Hamilton equations, given by

$$\dot{x} = \{x, H_s\}$$

$$\dot{y} = \{y, H_s\}$$

and, in the particular case of  $\theta_x$  and  $\theta_y$ , by equations

$$\hbar N \dot{\theta}_x = \frac{wy}{2} + \frac{u_a x}{2} + \frac{x \tau_a \cos(2\theta_x)}{\sqrt{1 - x^2}} \quad (\text{B.4})$$

$$\hbar N \dot{\theta}_y = \frac{wx}{2} + \frac{u_b y}{2} + \frac{y \tau_b \cos(2\theta_y)}{\sqrt{1-y^2}} \quad (\text{B.5})$$

The calculation of the minimum-energy states requires that  $\theta_x = \theta_y = 0$ , since at the GS all the order-parameters phases are equal by default (phase coherence). Such minimum-energy configuration shows that equations (B.4) and (B.5), once one has replaced  $\theta_x$  and  $\theta_y$  with 0, exactly reproduce the one that determines the extremal points of the dimer effective potential within the Continuous Variable approach. The search of the GS thus appears to be closely related to imposing the stationarity condition for the effective potential, i.e. to the most important step of the CVP.

# Bibliography

- [1] V. Elser A. G. Basile. In: *Phys. Rev. E* 51.5688 (1995) (cit. on p. 15).
- [2] S. E. Koonin A. K. Kerman. In: *Ann. Phys. (NY)* 100.332-358 (1976) (cit. on p. 15).
- [3] A. Zenesini A. Richaud and V. Penna. «The mixing-demixing phase diagram of ultracold heteronuclear mixtures in a ring trimer». In: *Scientific Reports* (May 2019) (cit. on pp. 7, 66, 81).
- [4] Ensher J. R. Matthews M. R. Wieman C. E. Anderson M. H. and E. A. Cornell. «Observation of Bose-Einstein condensation in a dilute atomic vapor.» In: *Science* 198 (1995) (cit. on p. 3).
- [5] Wu Z. Anoshkin K. and E. Zaremba. «Persistent currents in a bosonic mixture in the ring geometry.» In: *Phys. Rev. A* 88.013609 (2013) (cit. on p. 3).
- [6] Dalibard J. Bloch I. and Zwerger W. «Many-body physics with ultracold gases.» In: *Rev. Mod. Phys.* 80.885 (2008) (cit. on p. 6).
- [7] I. Bloch. «Ultracold quantum gases in optical lattices.» In: *Nat. Phys.* 1.23 (2005) (cit. on p. 4).
- [8] S. N. Bose. «Plancks Gesetz und Lichtquantenhypothese.» In: *Zeitschrift für Physik* 26 (1924), p. 178 (cit. on p. 1).
- [9] Sackett C. A. Tollett J. J. Bradley C. C. and R. G. Hulet. «Evidence of Bose-Einstein Condensation in an Atomic Gas with Attractive Interactions.» In: *Phys. Rev. Lett.* 75.1687 (1995) (cit. on p. 3).
- [10] Kaufman M. Camesasca M. and Manas-Zloczower. «Quantifying fluid mixing with the Shannon entropy.» In: *Macromol. theory simulations* 15 (2006), 595–607 (cit. on pp. 36, 69, 73).
- [11] De Sarlo L. Barontini G. Minardi F. Catani J. and M. Inguscio. «Degenerate Bose-Bose mixture in a three-dimensional optical lattice.» In: *Phys. Rev. A* 77.011603 (2008) (cit. on p. 6).

- [12] Markic L. V. Cikojevic V. and J. Boronat. «Harmonically trapped bose-bose mixtures: A quantum monte carlo study.» In: *New J. Phys.* 20.85002 (2018) (cit. on p. 3).
- [13] C. N. Cohen-Tannoudji. «Nobel Lecture: Manipulating atoms with photons.» In: *Rev. Mod. Phys.* 70.707 (1998) (cit. on p. 2).
- [14] Esry B. D. and Greene C. H. In: *Phys. Rev. A* 59 (1999), 1457–1460 (cit. on p. 3).
- [15] K. B. et al. Davis. «Bose-Einstein Condensation in a Gas of Sodium Atoms.» In: *Phys. Rev. Lett.* 75.3969 (1995) (cit. on p. 3).
- [16] S. et al. De. «Quenched binary Bose-Einstein condensates: Spin-domain formation and coarsening.» In: *Phys. Rev. A* 89.033631 (2014) (cit. on p. 3).
- [17] Timmermans E. In: *Phys. Rev. Lett.* 81 (1998), 5718–5721 (cit. on p. 3).
- [18] T. Esslinger. *Experimental and Theoretical Aspects of Quantum Gases*. Lecture notes, 2017 (cit. on p. 2).
- [19] Lingua F. and Penna V. «Continuous-variable approach to the spectral properties and quantum states of the two-component BoseHubbard dimer.» In: *Phys. Rev. E* 95.062142 (2017) (cit. on pp. 7, 21, 32).
- [20] R. P. Feynman. «Quantum mechanical computers.» In: *Opt. News* 11.11 (1985) (cit. on p. 4).
- [21] R. P. Feynman. «Quantum mechanical computers.» In: *Found. Phys.* 16.507 (1986) (cit. on p. 4).
- [22] Grinstein G. Fisher Matthew P. A. and Daniel S. Fisher. «Boson localization and the superfluid-insulator transition.» In: *Phys. Rev. B.* 40 (1) (1989), 546–70 (cit. on p. 8).
- [23] R. Franzosi and V. Penna. In: *Phys. Rev. A* 63.043609 (2001) (cit. on p. 20).
- [24] D. G. et al. Fried. «Bose-Einstein Condensation of Atomic Hydrogen.» In: *Phys. Rev. Lett.* 81.3811 (1998) (cit. on p. 3).
- [25] C. E. MacPhee H. Grubmüller U. Zachariae G. B. Brandani M. Schor and D. Marenduzzo. In: *PLoS ONE* 8.e65617 (2013) (cit. on p. 73).
- [26] H. Gersch and G. Knollman. «Quantum Cell Model for Bosons.» In: *Phys. Rev.* 129 (2).959 (1963) (cit. on p. 8).
- [27] T. Giamarchi and H. J. Schulz. «Anderson localization and interactions in one-dimensional metals.» In: *Phys. Rev. B.* 37 (1) (Jan. 1988), 325–340 (cit. on p. 8).
- [28] Mandel O. Esslinger T. Hänsch T. W. Greiner M. and I. Bloch. «Quantum phase transition from a superfluid to a Mott insulator in a gas of ultracold atoms.» In: *Nature* 415.39 (2002) (cit. on pp. 5, 6).

- [29] C. Gross and I. Bloch. «Quantum simulations with ultracold atoms in optical lattices.» In: *Science* 357.995 (2017) (cit. on p. 6).
- [30] Penna V. Guglielmino M. and B. Capogrosso-Sansone. «Mott-insulator-to-superfluid transition in Bose-Bose mixtures in a two-dimensional lattice.» In: *Phys. Rev. A* 82.021601 (2010) (cit. on p. 6).
- [31] Ma H. and Pang T. In: *Phys. Rev. Lett.* A 351 (2006), 92–96 (cit. on p. 3).
- [32] Pu H. and Bigelow N. P. In: *Phys. Rev. Lett.* 80 (1998), 1130–1133 (cit. on p. 3).
- [33] Chang J. Engels P. Hamner C. and M. Hoefer. «Generation of dark-bright soliton trains in superfluid-superfluid counterflow.» In: *Phys. Rev. Lett.* 106.065302 (2011) (cit. on p. 3).
- [34] T.-L. Ho and C. V. Ciobanu. In: *J. Low Temp. Phys.* 135.257 (2004) (cit. on p. 20).
- [35] Chang J. J. Hamner C. Hoefer M. A. and P. Engels. «Dark-dark solitons and modulational instability in miscible two-component Bose-Einstein condensates.» In: *Phys. Rev. A* 84.041605 (2011) (cit. on p. 3).
- [36] Jean Dalibard Immanuel Bloch and Wilhelm Zwerger. «Many-body physics with ultracold gases.» In: *Rev. Mod. Phys.* 80.885 (July 2008) (cit. on p. 5).
- [37] D. M. Jezek and P. Capuzzi. «Interaction-driven effects on two-component Bose-Einstein condensates.» In: *Phys. Rev. A* 66.015602 (2002) (cit. on p. 3).
- [38] W. Nobel lecture Ketterle. «When atoms behave as waves: Bose-Einstein condensation and the atom laser.» In: *Rev. Mod. Phys.* 74 (2002), p. 1131 (cit. on p. 3).
- [39] Ho T. L. and Shenoy V. B. In: *Phys. Rev. Lett.* 77 (1996), 3276–3279 (cit. on p. 3).
- [40] V. Penna L. Amico. In: *Phys. Rev. Lett.* 80.2189 (1998) (cit. on p. 16).
- [41] K. L. et al. Lee. «Phase separation and dynamics of two-component Bose-Einstein condensates.» In: *Phys. Rev. A* 94.013602 (2016) (cit. on p. 3).
- [42] M. et al. Lewenstein. «Ultracold atomic gases in optical lattices: mimicking condensed matter physics and beyond.» In: *Adv. Phys.* 56.243 (2007) (cit. on p. 6).
- [43] Halperin B. I. Ma M. and P. A. Lee. «Strongly disordered superfluids: Quantum fluctuations and critical behavior.» In: *Phys. Rev. B.* 34 (5) (Sept. 1986), 3136–3143 (cit. on p. 8).
- [44] Modugno M. Fort C. Minardi F. Maddaloni P. and M. Inguscio. «Collective Oscillations of Two Colliding Bose-Einstein Condensates.» In: *Phys. Rev. Lett.* 85.2413 (2000) (cit. on p. 3).

- 
- [45] G. Grinstein Matthew P. A. Fisher Peter B. Weichman and Daniel S. Fisher. «Boson localization and the superfluid-insulator transition.» In: *Phys. Rev. B* 40.546 (July 1989) (cit. on p. 5).
- [46] G. et al. Modugno. «Bose-Einstein condensation of potassium atoms by sympathetic cooling.» In: *Science* 294.1320 (2001) (cit. on p. 3).
- [47] Ao P. and Chui S. T. In: *Phys. Rev. A* 58 (1998), 4836–4840 (cit. on p. 3).
- [48] V. Penna P. Buonsante. In: *J. Phys. A: Math.* 41.175301 (2008) (cit. on p. 16).
- [49] V. Penna P. Buonsante and A. Vezzani. In: *Phys. Rev. A* 84.061601(R) (2011) (cit. on pp. 21, 24).
- [50] O. Penrose and L. Onsager. «Bose-Einstein Condensation and Liquid Helium.» In: *Phys. Rev.* 104 (1956), p. 576 (cit. on p. 2).
- [51] F. et al. Pereira Dos Santos. «Bose-Einstein Condensation of Metastable Helium.» In: *Phys. Rev. Lett.* 86.3459 (2001) (cit. on p. 3).
- [52] W. D. Phillips. «Nobel Lecture: Laser cooling and trapping of neutral atoms.» In: *Rev. Mod. Phys.* 70.721 (1998) (cit. on p. 2).
- [53] L. Pitaevskii and S. Stringari. *Bose-Einstein condensation and Superfluidity*. Oxford University Press, 2016 (cit. on pp. 2, 3).
- [54] F. Riboli and M. Modugno. «Topology of the ground state of two interacting Bose-Einstein condensates.» In: *Phys. Rev. A* 65.063614 (2002) (cit. on p. 3).
- [55] A. Richaud and V. Penna. «Pathway toward the formation of supermixed states in ultracold boson mixtures loaded in ring lattices.» In: *Phys. Rev. A* 100.013609 (2019) (cit. on pp. 24, 73).
- [56] A. et al. Robert. «A Bose-Einstein condensate of metastable atoms.» In: *Science* 292.461 (2001) (cit. on p. 3).
- [57] Bohn J. L. Halmo L. E. Ronen S. and M. Edwards. «Dynamical pattern formation during growth of a dual-species Bose-Einstein condensate.» In: *Phys. Rev. A* 78.053613 (2008) (cit. on p. 3).
- [58] Zheng W. M. Shi H. and Chui S. T. In: *Phys. Rev. A* 61.063613 (2000) (cit. on p. 3).
- [59] R. W. Spekkens and J. E. Sipe. In: *Phys. Rev. A* 59.3868 (1999) (cit. on p. 20).
- [60] A. A. Svidzinsky and S. T. Chui. «Symmetric-asymmetric transition in mixtures of Bose-Einstein condensates.» In: *Phys. Rev. A* 67.053608 (2003) (cit. on p. 3).
- [61] A. Richaud V. Penna. «The phase-separation mechanism of a binary mixture in a ring trimer». In: *Scientific Reports* (July 2018) (cit. on pp. 7, 32, 34, 36, 37, 39, 56, 59).

- [62] Isaieva K. O. Vilchinskii S. I. Yakimenko A. I. and M. Weyrauch. «Stability of persistent currents in spinor Bose-Einstein condensates.» In: *Phys. Rev. A* 88.051602 (2013) (cit. on p. 3).
- [63] M. et al. Zaccanti. «Observation of an Efimov spectrum in an atomic system.» In: *Nat. Phys.* 5.586 (2009) (cit. on p. 3).